UNIVERSITY OF NAPOLI *"FEDERICO II"*

POLYTECHNIC AND SCIENCE SCHOOL

Ph.D. School in Chemical Sciences (36° Cycle)

Coordinator: Prof. Angelina Lombardi

Microbial polysaccharides as flexible and renewable resources for innovative applications: structural and functional studies

Ph.D. Candidate
Samantha Armiento

Tutor

Prof. Antonio Molinaro/Cristina De Castro

2020-2024

Table of Contents

Abbreviations

AAPM Partially methylated and acetylated alditols
AcOH Acetic Acid
AMBIC Ammonium Bicarbonate
APCs Antigen-Presenting Cells
BB Blocking Buffer
BCIP 5-Bromo-4-chloro-3-indolyl-phosphate
BMDC Bone Marrow-derived Dendritic Cell
BLG β-Lactoglobulin
BSA Bovine Serum Albumin
ButOH Butanol
CDAP 1-cyano-4-dimethylaminopyridinium
CDC Center for Disease Control and Prevention
CFU Colony Forming Unit
CMA Cow's Milk Allergy
CM Cytoplasmic Membrane
CNRS Centre National de la Recherche Scientifique
COSY Correlation Spectroscopy
CPS Capsular Polysaccharide
CSDB Carbohydrate Structure Database
DC Dendritic cell
DMEM Dulbecco's Modified Eagles Medium
DMSO Dimethyl sulfoxide
DNAse Deoxyribonuclease
ELISA Enzyme-linked Immunosorbent Assay
EPS Exopolysaccharide
EtOH Ethanol
FBS Fetal Bovine Serum
GI Gastrointestinal
GC-MS Gas Chromatography – Mass Spectrometry
GRAS Generally Recognized as Safe
HF Hydrofluoric Acid
HMBC Heteronuclear Multiple Bond Correlation
HPLC High-Performance Liquid Chromatography
HR-MAS High resolution-Magic Angle Spinning
HSQC Heteronuclear Single Quantum Coherence
HSQC-TOCSY Heteronuclear Single Quantum Coherence – Total Correlation Spectroscopy
IBD Intestinal Bowel Disease
Ig Immunoglobulin
IL Interleukin
LAB LactobacilliLOS Lipooligosaccharide
LPS Lipopolysaccharide

LTA Lipoteichoic Acid
MAMP Microbial-associated molecular pattern
MeOH Methanol
MGA Acetylated Methyl Glycosides
MOI Multiplicity of Infection
MPGs Microbially Produced Glycans
*Muc*2 Mucin2
MW Molecular weight
NBT Nitro Blue Tetraziolium
NF-κB Nuclear Factor kappa B
NMR Nuclear Magnetic Resonance
NOESY Nuclear Overhauser Enhancement Spectroscopy
ODNs Oligodeoxynucleotides
OM Outer Membrane
OMG Octyl Methyl Glycosides
ON Overnight
OPA Opsonophagocytic Assays
OPIA Opsonophagocytic Inhibition Assay
P Phosphate
PBMC Peripheral Blood Mononuclear Cells
PBS Phosphate-buffered saline
PCR Polymerase Chain Reaction
PG Peptidoglycan
PMAA Partially Methylated Acetylated Alditols
PMN Polymorphonuclear leukocytes
PRR Pattern Recognition Receptor
R Substituent
RBC Red Blood Cells
rDC Regulatory Dendritic Cells
RNAse Ribonuclease
ROESY Rotating frame Overhauser Effect Spectroscopy
RT Room temperature
SDS Sodium Dodecyl Sulfate
SDS-PAGE Sodium Dodecyl Sulfate-PolyAcrylamide Gel Electrophoresis
SNFG Symbol Nomenclature for Glycans
SSCN Synthesis and Structure of Carbohydrates in Naples
STD Standard
TA Teichoic Acid
TCA Trichloroacetic Acid
TFA Trifluoroacetic Acid
TMB Tetramethylbenzidine
TNFα Tumour Necrosis Factor alpha
TLR Toll-Like Receptor

TOCSY Total Correlation Spectroscopy
UPLC Ultra-Performance Liquid Chromatography
Vr Retention volume
WB Washing Buffer
WHO World Health Organisation
WTA Wall-teichoic Acid

Monosaccharides abbreviations and symbols

	MurNAc	N-acetylmuramic acid
	Gal	galactose
	GalN	galactosamine
	GalNAc	N-acetylgalactosamine
	Glc	glucose
	GlcN	glucosamine
	GlcNAc	N-acetylglucosamine
	Hep	L-*glycero*-D-*manno*-heptosepyranonse
	Kdo	3-deoxy-D-*manno*-oct-2-ulosonic acid
	Rha	rhamnose
	Rib	ribose

Other residues abbreviations and symbols

	Gro	glycerol
	*P*	phosphate
	Rib-ol	ribitol

This Ph.D. thesis used the Symbol Nomenclature for Glycans (SNFG) (Varki et al., 2015).

Abstract

The term “microbiota” stands for the complex of microorganisms present in a defined environment, which coexist with their hosts without damaging them. The balance of the microbiota can play a fundamental role in health and disease conditions of the host with which it is in symbiosis. An imbalance can contribute to the decrease of the host's immune defenses and favor and exacerbate the virulence of even opportunistic commensal bacteria, which in this case become pathogenic. Polysaccharides of the bacteria cell surface are one of the principal molecules which interact with the host immune system. Among these, the most important are teichoic acids (TA), capsular polysaccharides (CPS) and exopolysaccharides (EPS). In particular, many CPS from commensals have been linked to beneficial effects to the host immune system, while TAs of Gram-positive bacteria seem to play crucial roles in microbe/host colonization or infection. Specifically, lipotheicoic acids have been identified as pathogen-associated molecular pattern molecules (PAMP) that activate the innate immune system via Toll-like receptor-2. In this context, the main effort of this Ph.D. thesis is to isolate polysaccharides produced by Gram-positive bacteria of the human and plants microbiota with the aim to structurally characterized them and to investigate their immunological properties. Specifically, as Gram-positive bacteria sources there were employed *Lactobacillus reuteri*, *Lactobacillus rhamnosus* GG ATCC 53103, *Lacticaseibacillus paracasei* CBA L74, *Bacillus subtilis* 168, *Ruminococcus gnavus* ATCC 35913, and *Enterococcus faecium* U0317.

Regarding with ***L. reuteri***, it is a pro-biotic, facultative anaerobic bacterium, that colonizes mostly the gastro-intestinal human tract. The abundance of *L. reuteri* varies among different individuals. Notably, the decrease of *L. reuteri* in humans in the past decades is correlated with an increase in the incidences of inflammatory diseases over these periods. Probably, many health-promoting properties of this bacterium are mediated by carbohydrate polymers that coat its cell-surface. In this part of work, the capsular material from *Lactobacillus reuteri* has been purified and analyzed and the obtained results demonstrate that the coat of this bacterium consists of a heterogeneous mixture of three types of glycans, a glucogalactan, a galactan, and a polyglycerol phosphate-based teichoic acids. The identification of the three glycans was possible after extensive purification steps which included both size exclusion and ion exchange chromatography, and that led to the isolation of the teichoic acid in pure forma and to a mixture of the two neutral polysaccharides. Each sample was then extensively characterized by 2D NMR spectroscopy and the structural data collected were counterchecked by GC-MS analysis.

Regarding with ***L. rhamnosus***, evidence suggests that it could elicit a tolerogenic action in children with cow’s milk allergy (CMA), but it is unclear if this effect could be induced by inactivated LGG or by its derived postbiotic components, such as its capsular polysaccharide. Thus, the latter was isolated and its chemical structure was confirmed, by NMR analysis, to be the same previously reported in literature. Moreover, it was performed an in-vitro investigation on the tolerogenic action elicited by the direct interaction between

heat inactivated LGG or LGG-derived postbiotic components (capsular polysaccharide, CPS; and non methylated CpG motifs DNA sequence, ID35) and human enterocytes or peripheral blood mononuclear cells (PBMCs). Specifically, there were investigated the expression levels of *Muc2*, *lactase*, and of the Tregs DCs-mediated, along with the pro-inflammatory cytokine production, by real time PCR, ELISA, and flow cytometry experiments. Finally, the obtained results suggest that the tolerogenic action elicited by *L. rhamnosus* in children with CMA is mediated by, at least, two postbiotic compounds, that are its CPS and its ID35 factor. Therefore, the aforementioned CPS isolated from *L. rhamnosus* could be a potential postbiotic candidate for the treatment of cow's milk allergy in childhood.

Regarding with ***L. paracasei***, it populates the human gut microbiota and is on markets as lactic ferment for infants to promote the maturation and the strengthening of their immune system. These activities may be addressed to the cell-surface glycan components of this bacterium. For this reason, *L. paracasei* cell-surface polysaccharides were isolated and studied by NMR spectroscopy and GC-MS techniques. In conclusion, a phosphoglycerol based teichoic acid polymer, and two capsular polysaccharides have been identified, one of which (CPS-1) with a repeating unit consisting of several hexoses and deoxyhexoses and a branched aminohexose, and the other (CPS-2), with a lower molecular weight, with a repeat consisting of a galactosamine and several rhamnoses, including a branched one with a non-stoichiometric substituent, in turn linked at one side to a terminal glucose, and at the other to a rhamnose. Specifically, this substituent can sometimes be a glucosamine and sometimes a galactosamine (10:1 ratio), making the entire structure non-regular and heterogeneous. Although the structure of teichoic acid has already been widely reported in the literature, especially for many species of lactobacillus, the structures described for the CPSs isolated from *L. paracasei* represent a total novelty. Moreover, by HR-MAS NMR spectroscopy analysis there were investigated the level of expression and of exposition of these glycans on the bacterium cell-surface. Finally, it was observed that, while the teichoic acid NMR signals were not present in the acquired spectra, the CPS-2 signals were the most evident in live cells, suggesting teichoic acid as the innermost component and CPS-2 as the one most exposed on the cell surface of *L. paracasei*. Lastly, from the HR-MAS NMR analysis of the cell surface of the bacterium during its different growth phases (lag, exponential and stationary), it emerged that the NMR signals of *L. paracasei* polysaccharides are generally more abundant in the exponential phase, compared to the lag one and, above all, to the stationary one.

Regarding with ***B. subtilis***, some pieces of evidence indicate that this bacterium is able to trigger defense responses in the plants. Hence, to understand if the glycans could play any role in such process, a study was undertaken to disclose their structure, a prerequisite to proceed with the biological studies. Accordingly, from the bacterium were isolated and characterized by GC-MS and NMR analysis a polyglycerol phosphate-based teichoic acid (glycan-1) and a capsular polysaccharide (glycan-2), this last made of GalNAc and Glc units along with phosphate linked as diester. Besides, by Arabidopsis infiltration assays it was discovered that the glycan-1 is able to trigger a dose-depending inflammatory response in the plant, which can culminate in a leaf necrosis, while the glycan-2 did not cause any

changes in leaf phenotype, suggesting that it does not exert any type of immunological activity on the plant.

Regarding with ***R. gnavus***, it is a prevalent member of the human gut microbiota and over-expressed in inflammatory bowel diseases. In particular, it has been previously reported in literature that there are two different clades of *R. gnavus*, and only one of these is enriched in IBD patients. This evidence could be addressed to a strain-dependent immunomodulatory activity of this bacterium, lastly dependent on the specific cell surface glycosylation pattern. *R. gnavus* ATCC 29149 was previously shown to produce a pro-inflammatory exopolysaccharide (glucorhamnan). In this part of the Ph.D thesis polysaccharides from *R. gravus* E1 and ATCC 35913 strain were isolated and structurally characterized, and their immunological activity was evaluated in comparison to that of the type strain (ATCC 29149), with the aim of seeing whether there may be any differences between them. Thus, by NMR spectroscopy and GC-MS studies it was discovered that the ATCC 35913 purified polysaccharide showed branched repeating units with a backbone composed of four α-L-rhamnose (α-Rha) units, with alternate 2- and 3-linkages, while the side chain was a single β-D-glucose (β-Glc) residue linked to O-2 of one of the 3-Rha units. This glucorhamnan differs from that of ATCC 29149 in terms of number of Rha units and length of the side chain, while *R. gnavus* E1 strain shared the same glucorhamnan structure as ATCC 35913. Next, by immunological assays it was observed that *R. gnavus* ATCC 35913 and its related EPS are the most immunogenic compounds, in terms of induction of a large array of pro-inflammatory cytokines in bone-marrow derived dendritic cells and of the Nf-kB mediated response in human THP1-Blue™ reporter cells. The strain-specific differences in *R. gnavus* cell surface glycosylation and host response underscore the importance of studying *R. gnavus*-host interaction at the strain level.

Regarding with ***E. faecium***, it is a bacterium belonging to the LAB group, which can be commensal in human GI tract. However, early in its evolution, it has acquired characteristics such as antibiotic resistance and the ability to prosper in hostile environments, that allowed it to become, in the past two decades, a worldwide cause of nosocomial infections. Therefore, finding novel alternatives for *E. faecium* treatment prevention, such as vaccines, is crucial. In this part of study, various techniques to discover a novel capsular polysaccharide were applied. Firstly, there was identified an encapsulated *E. faecium* strain by evaluating the opsonophagocytic activity of fifteen strains with antibodies targeting the well-known lipoteichoic acid antigen. This activity was attributed to an unknown polysaccharide. Then, guided by immunodot-blot analysis, this glycopolymer was isolated and structurally characterized by using NMR spectroscopy and GC-MS analysis. The elucidated structure presents a branched repeating unit, with the linear part being: →)-β-D-Gal-(1→4)-β-D-Glc-(1→4)-β-D-Gal-(1→4)-β-D-GlcNAc-(1→, further decorated with a terminal α-D-Glc and a D-phosphoglycerol moiety, attached to O-2 and O-3 of the 4-linked Gal unit, respectively. This polysaccharide was conjugated to BSA and the synthetic glycoprotein used to immunize mice. The resulting sera exhibited good opsonic activity, suggesting its potential as a vaccine antigen, namely with promising applications in immunotherapy.

Thanks to the work carried out together with my research group and various collaborators, during my doctoral period I was able to participate in the publication of the following manuscripts:

1. Speciale I, Notaro A, Garcia-Vello P, Di Lorenzo F, Armiento S, Molinaro A, Marchetti R, Silipo A, De Castro C. 2022. Liquid-state NMR spectroscopy for complex carbohydrate structural analysis: A hitchhiker's guide. *Carbohydr Polym*, 277:118885.

2. Laverde D, Armiento S, Molinaro A, Huebner J, De Castro C, Romero-Saavedra F. 2023. Identification of a capsular polysaccharide from *Enterococcus faecium* U0317 using a targeted approach to discover immunogenic carbohydrates for vaccine development. *Carbohydr Polym*, 121731.

Furthermore, I isolated a CPS from *L. rhamnosus* GG cells, confirming the chemical structure already described in literature but, currently, the study of its immunological activity represents a scientific novelty. Instead, from *R. gnavus* ATCC 35913 and E1 strains, and *L. paracasei* CBA L74 I discovered new glycans, not yet described in literature. Therefore, together with some collaborators who are developing studies aimed at discovering the potential immunological activities of these polysaccharides, the following articles are currently in preparation:

3. Cozzolino M, Oglio F, Paparo L, Di Sarra C, Armiento S, De Castro C, Pisapia L, Coppola S, Molinaro A, Carucci L, Berni Canani R. 2023. Postbiotic effects elicited by heat inactivated *Lacticaseibacillus rhamnosus* GG against cow's milk allergy in human cells. In preparation.

4. Laplanche V*, Armiento S*, Notaro A, Šuligoj T, H. Crost E, Lamprinaki D, Vaux L, Gotts K, De Castro C, Juge N. *Contributed equally. 2023. The human gut symbiont *Ruminococcus gnavus* displays strain-specific cell surface glycosylation glucorhamnan polysaccharides modulating the host immune response. In preparation.

5. Armiento S, Cozzolino M, Oglio F, Guerardel J, Trivelli X, Berni Canani R, Molinaro A, De Castro C. The probiotic *Lactobacillus paracasei* displays on its cell-membrane a teichoic acid and two peculiar capsular polysaccharides able to modulate the host immune response. In preparation.

Therefore, part of this Ph.D. thesis was adapted from the aforementioned articles co-written by the author of the present thesis.

List of Figures

List of Tables

Chapter 1

Introduction

1.1. Bacterial microorganisms

Bacteria are tiny, single-celled organisms invisible to the naked eye. They can be found almost everywhere on earth and are vital to the planet's ecosystems. For example, bacteria break down dead matter in the environment, releasing nutrients and carbon dioxide, that is essential for plants growth (Lacaze, Zboralski, & Joly, 2021). Some bacteria live in or on other organisms including plants, animals and humans. From the latest recent research it has emerged that the ratio between bacterial and human cells is approximately 1:1 (Sender, Fuchs, & Milo, 2016).

Though small, bacteria are powerful and complex. They can also survive in extreme conditions of temperature and pressure (Rampelotto, 2013). They have a tough protective coat that boosts their resistance to white blood cells in the body. In addition, some bacteria have a tail, known as flagellum, that helps them to move around. Other bacteria have sticky, hair-like appendages that help them stick to one another or onto hard surfaces (Van Gerven, Waksman, & Remaut, 2011). Bacteria cell structure is simpler than that of many other organisms. Their genetic information is contained in a single loop of DNA. Some bacteria have an extra circle of genetic material, called plasmid, rather than a nucleus. This plasmid often contains genes that give the bacterium some advantage over other bacteria or resistance to antibiotics (Tsang, 2017).

Bacteria are classified into five groups according to their basic shapes: spherical (cocci), rod (bacilli), spiral (spirilla), comma (vibrios) or corkscrew (spirochaetes) (*Chapter 1 - Basic Biology of Oral Microbes*, 2015). In addition, according to the Microbiology Society, they can be single-celled microorganisms, but they may also exist in clusters, chains, and pairs. Bacteria are also described as aerobic, anaerobic, or facultative anaerobes. These terms describe how they respond to oxygen. While aerobic bacteria need oxygen to live, anaerobic bacteria will die. Facultative anaerobes live best with oxygen but do not need it to survive.

Last but not least, bacteria can also be classified as harmless, helpful, or pathogenic (harmful). Thus, while some bacteria can be used to make medicines and vaccines, others can cause diseases and illnesses. If you consume or come in contact with harmful bacteria, they may reproduce in your body and release toxins that can damage your body's tissues and make you feel ill. In some cases, you may need antibiotics to stop pathogenic bacteria from reproducing and attacking your body. While antibiotics are sometimes necessary for healing, the Centers for Disease Control and Prevention (CDC) estimate that more than 28% of related prescriptions are not necessary. It is important to receive an accurate diagnosis from your doctor since un incorrect assumption of antibiotics can promote the bacteria resistance to them, and your health could be seriously compromised. Concerning with bacteria that inhabit the soil, some of these can cause food spoilage and crop damage, especially the endospore-producing bacteria. These are dangerous pathogens that can form endospores, namely dormant structures extremely resistant to hostile physical and

chemical conditions such as heat, UV radiation and disinfectants. This makes destroying them very difficult. Despite that, relatively few species of bacteria are parasites or pathogens that cause disease in animals, plants and humans (Balloux & van Dorp, 2017). Indeed, according to the National Human Genome Research Institute (NHGRI), most bacteria are harmless for people. Most of the beneficial bacteria in the human body are located in your digestive system, hence the term "gut microbiome". As an example, in our gut, we have bacteria that are very necessary to help our body functions (e.g. breaking down food and keeping harmful bacteria from moving in). Indeed, some people take probiotics on a regular basis or while taking antibiotics to support gut health. These supplements contain strains of helpful bacteria, such as Bifidobacteria and Lactobacillus, used also in food production to make fermented foods (Soemarie, Milanda, & Barliana, 2021).

1.1.2. Bacterial microbiota

The term "microbiota" stands for an assemblage of microorganisms that form an ecological community in a specific area (Altveş, Yildiz, & Vural, 2020). All multicellular organisms benefit from their own microbiota, which play important roles in maintaining the host nutritional health and immunity (Ikeda-Ohtsubo et al., 2018). The theory of the coevolution arises from the close relationships between hosts and their associated microorganisms, that adapt mutually, with respect to each other (O'Brien, Webster, Miller, & Bourne, 2019).

Microbial compartmentalization depends strongly on biotic and abiotic gradients that exist in both the gut and root. Along the soil-root, we can distinguish a soil, a rhizosphere, a rhizoplane, and an endosphere compartment. Bacterial diversity in soil is high (Schloss and Handelsman, 2006). The rhizosphere is the area of the soil directly influenced by root exudation, while the root compartment is divided into the rhizoplane and the endosphere. The rhizoplane harbors microbes closely adhered to the root surface, while in the endosphere we find microbes settled in the interior of roots. Microbial density is high in the rhizosphere, and species richness gradually decreases along the soil-endosphere (Hacquard et al., 2015).. A similar heterogeneity of microbial density exists along the human digestive track (Stearns et al., 2011). Bacterial density is lowest in the stomach and duodenum and increases along the length of the small intestine, with a higher density in the distal ileum. Moreover, like to the compartmentalization in the root, a decrease in bacterial density is observed from the lumen to the epithelial surface of the digestive tract.

Moreover, within the microbiota, we can distinguish a "core" from a "transient microbiota". The first one appears to remain constant during the time, and is constantly associated with a given host genotype or a specific environment (Gabriele Berg et al., 2020). In contrast, the transient microbiota changes over time, depending on the host's genes (Hacquard et al., 2015), diet (Eilam et al., 2014) and lifestyle, drugs (Altveş et al., 2020), environment (Hacquard et al., 2015), pregnancy, age, microbe-microbe interactions (Hacquard & Schadt, 2015) and on the immune system.

Although the infancy or the seedling stage for plants are critical parameters for microbiota assembly, very little is known about the earliest steps driving host bacteria colonization. Assembly of the infant gut microbiome begins at birth, and diversity levels slowly increase until 2-3 years of age, where Bacteroidetes is co-dominant with the phylum of Firmicutes after the introduction of solid foods (Koenig et al., 2011). On the contrary, in adulthood the microbiota becomes more stable in terms of composition. Instead, despite a higher variability observed during the seedling stage(Chaparro, Badri, & Vivanco, 2014), microbiota acquisition from soil occurs relatively rapidly in plants, within 2 weeks (J. Edwards et al., 2015), and the structure of the root microbiota during the plant life cycle appears rather stable since birth.

Microbial diversity is one of the key factor in preventing diseases in the human gut (Larsen & Claassen, 2018) as well as in plants (Gabriele Berg et al., 2017). According to the "microbioma" definition of Lederberg and McCray (Lederberg & McCray, 2001), microorganisms can be divided into beneficial, pathogenic, and neutral based on their interactions with the host. However, recent studies on opportunistic pathogens showed that host-microbe interactions depend not only on a single subject, but on the entire microbiome (G. Berg & Martinez, 2015). Studies observe the presence of four dominant phyla in the gut microbiota, where Firmicutes and Bacteroidetes represent more than 90% of the total population, while Proteobacteria and Actinobacteria are almost the rest (Magne et al., 2020). Homeostatic balance between both microbe-microbe and host-microbe interactions is critical for a healthy host-microbiota environment (Sekirov, Russell, Antunes, & Finlay, 2010). The alteration of this balance is called dysbiosis. Many factors can generate a dysbiosis, leading to an increased exposure to infections and to many other diseases such as auto-immune (Flandroy et al., 2018), chronic and/or metabolic pathologies (B. Wang, Yao, Lv, Ling, & Li, 2017). The consequences can extend also to cancer and central nervous system disorders (Treisman, 2017). Moreover, the reduced exposure to microorganisms in early human life can lead to several allergies. In many epidemiological studies, it has been observed that children growing up on natural environments are more protected from asthma and other allergic symptoms than children growing up on urban areas (von Mutius & Vercelli, 2010).

The human-gut and root microbiota share a several of common beneficial effects for their hosts. First of all, it protects the organism from external pathogens through competitive colonization or production of antimicrobial agents like bacteriocins (Garcia-Gutierrez, Mayer, Cotter, & Narbad, 2019). Additionally, it provides energy, vitamins and nutrients to the host by increasing their bioavailability (Bulgarelli, Schlaeppi, Spaepen, Ver Loren van Themaat, & Schulze-Lefert, 2013) (Martins dos Santos, Müller, & de Vos, 2010). Moreover, it can increase host tolerance against abiotic stresses and affect plant flowering plasticity (Panke-Buisse, Poole, Goodrich, Ley, & Kao-Kniffin, 2015). Finally, the human-gut microbiota modulates many fundamentals biological processes such as substances absorption by

intestinal epithelium, endocrine secretion, genes expression, and the development of the immune system (Flandroy et al., 2018).

1.2. Antibiotic resistance

Antibiotics are medications used to destroy or slow down the bacterial growth. They essentially work by killing bacteria or preventing their reproduction in the host organism, thus they are intended to treat and prevent bacterial infections.

Depending on their final effects, antibiotics can be classified as bacteriostatic or bactericidal. Generically, an antibiotic able to stop the bacterial growth is defined as bacteriostatic, while an antibiotic that kills the bacterium is defined bactericidal (Patel, Wermuth, Calhoun, & Hall, 2023). To be more precisely, we must introduce the concepts of "minimum inhibitory concentration" (MIC), and "minimum bactericidal concentration" (MBC). The MIC is the lowest antibiotic concentration that inhibits visible bacterial growth after 24 h, while the MBC is the lowest antibiotic concentration that reduces bacterial density by 1000-fold after 24 h. Thus, bacteriostatic activity is defined by an MBC to MIC ratio greater than 4, whereas a bactericidal activity is defined by an MBC to MIC ratio less than or equal to 4 (Pankey & Sabath, 2004).

The clinical antibiotic efficacy depends on many factors as pharmacokinetic and pharmacodynamic profiles, the specific bacterial target, bacterial load and site of infection. Furthermore, the bacteriostatic and bactericidal activity of some antibiotics may vary depending on the bacterial strain considered (Nemeth, Oesch, & Kuster, 2015). Additionally, antibiotics not only act on pathogenic bacteria but also may have an impact on beneficial bacteria, which can leads to biological imbalances, namely dysbiosis (Arboleya et al., 2016). This effect is particularly caused by using broad-spectrum antibiotics: while narrow-spectrum antibiotics target a few types of bacteria, the antibiotics with a broad-spectrum of action target many types of bacteria. The improper use of the latter may cause more side effects such as rush or diarrhea, in respect to the administration of a narrow-spectrum antibiotic when the specific etiological agent responsible for the infection is well diagnosed.

Especially in early life, the antibiotic consumption may negatively impact the formation of a healthy microbial community. Studies on infants highlighted that the use of antibiotics or even the exposure to them during the intrauterine life, is related to an increase in the Proteobacteria phylum, since it contains resistance genes for many antibiotics, and a decrease in Bifidobacteria, which are considered beneficial to the host (Francino, 2015). Likewise, another study on children using macrolides in their first year of life, reported a decrease in Actinobacteria and an increase in Bacteroidetes and Proteobacteria, along with an increment of resistance genes. This dysbiosis was linked to the asthma development or to the body mass increment in these children (Korpela et al., 2016). In addition, the intestinal environment provides a suitable environment for the horizontal transfer of multiple resistance genes between bacteria, which increases the risks linked to the inappropriate use of antibiotics (Flandroy et al., 2018).

Widespread antibiotic bacteria resistance determines hundreds of thousands of deaths every year. The most worrying factors for the global public health are represented by the constantly growing number of bacteria resistant to the commonly used antibiotics, and the speed with which resistance genes can spread among microorganisms (Urban-Chmiel et al., 2022).

The bacteria resistances against external threats can be primary or secondary. Primary resistance arises from a spontaneous, random mutation and can appear even in absence of drugs. This type of resistance is encoded through chromosomes and is not transmitted to other bacterial species. The frequency of occurrence of spontaneous bacteria mutations is low. On the other hand, secondary bacteria resistance arises from contact with external potentially harmful agents such as antibiotics. The secondary genetic resistance mechanism is extrachromosomal and much more complex. The genes responsible for this phenomenon are located in small circular molecules of DNA in the cytoplasm, named plasmids. One plasmid may contain genes for the resistance to several different antimicrobials. Plasmids can transfer these genes from one bacterium to another, mainly via conjugation and transduction. During conjugation, plasmids are transferred directly by contact between bacterial cells through strands of protein produced by them. In this process can participate different species and genera bacteria, even phylogenetically remote. During transduction, plasmids are transferred between cells through bacteriophages, namely bacterial viruses that introduce DNA in the bacterium by attaching to a receptor on its cell surface.

Antimicrobial resistance mechanisms can be summarized into: limiting the uptake of a drug; modifying a drug target; inactivating a drug; active efflux of a drug. Instead of Gram-negative, the drug uptake limitation and the drug active efflux occur less in Gram-positive bacteria, because of structural differences in their cell membrane (Reygaert, 2018).

Horizontal gene transfer makes resistance genes available for a great number of bacteria, even breaking the barrier between environmental (non-pathogenic) bacteria and microbial pathogens in a living environment (Martinez, 2012). However, this process is much more frequent between bacteria that are tightly phylogenetically related (Smillie et al., 2011). Thus, pathogens transfer of resistance genes is supposed to be an event relatively common between human bacteria (Poirel et al., 2018), especially during treatment with antibiotics. In conclusion, a resistance factor transferred to a human pathogen, more probably spreads between commensals and pathogens around than to the environmental bacteria.

One of the major aim in clinical and, recently, also agricultural field are the avoiding of resistant bacterial strains selection during antibiotic treatments and the limiting of their diffusion. The currently implemented strategies for overcoming antibiotic resistance rely on the alternative use of antimicrobial peptides (Mourenza, Gil, Mateos, & Letek, 2020), the development of next-generation vaccines, and the use of new diet for animals, based on prebiotics, probiotics, and phytobiotics (Ruvalcaba-Gómez et al., 2022).

1.3. Cell membrane differences in Gram-positive and Gram-negative bacteria

In 1884 Christian Gram developed a staining procedure that allowed him to distinguish bacteria into two main groups, and this eponymous stain is still in use today. In particular, the group of bacteria that retain Christian's stain was named "Gram-positive", while the other do not, "Gram-negative". The Gram stain is essentially due to the structural differences in the cell envelope of these two groups of bacteria.

The bacteria cell envelope is a complex, dynamic structure, essential for the protection and the adaptation of the bacterium in its surrounding environment. Its composition varies between Gram- positive and Gram-negative bacteria. Basically, the Gram-negatives cell wall consists, from bottom to top, of a cytoplasmatic or inner membrane (IM), a thin (few nanometers) layer of peptidoglycan (PG) contained in the periplasmic space, and of an outer membrane (OM) (Glauert & Thornley, 1969), where there are attached proteins, and lipopolysaccharide (LPS) or lipooligosaccharide (LOS).

Among the components of the cell envelope, the one majorly conserved in bacteria is peptidoglycan, which has an important role in the stabilization of the cell membranes against high internal osmotic pressure, and because its rigidity, it determines the cell shape. The chemical structure of peptidoglycan in Gram-positive microorganisms is similar to that of Gram-negatives. It consists of a disaccharide-peptide repeating unit coupled through glycosidic bonds to form linear glycan strands. These strands are in turn crosslinked through the peptide stems attached to the disaccharide repeating unit to give a meshlike framework. More in details, there are many differences among Gram-positive and Gram-negative peptidoglycan structure. One of the most relevant difference consists to the peptide crosslinks between glycan strands (Vollmer, 2008).

The OM of Gram-negative bacteria consists of phospholipids, lipopolysaccharides, lipoproteins and integral membrane proteins such as porins, which limit the diffusion of hydrophilic molecules larger than about 700 Daltons (Nikaido, 2003). All of these molecules are synthesized in the cytoplasm or at the inner leaflet of the IM and are transported through the inner membrane and the periplasm to be assembled (Bos, Robert, & Tommassen, 2007). The OM represents a very selective permeability barrier.

The periplasm is an aqueous compartment delimiting the OM from the IM. It is densely packed with proteins and has different functions, including protein transport, folding, oxidation, and quality control, that makes it similar to the endoplasmic reticulum of the eukaryotic cell. The periplasm also contributes to the kidnapping of enzymes that may be toxic in the cytoplasm, to the signaling mechanisms, and to the regulations of the cell division. Additionally, it is important for the synthesis of molecules involving in maintaining the rigidity and the selective permeability of the OM, such as peptidoglycan, lipoproteins and glycerolphospholipids (Miller & Salama, 2018).

The IM is a phospholipid bilayer. It contains all of the proteins that in the eukaryotic cells are located in intracellular organelles and are involved in energy production, lipid biosynthesis, and protein transport and secretion (Miller & Salama, 2018).

Differently, the Gram-positive cell wall lacks the outer membrane along with its associated LPS or LOS, the periplasm and has a thicker (30-100 nm) PG, composed of many layers (Fig. 1). Moreover, in Gram-positive bacteria we also have negatively charged polymers named teichoic acids (TA). They may be directly attached to the peptidoglycan, namely wall-teichoic acids (WTAs), or anchored to the inner membrane, namely lipoteichoic acids (LTAs).

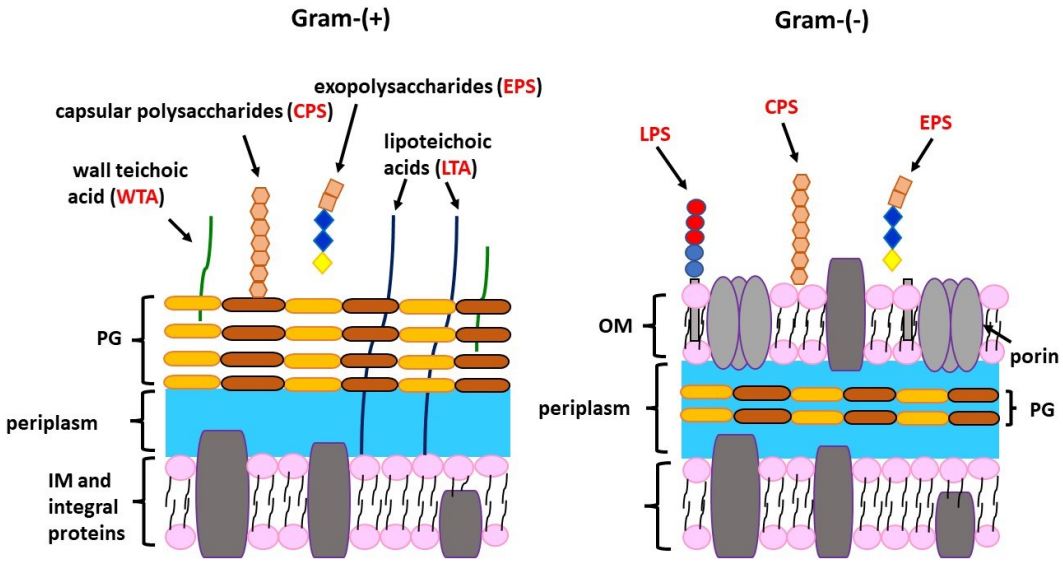

Figure 1. Gram-positive and Gram-negative cell envelope. These last one are distinguished from the first one for their extra outer membrane layer (OM), that covers a thinner peptidoglycan (PG) and the inner membrane (IM). The acronyms LPS, CPS, and EPS stand for lipopolysaccharide, capsular polysaccharide and exopolysaccharide, respectively.

The IM in Gram-positive bacteria is mainly stabilized by peptidoglycan, that in turns also help them to withstand the turgor pressure exerted on the plasma membrane. In addition, the surfaces of Gram-positive microorganisms are decorated with different proteins, some of which analogous to the proteins found in the periplasm of Gram-negative bacteria (Dramsi, Magnet, Davison, & Arthur, 2008). Some of them are linked to lipid anchors inserted in the membrane and others are covalently attached to or tightly associated with peptidoglycan (J. R. Scott & Barnett, 2006). Still others are linked to teichoic acids.

All together, TA constitutes over 60% of the mass of the Gram-positive cell wall, making them one of the most important determinants of the cell envelope structure and functions.

Deleting the pathways for the biosynthesis of TA produces organisms that have cell division and morphological defects as well as other growth defects.

1.4. Bacterial glycans

The bacterial surface is covered by a complex blend of different glycoconjugates, each with a different activity profile. They may have several different structural formats, with varying distributions. Some of them are associated to particular type of bacteria, such as LPS in gram-negative outer membranes, or WTAs in gram-positive peptidoglycan. Conversely, other glycoconjugates as glycoproteins, capsular polysaccharides (CPSs) and exopolysaccharides (EPSs), are present in both of them.

CPSs and EPSs are long polysaccharide chains that can be several 100 µm thick. When present, they form the outermost layer of bacteria (Martens, Roth, Heuser, & Gordon, 2009). Often, determining whether or not glycans are attached to the cell surface is difficult, thus "microbially produced glycans" (MPGs) is a generic term which refers to both CPSs and EPSs. Usually, EPSs are loosely associated with microbial cell surface or released by bacteria in extracellular media, and determine biofilm physicochemical properties (Costerton et al., 1987). Moreover, over the last decade EPSs from certain bacteria have also been shown to inhibit biofilm formation by other microbial species (Valle et al., 2006). On the other hand, CPSs are firmly attached to the microbial cell surface and characteristically retained on it after centrifugation, forming a surface-covering capsule revealed through microscopy (Whitfield, Wear, & Sande, 2020). CPSs represent one of the major bacteria virulence factor that confer them protection against environmental stressors, and most notably against the host-immune system during infection. Although there is a high percentage of encapsulated invasive-pathogens between bacteria, also non-pathogenic and commensal bacteria benefit from the ability to envelope themselves with a capsule (Dasgupta & Kasper, 2010). In Gram-negative bacteria, capsular polysaccharides are often attached to the outer membrane at their reducing end through covalently-linked lipids inserted into the membrane. This provides a hydrophilic surface, with high molecular weight polysaccharides that prevent cell desiccation in harsh environmental conditions, protect by pathogens infections, and hinder host immune responses by physically restricting access to cell surface antigens. Quite often, the structure of the CPS is the same of the EPS, so that the distinction between EPS and CPS is somewhat artificial. The molecular compositions of CPSs vary extensively between organisms and even between strains within a single species, but, despite this diversity, some species from distinct orders have been shown to biosynthesize identical CPS structures (Cress et al., 2014). Capsules composition may vary also with diet and different capsules may provide optimal access to various nutrients and more efficient use of the bacterial cell's resources (Porter & Martens, 2017). Moreover, some bacteria express CPSs that are phase variant and are able to switch between a reversible on-off phenotype (Krinos et al., 2001). These phase variation is thought to equip bacteria to adapt and survive in different niches and enables bacteria to alter their surface antigenicity (Porter & Martens, 2017). The differences between capsule structures were originally

investigated to classify strains of capsular bacterial depending on their interaction with human serum antibodies. Thus, bacteria were serotyped through differentiation of their capsular polysaccharide antigens (Lancefield, 1933). For example, *K. pneumoniae* has been historically classified by capsule (renamed K antigen) serotyping and to date 79 capsule types have been identified (Opoku-Temeng, Kobayashi, & DeLeo, 2019). However, purified CPSs may often mimic human glycans, resulting non-immunogenic for this host (M. S. Edwards, Kasper, Jennings, Baker, & Nicholson-Weller, 1982). On the other hand, capsule-deficient mutants generally exhibit decreased virulence, invasive properties and serum sensitivity (Hérias, Midtvedt, Hanson, & Wold, 1997). The chemical-structural differences between CPSs may involve their monosaccharide components (Fig. 2), which can vary in their stereoisomers (D or L), in the number of carbon molecules forming the sugar ring structure (furanose or pyranose), and in the configuration of the anomeric center (α or β). CPSs can be further diversified by branching and glycosidic linkage patterns, covalent coupling to other biological molecules such as lipids and proteins, and by the formation of secondary structures. Anyway, among the most recurring monosaccharide units of capsules, we can find:

-hexoses, such as glucose, galactose and mannose, which can be not-substituted or replaced with amino (amino sugars), acetyl or, less often, phosphate groups;

-deoxyhexoses, such as rhamnose and fucose;

-pentoses, such as xylose and arabinose.

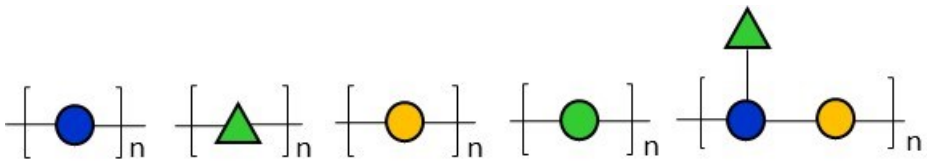

Figure 2. Generical exemplification of some of the most common CPS and EPS structures found to date. Structures are reported according to the Symbolic Nomenclature for Glycans (SNFG).

Wall-teichoic and lipoteichoic acids are anionic cell surface polymers present in a wide range of Gram-positive organisms. The WTAs are attached via a phosphodiester linkage to the C-6 hydroxyl of MurNAc residues of the peptidoglycan. Although structural variations sometimes occur, the most common WTAs are composed of a polyglycerol phosphate (polyGro*P*) or a polyribitol phosphate (polyRib-ol*P*) chain (Fig. 3), containing up to almost 60 repeating units (Silhavy, Kahne, & Walker, 2010). WTAs extend perpendicularly through the peptidoglycan mesh into a sort of "fluffy" layer. The Rib-ol*P* or Gro*P* repeats can be substituted with different chemical groups, typically amino acids as D-alanyl or glycosyl moieties, mostly composed by glucose, glucosamine and galactose. The nature and extent

of the modifications significantly affect the WTAs functions (Stephanie Brown et al., 2012). LTAs have chemical structures similar to WTAs, but they also differ in something. For example, their glycerolphosphate repeats have an opposite chirality in respect to those found in WTAs (A. Walter et al., 2020). Furthermore, rather than being attached to peptidoglycan, they are anchored to the membrane through a lipid anchor consisting of glycolipids such as a diglycosylated diacylglycerol in *S. aureus* (Kiriukhin, Debabov, Shinabarger, & Neuhaus, 2001), and usually contain fewer Gro*P* repeating units. Teichoic acids functions are various. One of this is their capability to bind cations, since their anionic nature. This activity contributes (Silhavy et al., 2010) to the cation homeostasis (Marquis, Mayzel, & Carstensen, 1976). Additionally, the networks of metal cations between WTAs influence the integrity and porosity of the cell wall (Silhavy et al., 2010).

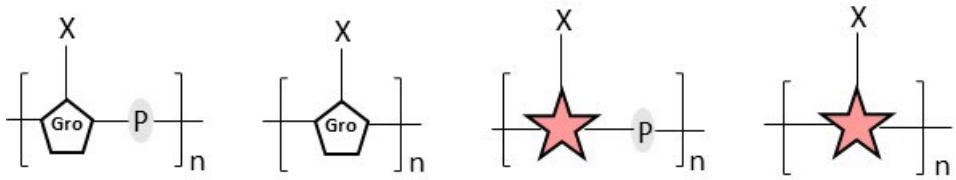

Figure 3. TA structures, consisting of poly-glycerol or poly-ribitol chains that sometimes can be substituted with amino acids or sugars. Hence, X stands for -H or a generic amino acid or sugar. Structures are reported according to the Symbolic Nomenclature for Glycans (SNFG), thus ★ = Rib.

LPS is produced by most Gram-negative bacteria. It is a glycolipid made of three structural domains (Fig. 4):

-the lipid A, that is the hydrophobic portion of the molecule. It is an acylated β-1'-6-linked glucosamine disaccharide that forms the outer leaflet of the OM. In *E. coli* and *Salmonella*, the glucosamines are phosphorylated at the 1 and 4' positions and acylated at the 2, 3, 2' and 3' positions. Two additional secondary acyl chains are also typically present in the distal glucosamine so that mature lipid A is mostly hexa-acylated (Raetz & Whitfield, 2002);

-the core oligosaccharide, that is an oligosaccharide linked in position α-2 to the C-6 atom of the GlcN of the lipid A (Heinrichs, Yethon, & Whitfield, 1998). The core structure usually contains 3-deoxy-D-*manno*-oct-2-ulosonic acid (Kdo), heptose, and various hexose residues, which can be modified with different groups such as phosphates and phosphoethanolamine (Whitfield, Kaniuk, & Frirdich, 2003);

-the O-antigen, that is an extended polysaccharide with a high molecular weight (10-60 kDa), linked to the core oligosaccharide. It is composed by a variable number of repeating units, each consisting of 3 to 6 sugar residues (Sergei Kalynych, Renato Morona, & Miroslaw Cygler, 2014). Some Gram-negative bacteria do not synthesize this LPS region. In such cases,

LPS composed of only lipid A and the core oligosaccharide is defined as "rough" and is typically named lipooligosaccharides, or LOS. On the contrary, the "smooth" LPS includes the O-antigen and is named lipopolysaccharides. The overall structure of LPS is conserved, but many variations can occur between species and strains. The O-antigen represents the most variable component of LPS (L. Wang, Wang, & Reeves, 2010).

The LPS populates much of the Gram-negative cell surface and forms a selective barrier that protects the cell from the toxic molecules. The selectivity is linked to LPS amphipathic nature: the lipid A provides a hydrophobic character that inhibits the passage of hydrophilic molecules through the OM, while the core oligosaccharide and the O-antigen provide an extensive hydrophilic character that makes the OM particularly impervious to hydrophobic molecules. In addition, LPS reinforces the barrier function of the OM thanks to the ability to pack densely within its outer leaflet. The tight packing is promoted by the acyl chains, that are largely saturated and therefore interact with each other, resulting in low fluidity within the membrane bilayer (Nikaido, 2003). Especially, LPS molecules bind firmly to each other especially in presence of cations as Mg^{2+}, that neutralize the negative charges of its phosphate groups. On the other hand, the negative charges of the LPS's phosphate groups represent a very effective barrier for the entry of hydrophobic molecules. Another important role played by LPS involves the bacterial pathogenicity. It is generally recognized by the host immune system as a pathogen associated molecular pattern (PAMP). Mammals have evolved multiple receptors for the PAMP, the so-called pathogens related receptors (PRRs), but LPS is not immuno-stimulatory in all eukaryotes (Gauthier, Rotjan, & Kagan, 2022). To better adapt to their varying environments, Gram-negative bacteria may often modify their LPS biosynthesis pathways, synthetizing LPS with different chemical structures. The most frequent modifications include: changes in the number and type of acyl chains, as well as the number of phosphates in lipid A (Mendoza, 2014), and addition of covalent modifications to lipid A, generally at the 1 and 4' phosphates, and at the core oligosaccharide (Maldonado, Sá-Correia, & Valvano, 2016).

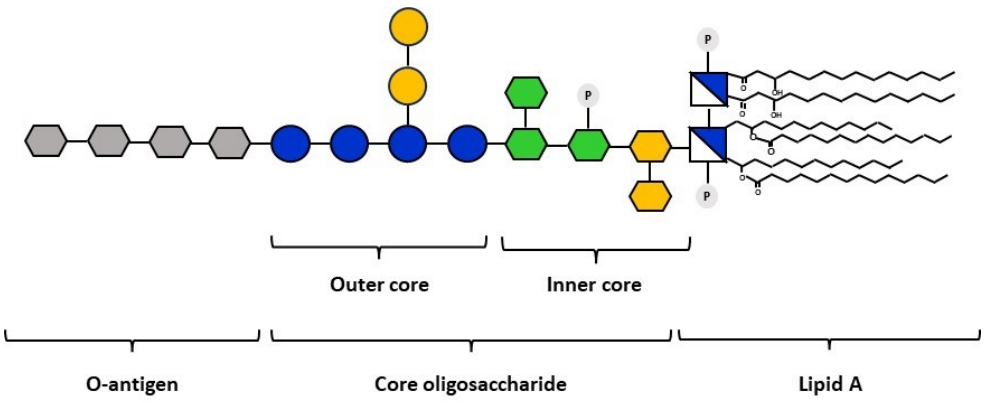

Figure 4. Schematic representation of a generic LPS. Structures are reported according to the Symbolic Nomenclature for Glycans (SNFG).

1.4.1. Polysaccharides immunomodulatory activity

Polysaccharides of the bacteria cell surface are one of the principal molecules involved in the modulation of the host immune system. Anyway, about the polysaccharides-host immune cells interactions, the structure-activity relationships, the interaction mechanisms and the final effects still remain not completely discovered and therefore subject of further investigation.

In general, in Gram-negative bacteria, the ability to trigger the host immune response varies with the structure of the LPS. The most conserved feature of LPS is the lipid A, for which host toll-like receptor 4 (TLR4) is the primary receptor (A. J. Scott, Oyler, Goodlett, & Ernst, 2017). However, there is a considerable structures diversity even within lipid A. Consequently, while the classical, hexacylated, bisphosphorylated lipid A molecule produced by *E. coli* and *Salmonella* is highly immunogenic, other forms of lipid A are less so. Really, some forms of lipid A not only inhibit a more immunogenic host response, but elicit no response themselves (Coats, Pham, Bainbridge, Reife, & Darveau, 2005). The production of less immunogenic lipid A is a strategy used by certain pathogens to evade the host immune response (Montminy et al., 2006). Alternatively, some Gram-negative bacteria evade the host immune response by masking the more conserved aspects of their LPS with a high variability of their O-antigen. Although the O-antigen induces the production of antibodies, the length of its chain prevents the antibody-mediated deposition of complement at the bacterial cell surface, protecting bacteria from lysis by complement. In addition, the O-antigen also contributes to pathogen evasion of phagocytosis by immune cells (S. Kalynych, R. Morona, & M. Cygler, 2014).

From an immunological point of view, we can consider teichoic acids of Gram-positive as equivalents of LPS (or LOS) of Gram-negative bacteria. In the last decades, LTA have become increasingly recognized as an immuno-stimulatory principle. For example, it has been observed that some LTAs isolated from different bacterial species are able to induce monokine production in human monocytes (Bhakdi, Klonisch, Nuber, & Fischer, 1991). Moreover, other studies discovered that in *S. aureus*, WTA plays an important role in its interaction with the human host. This interaction involves a wide range of resident and circulating immune cells, epithelial and endothelial cells, as well as humoral immune components. The consequences are various and often not fully understood. Several of them have antibacterial effects, whereas others could be beneficial for the bacterium survival during infection or colonization processes (R. van Dalen, A. Peschel, & N. M. van Sorge, 2020).

Finally, also CPSs and EPSs (or more in general MPGs) from commensal and pathogenic bacteria can modulate the innate and adaptive host-immune systems, especially in the human-gut environment. Many MPGs (CPSs and EPSs) enable bacteria to evade innate and adaptive immune responses by forming a protecting shield around them. For examples, CPSs protect bacteria from antimicrobial factors (Lebeer, Claes, Verhoeven, Vanderleyden,

& De Keersmaecker, 2011), complement deposition on the bacterial surface and consequently complement-mediated lysis (Attridge & Holmgren, 2009), and from phagocytosis by innate immune cells (Hsieh et al., 2020). MPGs can also enhance the host immune tolerance by inducing the innate immune system to produce more anti-inflammatory cytokines (Paynich, Jones-Burrage, & Knight, 2017) or fewer pro-inflammatory cytokines (Schiavi et al., 2016). In addition, they can promote the correct maturation of the innate immune cells to make them better antigen-presenting cells (APCs) for the adaptive immune system. Thus, MPGs can also modulate the adaptive immune responses, for example by blocking B cell and antibody responses (Dertli et al., 2013) or by eliciting the clonal expansion of CD4+ T-cell populations (Mazmanian & Kasper, 2006).

1.4.2. Potential therapeutic applications of microbial polysaccharides

According to the World Health Organization, the term "probiotics" stand for live, beneficial, non-pathogenic bacteria that provide health benefits to the host when administered in sufficient amount. The history of probiotics is quite old. In 1899, Tissier from the Pasteur Institute was the first to mention the role of a specific microorganism in relieving diarrhea. In 1917, Alfred Nissle used a subspecies of *E. coli* to treat shigellosis (Sonnenborn, 2016). The most important prerequisites for becoming a potential probiotic are: to survive in low pH and enzyme-enriched environments, epithelium adhesion for host-probiotic interactions, competition with pathogenic microorganisms and, last but not least, safety. Additionally, probiotic properties contribute to the beneficial effects on host health and disease prevention and/or amelioration. It has been suggested that selected cell components, including capsular polysaccharides (CPS), may be involved in several effects elicited by probiotics (Cicenia et al., 2014) (J. E. Aguilar-Toalá et al., 2018). These bacterial cell components could be considered as postbiotics. Postbiotics are considered as inactivated probiotics, namely metabolites or any released bacterial molecule capable of conferring, directly or in an indirect way, beneficial effects to the host (José Eleazar Aguilar-Toalá et al., 2021). Since they not include living microorganisms, the risks associated with the use of postbiotics in human nutrition are lower than those resulting from the use of probiotics. Lastly, it could be much easier to add postbiotics to other foods as milk infant formula ((Vieira, Fukumori, & Ferreira, 2016) (Żółkiewicz, Marzec, Ruszczyński, & Feleszko, 2020). Thus, polysaccharides secreted by bacteria can potentially be utilized as postbiotics to restore beneficial gut microbiota composition and to consequently fix metabolic and immune host disorders (Khan, R., Shah, M.D., et al. 2022). Indeed, polysaccharides from beneficial bacteria can promote the correct growth and maturation of both immune system and gut of the host. For example, a study found that an EPS produced by *L. plantarum* was able to promote the intestinal homeostasis by modulating the intestinal stem cells proliferation and differentiation, and by altering the structure of the gut microbiota (Xingtao Zhou et al., 2021). Additionally, some EPSs produced by commensals can be metabolized by some other commensals, promoting the growth of health-promoting members of the gut community (Hongpattarakere, Cherntong, Wichienchot, Kolida, & Rastall, 2012). On the

contrary, other microbial polysaccharides can exhibit an antimicrobial activity against a variety of bacterial pathogens, for example by interfering with their biofilm formation, efflux pump, membrane and nucleic acid synthesis (Z. Wang et al., 2021).

Moreover, polysaccharides on the bacterial cell surface are highly conserved and accessible polymers, so they may be excellent immunological targets. It has already been demonstrated that microbial polysaccharides can induce the host's immune response at various levels. For example, a study revealed that an isolated unconjugated α-1,4/β-1,4-GlcNAc-modified WTA was able to induce a high anti-WTA IgG response, that in turns reduces susceptibility to systemic *S. aureus* infection in a murine intradermal infection model (Rob van Dalen, Andreas Peschel, & Nina M. van Sorge, 2020). Consequently, microbial polysaccharides have been extensively studied as antigens for the development of glycoconjugate vaccines (Rohokale & Guo, 2023). These last one are composed by a bacterial polysaccharide covalently linked to a protein. Most polysaccharides are not good vaccine candidates because, on their own, they are unable to interact with the receptors on T cells of the human acquired immunity (Rappuoli, 2018). T cells are responsible for the correct antibody maturation and production of B lymphocytes with immune memory. However, through peptides derived from the processing of protein covalently linked to polysaccharide, T cells are engaged and stimulated (Rappuoli & De Gregorio, 2011).

1.5. Lactobacilli

Lactobacilli are Gram-positive, non-spore forming rods or coccobacilli, usually non-motile bacteria of the family Lactobacillaceae (Tannock, 2004). *Lactobacillus* is the largest genus within the group of lactic acid bacteria (LAB), that to date contains 166 species (De Angelis & Gobbetti, 2011). LAB are widespread in nature, especially in conditions of high concentrations of soluble carbohydrate, protein breakdown products, vitamins and a low oxygen tension. Consequently, they are common in milk and dairy products, other fermented foods (meats, vegetables, breads), intact and rotting vegetable material, silage, and intestinal tracts and mucous membranes of humans and animals (Aguirre & Collins, 1993). Hence, various species of this genera are used in industry for the production of foods that require lactic acid fermentation, notably dairy products, but also vegetables, beverages and some sausages. Lactobacilli are also known for their ability to produce lactic acid as a by-product of glucose metabolism. The amount of lactic acid produced varies. In several species, including *L. casei*, and *L. plantarum*, glucose metabolism is described as homofermentative, since lactic acid is the primary byproduct. In other species, such as *L. brevis*, glucose metabolism is heterofermentative, because lactic represents the 50% of metabolic byproducts while ethanol, acetic acid, and carbon dioxide are the other 50%. Lactobacilli can survive in both aerobic and anaerobic environments. They are commensals of animal and human mouth, vagina and gastrointestinal tract. Usually, commercial preparations of lactobacilli are used as probiotics to restore normal flora after dysbiosis caused by antibiotic therapy.

The general utility of the Lactobacillus species is related to their GRAS (generally recognized as safe) status. The two most relevant beneficial roles of lactobacilli are as starter cultures (to produce acid rapidly) and as probiotic cultures. Probiotics, particularly Lactobacillus species, are used to improve gut health, mainly through an improvement of the microecology of the gut and the synthesis of antibacterial substances. Moreover, the probiotic lactobacilli may also decrease the occurrence of infections by enhancement of immune function.

1.5.1. *Lactobacillus reuteri*

The polysaccharides from *L. reuteri* were studied in a frame of collaboration with Prof. Sin Hyeog Im research group from Pohang University of Science and Technology, which gave us the raw extract from this strain. Specifically, *L. reuteri* is a Gram-positive bacterium, belonging to the Lactobacillaceae family, that colonizes a large number of mammals. In humans, *L. reuteri* is found in different body sites, including the gastrointestinal and the urinary tracts, skin, and breast milk. The abundance of this bacterium varies among different individuals. Several beneficial effects to the host together with safety and tolerance proven by many clinical studies, make *L. reuteri* a well-studied probiotic bacterium. Among the benefits, it can produce antimicrobial molecules that inhibit the colonization of pathogenic microbes and remodel the commensal microbiota composition in the host. In addition, *L. reuteri* can benefit the host immune system, for instance decreasing the production of pro-inflammatory cytokines and promoting regulatory T cell development and function. Finally, showing the ability to strengthen the human intestinal barrier, the colonization of *L. reuteri* may decrease the microbial translocation from the gut lumen to the tissues. This type of translocation may be linked to a beginning of inflammation. Consistently, the decrease in the abundance of *L. reuteri* in humans in the past decades is linked to an increase of inflammatory diseases within the same period (Mu, Tavella, & Luo, 2018; Qin et al., 2010). The antimicrobial and immunomodulatory effects of the bacterium are linked to its metabolite production profile. For example, most *L. reuteri* strains are able to produce and secrete reuterin, a well-known antimicrobial compound (Talarico, Casas, Chung, & Dobrogosz, 1988). Moreover, the EPS produced by *L. reuteri* is important for biofilm formation, that can help its adhesion to the human intestinal epithelial cells (Salas-Jara, Ilabaca, Vega, & García, 2016) to the detriment of the adhesion of other, potentially pathogenic, microorganisms (Kšonžeková et al., 2016). More importantly, EPS-mediated blocking of adhesion also suppresses gene expression of proinflammatory cytokines, including IL-1β and IL-6, triggered by pathogens (Mu et al., 2018). Lastly, EPS from some specific strain of *L. reuteri* is required for the *L. reuteri*-mediated induction of Treg cells, highlighting its importance in the bacterium immunomodulatory activity (Sims et al., 2011).

1.5.2. *Lactobacillus rhamnosus GG*

L. rhamnosus GG (ATCC 53103) polysaccharide was studied in a frame of a collaboration with Prof. Roberto Canani's research group from CEINGE-Biotecnologie Avanzate of Naples, which gave us the starting material from that the bacterium was isolated, and performed

the related immunological assays described in the following chapters. Specifically, *L. rhamnosus* GG is a strain of *L. rhamnosus* isolated in 1983 by Sherwood Gorbach and Barry Goldin (from which 'GG' derives the suffix "GG"), from the intestinal tract of healthy humans (Silva, Jacobus, Deneke, & Gorbach, 1987). The term "ATCC 53103" indicates the number of the American Type Culture Collection. *L. rhamnosus* is a short, Gram-positive, homofermentative, facultative anaerobic and non-spore-forming and rod bacterium, that often appears in chains. While it is able to survive into the acidic and harsh environments of the stomach and intestine to colonize the digestive tract and balance intestinal microbiota, evidences suggests that *L. rhamnosus*, differently from the other probiotic lactobacilli, is only a transient inhabitant of the human gut (*Chapter 1 - Basic Biology of Oral Microbes*, 2015; J. Walter, 2008). Anyway, it is able to bind to the gut mucosa (Ardita et al., 2014) and all these features make it one of the most well-studied probiotic supplements for the treatment of several human diseases. Thus, some strains of *L. rhamnosus* are widely used as probiotics to restore, for example, the commensal microflora during an active infection (de Vrese, Laue, Papazova, Petricevic, & Schrezenmeir, 2019). Moreover, it is also used in the fermentation of different dairy products, such as milk. In this context, *L. rhamnosus* supplementation on cow's milk has been proposed for allergy prevention and treatment. Several preclinical and clinical evidences suggest that it may be helpful in promoting gastrointestinal symptoms resolution and immune tolerance acquisition in children with cow's milk allergy, which represents one of the most common food allergies in early childhood (Flom & Sicherer, 2019) (Thang, Baurhoo, Boye, Simpson, & Zhao, 2011) (Basturk, Isik, Atalay, & Yılmaz, 2020) (Tan, Zhou, Li, Lu, & Qiu, 2021).

1.5.3. *Lacticaseibacillus paracasei*

Also *L. paracasei* CBA L74 polysaccharides were studied in a frame of a collaboration with Prof. Roberto Canani's research group, which gave us the commercial milk powder fermented with this bacterium in a first time, and the freeze-dried bacterium alone in a second time. The latter was grown in a different medium, the MRS broth. Finally, the polysaccharides were extracted from the bacterium grown in these two different matrix, and their NMR profiles were compared to see if there may be differences in their nature and chemical structure. *L. paracasei* is a gram-positive, homofermentative species of lactic acid bacteria commonly used in dairy product fermentation and as probiotic cultures. The Lactobacillus casei group of bacteria, consisting of the closely related *L. casei*, *L. paracasei*, *L. rhamnosus* and *L. zeae* are among the most studied lactobacilli due to their commercial, industrial, and health potential (Sun et al., 2015). *L. paracasei* strains have been isolated from several different environments, including dairy products, plants, and from the human and animal gastrointestinal tracts (Smokvina et al., 2013). The fermentation of dairy products with lactobacilli is considered an advantage for the human health, making these products (such as fermented milk–based infant formulas) useful strategy against pediatric infections. The efficacy of these fermented foods is believed to be strain-specific and dose-dependent (Granier, Goulet, & Hoarau, 2013). The *L. paracasei* positive effects on human

health were demonstrated by different clinical studies. For example, it is discovered that dietary supplementation with cow's milk or rice fermented with *L. paracasei* CBA L74 prevents common infection diseases in children. The supposed mechanism behind this effect is a stimulation and regulation of the infant innate and acquired immunity through a direct interaction with the enterocytes (Paparo et al., 2018) (Nocerino et al., 2017) (Berni Canani et al., 2017). Moreover, despite studies to date have not been conclusive, different investigations have shown that lactobacilli may have a potential role also in the prevention and treatment of some type of allergies, such as the atopic dermatitis. For instance, a study analyzed the association between the consumption of fermented dairy products and the development of allergy and allergic sensitization in Japanese students, highlighting a significant reduction in allergy development among the students consuming fermented milk (Enomoto, Shimizu, & Shimazu, 2006).

1.6. *Bacillus subtilis*

Polysaccharides from *B. subtilis* 168 were studied in collaboration with Prof. Lipka Volker's research group from Georg-August Universitat, which gave us the raw extract from this bacterium and investigated the immunological activities of the isolated and purified products. *B. subtilis* is a Gram-positive, obligate aerobic bacterium with a road shape and flagella. Its ability to form a protective endospore allows it to survive in extreme environmental situations. This bacterium is also known as hay or pasture bacillus because of it inhabits the soil and contributes to plant microbioma. Indeed, it is one of the most widely used and studied plant-growth promoting rizhobacteria and a highly promising candidate for agricultural applications. *B. subtilis* is able to promote plant growth as well as control plant pathogens through diverse mechanisms, including the improvement of nutrient availability and alteration of phytohormone homeostasis as well as the production of antimicrobials and triggering induced systemic resistance, respectively (Blake, Christensen, & Kovács Á, 2021). Next to direct inhibition of pathogens, *B. subtilis* is able to boost plant defences by eliciting its induced systemic resistance, in which inoculation of the roots with beneficial bacteria enhances the defence capacity of the entire plant against various pathogens (Kloepper & Schroth, 1981). On the other hand, as for the root colonization, another study observed that *B. subtilis* strain RR4 suppresses various immune-related genes at the beginning of its colonization, to promote this process, while it induces defence responses gradually, at a later stage, to boost plant immunity (Rekha, Kumar, Ilango, Rex, & Usha, 2018). Therefore, like other bacteria, *B. subtilis* can exert an immunomodulatory activity on the host plant (pro or anti-inflammatory), depending on its survival needs. Even though its benefits for crop production have been extensively recognized, the success of its application often fails because the bacterium is not able to persist in the rhizosphere. Bacterial colonization of plant roots is a crucial step in the interaction between microbe and plant and seems, therefore, to be of great importance for its growth promotion and biocontrol effects. A successful root colonization depends on both bacterial components and motility, as well as on a signal interplay with the plant.

1.7. *Ruminococcus gnavus*

The cells of *R. gnavus* ATCC 29149 and E1 strains were gave us by Prof. Nathalie Juge's research team from Quadram Institute Bioscience, in a frame of a collaboration where they provided us the entire immunological data, described in the following paragraphs. Regarding *R. gnavus*, it is a strict anaerobic Gram-positive bacterium which belongs to the Clostridium XIVa cluster (C. Liu, Finegold, Song, & Lawson, 2008) (Togo et al., 2018). It is an early coloniser of the infant gut (Sagheddu, Patrone, Miragoli, Puglisi, & Morelli, 2016), which persists during the adulthood, where it is one of the common 57 species present in ≥90% of individuals at around 0.1% abundance (Kraal, Abubucker, Kota, Fischbach, & Mitreva, 2014). Different metagenomics studies showed that *R. gnavus* abundance in the gastrointestinal tract varies depending on the health conditions of the host (Crost, Coletto, Bell, & Juge, 2023). For instance, there is an enrichment of this bacterium in patients with inflammatory bowel disease (IBD) with respect to healthy individuals (S. Liu, Zhao, Lan, & Mou, 2021). Anyway, only specific clades of *R. gnavus* strains that live in humans are enriched in IBD patients (Hall et al., 2017). This evidence suggests that the effects of *R. gnavus* on the host immune response are likely to be strain-specific. Indeed, supplementation of humanised microbiota mice with *R. gnavus* ATCC 29149, the type-strain of this species, enhanced the expression of Reg3γ (Surana & Kasper, 2017), an antimicrobial peptide expressed by intestinal epithelial cells, which plays a pivotal role in maintaining gut homeostasis (Vaishnava et al., 2011). In addition, it has been seen that *R. gnavus* ATCC 29149 has an anti-inflammatory effect in mouse models of colitis (Grabinger et al., 2019). This anti-inflammatory activity has been attributed to *R. gnavus* cell-surface polysaccharides (Henke et al., 2021). In particular, *R. gnavus* type strain ATCC 29149 produces an EPS constituted by a trisaccharide rhamnose (Rha) backbone substituted with a sidechain made by two glucose, linked in positions α-1,6. This polysaccharide has been shown to have pro-inflammatory properties in vitro, as it induces the secretion of TNF-α (an inflammatory cytokine) involved into the binding to toll-like receptor 4 (TLR4) (Henke et al., 2019). Moreover, it has been also proven that the synthesised pentasaccharide repeat of the glucorhamnan is able to induce an immune response in vitro by releasing inflammatory cytokines such as TNF-α and IL-6 from bone marrow-derived dendritic cells (BMDCs) through TLR4 receptor recognition (Haynie et al., 2021).

1.8. *Enterococcus faecium*

The pure capsular polysaccharide of *E. faecium* U0317 strain was gave us by Dr. Luis Felipe Romero Saavedra's research team from Ludwig Maximilians University, with the aim to structurally characterize it. After that, the team conjugated the aforementioned CPS with a carrier protein and studied its immunogenic potential in mouse models. Specifically, *E. faecium* is a Gram-positive, opportunistic pathogen, belonging to the genus Enterococcus (Devriese, Baele, & Butaye, 2006). This genus was first discovered in 1899 in human fecal flora (Xuewei Zhou, Willems, Friedrich, Rossen, & Bathoorn, 2020), and is comprised into the group of LAB. Thus, *E. faecium* can be commensal in the human and animal GI tract,

representing a potential probiotic for the reduction of GI diseases. Indeed, in some instances, this bacterium can hinder the colonization of the host organism by pathogenic microbes (Hanchi, Mottawea, Sebei, & Hammami, 2018) as demonstrated by the fact that a specific strain of *E. faecium* is currently used as probiotic in animal feed, to avoid the addition of antibiotics to livestock feed, and the risk of the onset of antibiotic resistance (Bednorz et al., 2013). Anyway, the constant exposure to high levels of this microbe leads to immunosuppression, by reducing expression of IL-8, IL-10, and CD86, predisposing the livestock to acute infections (Siepert et al., 2014). Actually, unlike other LAB genera, Enterococcus has not yet obtained the GRAS status (Hanchi et al., 2018). The term "GRAS" is an acronym to indicate any substance "Generally Recognized As Safe" under the conditions of its intended use (sections 201(s) and 409 of the Federal Food, Drug, and Cosmetic Act). For these reasons, before adding an Enterococcus strain as probiotic in a functional food, there must be assessed its safety (Nascimento, Casarotti, Todorov, & Penna, 2019). Otherwise, early in its evolution, *E. faecium* acquired characteristics that allowed it to become, in the past two decades, a worldwide cause of nosocomial infections, particularly urinary tract, bloodstream, endocardium, and surgical sites, especially among immunocompromised patients (Agudelo Higuita & Huycke, 2014). The pathogenic potential of enterococci is linked to their resistance to several antibiotics, including vancomycin, and their ability to survive to several stressors and to prosper in harsh environments, including those of extreme temperature, pH and high osmolarity. This abilities are also partly mediated by their polysaccharides (Ramos, Sansone, & Morales, 2021) but, until now, only few polysaccharides from *E. faecium* strains have been isolated and their structures identified, with limited focus on immunological studies (Kodali et al., 2015) (Z. Zhou, Ding, Li, & Wu, 2017). Thus, the discovery of novel polysaccharides that enable *E. faecium* to resist opsonophagocytosis and could therefore be used as potential vaccine antigens is actually an important matter of research.

1.9. Aim of the thesis

The overarching goal of this Ph.D. thesis is to structurally characterize bacterial glycans from different human and plant sources, contributing to better understand the roles of these polysaccharides in microbiota-immune system interactions. Understanding how they can modulate the host immune system is of fundamental importance to refine targets of microbial manipulation and reduce uses of chemicals and antimicrobial agents in human medicine and agricultural field. In particular, this work focus on cell-membrane related glycans of: *Lactobacillus reuteri; Lactobacillus rhamnosus* GG ATCC 53103*; Lacticaseibacillus paracasei* CBA L74*; Bacillus subtilis* 168*; Ruminococcus gnavus* ATCC 35913*; Enterococcus faecium* U0317.

Chapter 2

Results and discussion

2.1. Structural characterization of *Lactobacillus reuteri* glycans

Glycans isolation was performed by Prof. Sin-Hyeog Im's research group form Pohang University of Science and Technology. Precisely, they detached the capsular material from *L. reuteri* cells by sonication, precipitated the supernatant with ethanol, and resuspended the solid in TRIS buffer to carry on enzymatic treatment to remove protein and nucleic acids. After that, I repeatedly purified the cell-wall components of *L. reuteri* by size-exclusion and anionic-exchange chromatographic techniques, and I was finally able to identify by NMR spectroscopy and GLC-MS analysis: wall- and lipo-teichoic (WTA and LTA, respectively) acids and two capsular polysaccharides (CPS).

2.1.1. Teichoic acids purification

The teichoic acids from *L. reuteri* were purified by anion-exchange chromatography on Q-sepharose® Fast Flow, using an increasing molarity of NaCl for the elution. After that, each obtained fraction was desalted on BioGel® P-10 resin, eluted in water with a flow rate of 12 mL/h. Thus, the fractions were finally separated according to chromatograms obtained through a refractive index detector connected at the end of the column and were analysed by ^{1}H NMR spectroscopy. The proton spectra of the various fractions showed that the teichoic acids were eluted with NaCl 400 mM, 700 mM and 1 M (Fig. 5) and the cleanest fractions were those eluted with 400 mM NaCl (D3 + D4, Fig. 5), pooled together, leading to a final yield of 20% (3.51 mg : 17.3 mg of purified glycans/crude product). Lastly, they were characterized by GC-MS and 2D NMR spectroscopy.

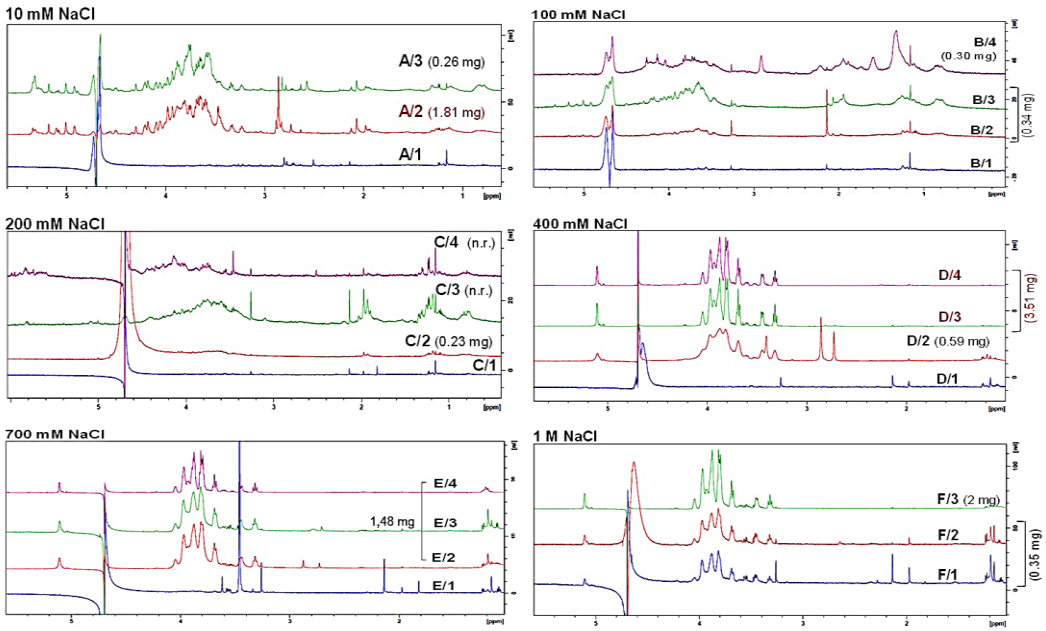

Figure 5. Proton spectra (600 MHz, 298 K, D_2O) of several chromatographic fractions. Each panel contains the fractions collected by desalting the eluate of the ion exchange chromatography obtained with a specific ionic strength. The amount of each sample is indicated next to the profile.

2.1.2. Teichoic acids compositional analysis

Monosaccharide analysis as acetylated O-methyl glycosides (MGA) was performed on the intact sample and also after dephosphorylation by HF treatment. Normally teichoic acids are poorly detected as MGA because methanolysis is unable to completely cleave the phosphodiester linkages between glycerol or ribitol molecules. Hence, the analysis was repeated by dephosphorylating the sample with aqueous HF before methanolysis and acetylation, and the relative amount of the glycerol (Gro) increased (Fig. 6, panel B), confirming the presence of teichoic acids (Garcia-Vello et al., 2020). In conclusion, glucose, galactose and glycerol were detected as the major sugar components of the sample, while ribose and the fatty acid 16:0 are present in smaller percentages and derive from nucleic acids and cell membrane lipid components, as demonstrated by following 2D NMR spectroscopic studies.

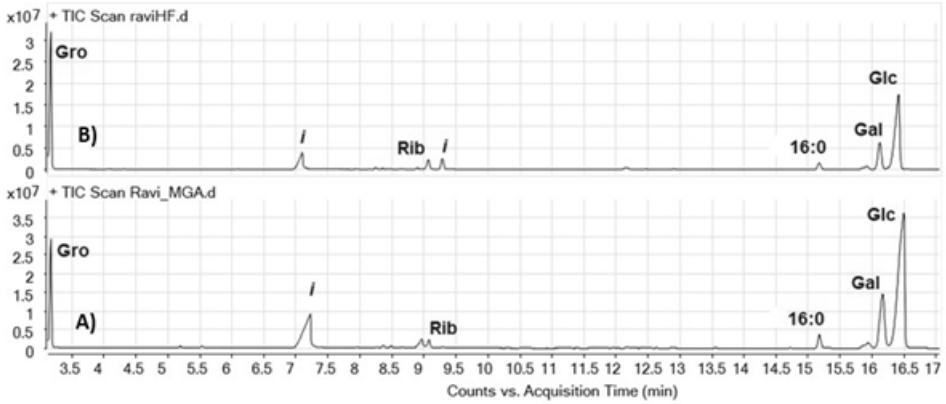

Figure 6. GC-MS compositional analysis of *L. reuteri* sample: A) without or B) with HF pretreatment to remove phosphate groups. In both panels, "*i*" stands for impurities.

2.1.3. NMR analysis of the *L. reuteri* teichoic acids

The structure of the teichoic acids was determined by analysing $^{1}H,^{1}H$ homo- and $^{1}H,^{13}C$ heteronuclear 2D NMR experiments, recorded by dissolving the glycans in D_2O. $^{1}H,^{1}H$ COSY and $^{1}H,^{1}H$ TOCSY experiments were used to disclose the protons of each spin system, while carbon atoms were identified through $^{1}H,^{13}C$ HSQC. The HSQC spectrum presents three anomeric signals between 5.2-5.1 ppm, that were labelled with a capital letter (A,B,C, Tab. 1, Fig. 7). Finally, the repeating unit sequence was inferred by analysis of long-range dipolar and scalar correlations from $^{1}H,^{13}C$ HMBC spectrum.

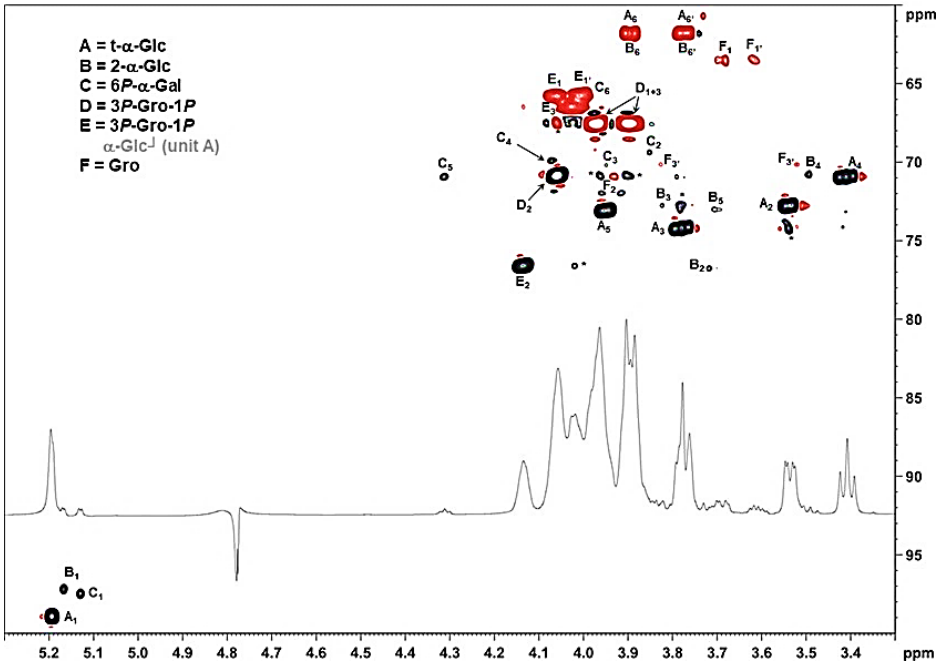

Figure 7. Expansion of HSQC spectrum (600 MHz, 298 K) of *L. reuteri* teichoic acids. Red densities correspond to -CH_2 groups. Letters refer to carbohydrate residues as defined in Tab. 1. Arabic numerals refer to the proton/carbon atoms in the respective residues.

Table 1. NMR chemical shifts of the *L. reuteri* teichoic acids, measured at 600 MHz, 298 K, in D_2O.

Residue	1	2	3	4	5	6
A	5.20	3.54	3.78	3.41	3.95	3.89;3.77
t-α-Glc*p*	*99.0*	*72.7*	*74.2*	*71.0*	*73.1*	*61.8*
B	5.17	3.71	3.82	3.49	3.69	3.89;3.77
2-α-Glc*p*	*97.2*	*76.7*	*72.8*	*70.8*	*73.0*	*61.8*
C	5.13	3.84	3.95	4.07	4.31	3.99 x 2
t-α-Gal6*P*	*97.5*	*69.3*	*70.2*	*69.9*	*70.9*	*65.5*
D	3.97;3.90	4.06	3.97;3.90			
P*-Gro-*P	*67.5*	*70.9*	*67.5*			
E*	4.06;4.01	4.14	4.03;4.03			
P*-(Glc*p*)-Gro-*P	*65.8*	*76.6*	*66.5*			
F*	3.69;3.60	3.94	3.83;3.61			
Gro	*63.6*	*72.0*	*70.1*			

* **E_3** and **E_1** can be exchanged.

NMR analysis started from H-1 of A (5.20 ppm) that displayed five correlations in the TOCSY spectrum (Fig. 8a), with that at 3.54 ppm in common with the COSY spectrum. Hence, this density was assigned to H-2, and by a similar approach H-3 (3.78 ppm), H-4 (3.41 ppm), H-

5 (3.95 ppm) and H-6,6' (3.89-3.77 ppm). The same approach was used to identify also signals B and C of lower intensity, so that some weaker TOCSY correlations do not appear in the spectrum. Anyway, the H-1 of B shows four correlations, up to the proton H-5, while the H-1 of C shows three correlations, up to the proton H-3. These information, along with the chemical shift values reported in literature (Speciale et al., 2022), led to identifying A and B as α-glucose residues and C as an α-galactose O-6 substituted with a phosphate group. The identification of the H-5 and H-6 of the residue C was possible through the HMBC spectrum. Moreover, the analysis of the HMBC spectrum (Fig. 8b) showed the connection of the anomeric proton of C with the signal at 76.7 ppm, identified as carbon 2 of the residue B. Finally, combination of COSY and HMBC allows to identified residues D, E and F as, respectively, a 2-linked 1,3-glycerol phosphate, a free linked 1,3-glycerol phosphate and a glycerol linked in position 1 or 3 (the C-1 and C-3 atoms are equivalent). Chemical shift values of these residues matched with those reported in literature (De Boer, Kruyssen, & Wouters, 1976) (Kozlova, Streshinskaya, Shashkov, Evtushenko, & Naumova, 1999). Since the ^{13}C value of the residue B is shifted to downfield (Tab. 1) in respect to the anomeric value of a reducing sugar, it denotes that it is linked in this position. Indeed, the HMBC spectrum confirm the B1-F3 correlation (Fig. 8b). Also, in the HMBC spectrum it can be found the A1E2 correlation, showing that the analysed sample contains a polyglycerol-phosphate not stoichiometrically substituted with a terminal α-glucose.

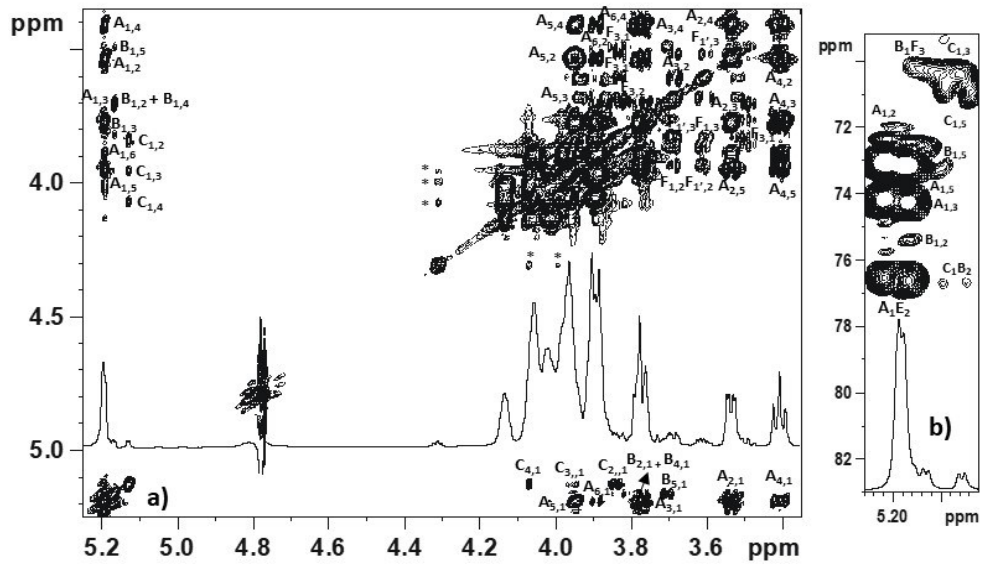

Figure 8. a) TOCSY spectrum (600 MHz, 315 K, D_2O) of the teichoic acids produced by *L. reuteri.* b) Expansion of the $^{1}H,^{13}C$ HMBC spectrum (600 MHz, 315 K, D_2O) of the teichoic acids produced by *L. reuteri*. Signals marked with (*) are due to minor impurities. In both panels, letters refer to carbohydrate residues as defined in Tab. 1, and arabic numerals to the atoms of the respective residues.

In conclusion, the main signals of the NMR spectra belong to the gro-type polymer, shown in Fig. 9a. The backbone of this polymer is made of polyglycerolphosphate, 1,3-linked (unit D); the position 2 of some of these Gro units (labelled E) is further substituted with a α-Glc (unit A). By integration of the D2 vs E2 densities in the HSQC spectrum (Fig. 7), it has been possible to evaluate the free-Gro vs the "linked Gro" ratio, that is 66%. The NMR spectra denoted the presence of other two monosaccharide, B and C, defined as a α-Glc and a α-Gal, respectively, linked together as shown in Fig. 9b, with the Gal unit further decorated at O-6 with a phosphodiester group, while the unit B is linked to a Gro unit (F). The search in the CSBD database of this small unit, disclosed that it exists in some bacteria (Werner Fischer, Laine, & Nakano, 1978), with some of the Lactobacillus genus (W. Fischer, Koch, Rösel, Fiedler, & Schmuck, 1980) (Shaw, Heatherington, & Baddiley, 1968). Here and in other bacteria, this unit seems located at the reducing terminal side of the teichoic acid chain, and its Gro unit (F) is further acylated with two fatty acids. In other words, this unit denotes the presence of a lipoteichoic acid, that in this case is missing the acyl units. Probably, this last one may have been lost during the extraction/purification procedures.

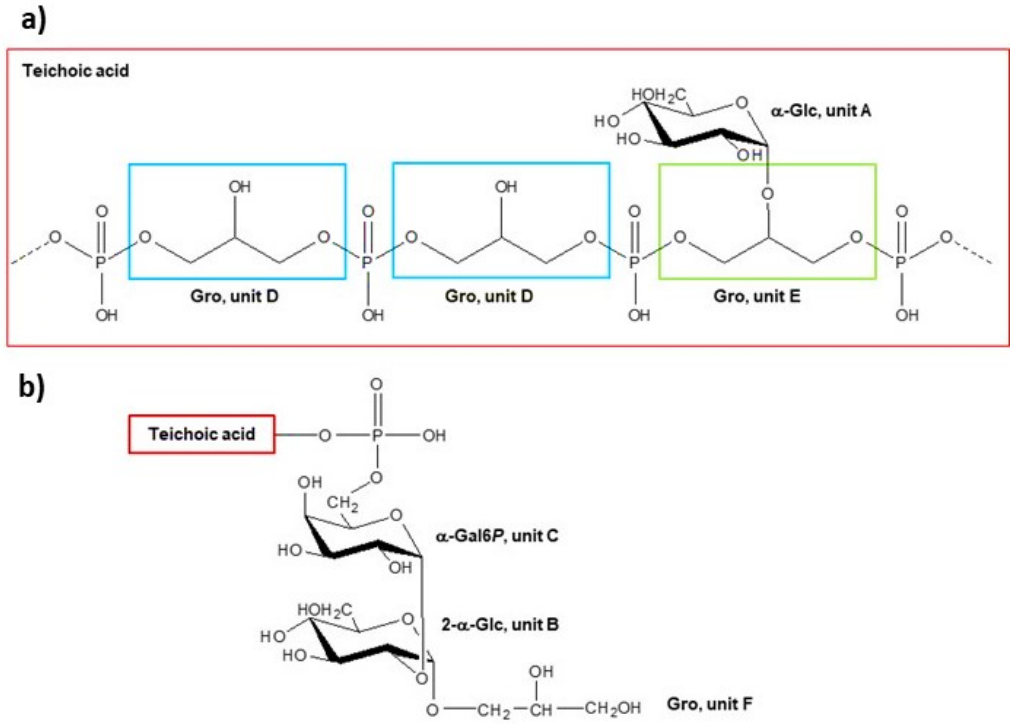

Figure 9. a) Model of the Gro-type teichoic acid found in this bacterium; b) second motif present in the NMR sample, probably the primer unit of a lipoteichoic acid.

2.1.4. Molecular weight evaluation of the *L. reuteri* teichoic acids

I performed the analysis by using the HPLC instrument equipped with a TSK-GPW5000 column, eluted in 50 mM ammonium bicarbonate at flow 0.8 mL/min. I calculated the molecular weight of the samples reported in Tab. 2, based on the calibration parameters of the column (Fig. 10), which gave the following equation: LogMW = -0,70Vr+10.8, with Vr = retention volume.

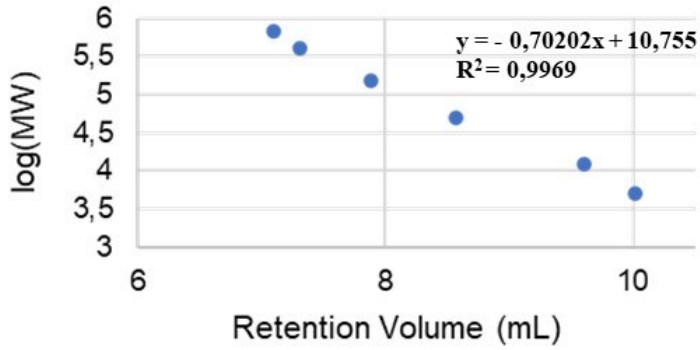

Figure 10. Calibration curve of TSK-GPW5000 column with different dextran standard of a known molecular weight, along with its equation. R^2 is an indicator between 0 and 1 that indicates the degree of correspondence between the estimated values for the trend line and the actual values. A trendline is most accurate when its R^2 value is equal to 1.

The idea that the motif C-B-F is the priming of the teichoic acid chain is reinforced and enriched through the data obtained by further separation of the fractions D2, E2+E3+E4, and F3, and the consequently evaluation of their MW. These three fractions present two components, baseline separated (Fig. 11), each with a certain MW (Tab. 2).

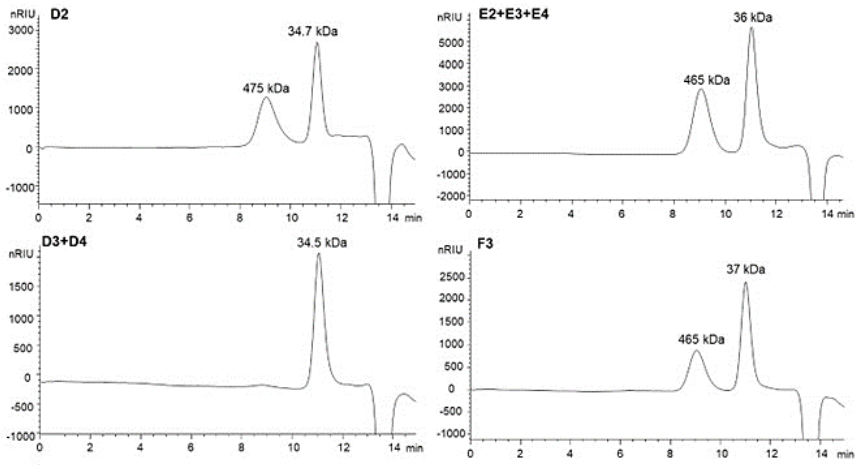

Figure 11. Chromatographic profiles of the several fractions of *L. reuteri* teichoic acids purified by a combination of ion exchange and size-exclusion chromatography, along with their reported MW.

Table 2. MW calculated for the different fractions.

Samples	tr (min)	Vr (mL)	Log (MW)	MW (Da)	MW (kDa)
Ravi/1/A2	9,024	7,2192	5,6868272	486213,727	486,2
	11,827	9,4616	4,112618	12960,38	13,0
Ravi/1/A3	9,109	7,2872	5,63909	435602	435,6
	12,411	9,9288	3,784634	6090,232	6,1
Ravi/1/D2	9,042	7,2336	5,676718	475026,8	475,0
	11,065	8,852	4,540569	34719,14	34,7
Ravi/1/D3+D4	11,071	8,8568	4,537199	34450,8	34,5
Ravi/1/F1+F2	11,154	8,9232	4,490585	30944,62	30,9
Ravi/1/F3	9,058	7,2464	5,667732	465299,2	465,3
	11,019	8,8152	4,566403	36847,1	36,8
Ravi/1/A2	9,024	7,2192	5,6868272	486213,727	486,2

Fractions D2, E2E3E4 and F3 were separated by size exclusion chromatography (Fig. 12), and analysed by ^{1}H NMR spectroscopy (Fig. 13). Summarizing, in the protonic profiles of fractions D2-B, D2-C, and D2-D it is possible to see how the anomeric peaks related to the unit B (5.17 ppm) and C (5.13 ppm) become more intense as their elution time is prolonged, namely from the first fraction D2-B to the last obtained fraction D2-D (Fig. 14a). In other words, the percentage of CBF motif increases as the elution time becomes greater (Fig. 14b), and this is in line with the hypothesis that LTAs have a lower MW in respect to the WTA, namely they are more retained in size-exclusion chromatography.

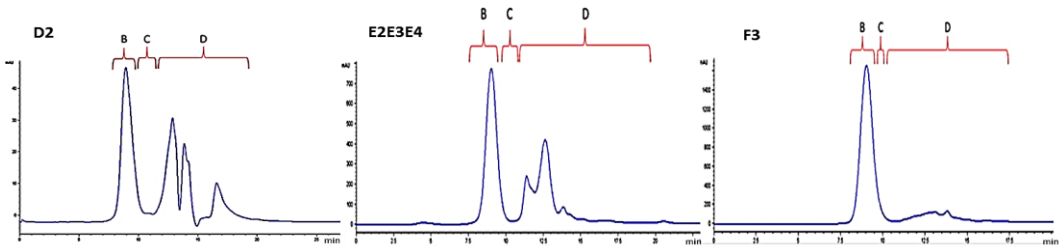

Figure 12. Chromatographic profiles observed for fractions D2, E2+E3+E4 and F3. The eluate was monitored by UV (206 nm) and each chromatogram reports how each fraction was collected.

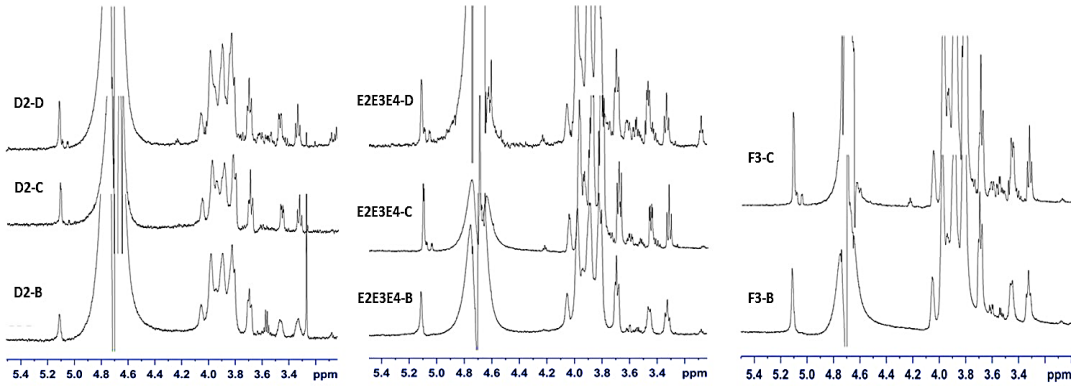

Figure 13. Proton spectra of the fraction D2, E2+E3+E4 and F3 after the additional purification by TSK-GPW5000.

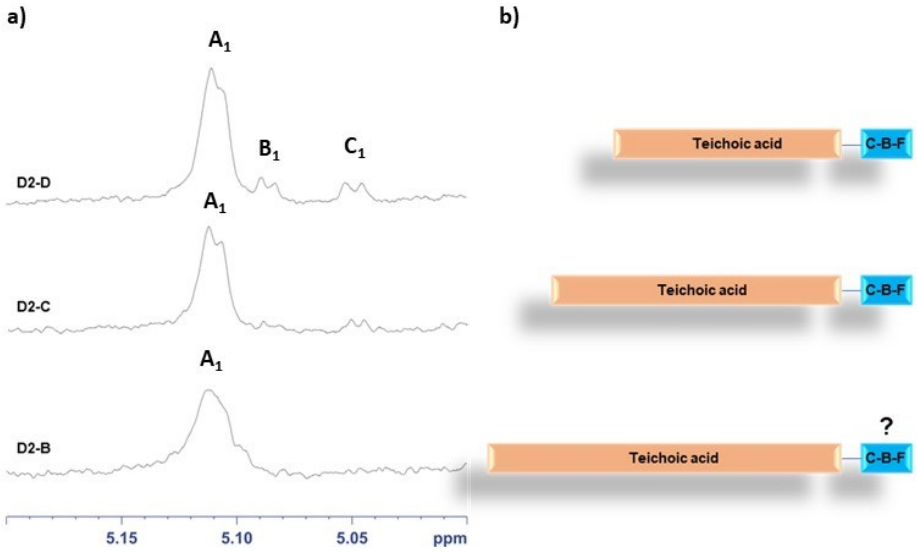

Figure 14. a) Expansion of the anomeric region of the three fractions D2-B, D2-C and D2-D obtained by purifying D2 on TSK-GPW5000. b) Qualitative model of the teichoic acid fraction, the pink area denotes the polyglycerol-phosphate backbone that is substituted with glucose (unit A), as depicted in Fig. 9a. The blue box instead is made of the units C-B-F.

2.1.5 Capsular polysaccharides purification

CPSs from *L. reuteri* were purified by an enzymatic hydrolysis of the crude sample in order to remove the nucleic acids and proteins, followed by a dialysis for the removal of salts present in the hydrolysis buffer. After that, the obtained product underwent to a size-exclusion chromatography on Sephacryl® S-300 HR, eluted in ammonium bicarbonate 50

mM. All the fractions were separated and collected according to the chromatogram given by the refractive-index detector connected to the column (Fig. 15).

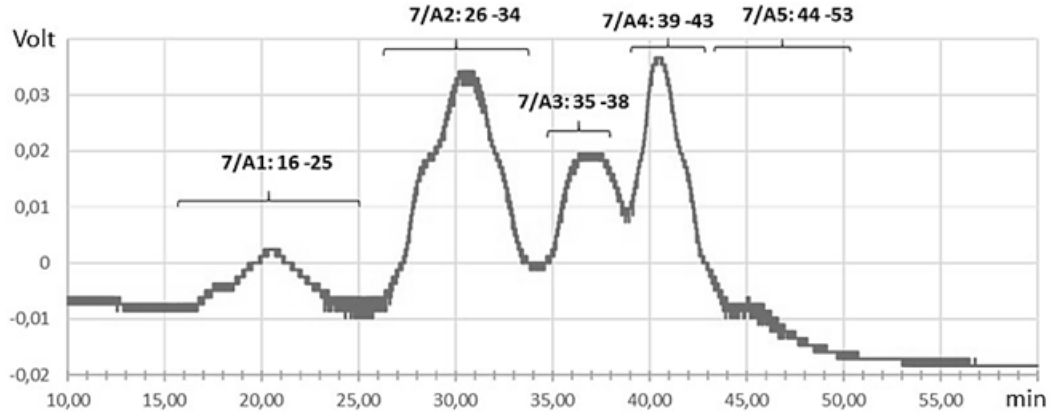

Figure 15. Chromatographic profile observed from size exclusion chromatography via Sephacryl® S-300 HR. The flow rate was set to 14 mL/h, and the eluate was monitored by RID signal (sensibility=5xe-3). The above chromatogram reports how each fraction was collected.

Each fraction was analysed by ^{1}H NMR spectroscopy, through which the purest fraction containing glycans was identified and further purified by an anion-exchange chromatography on Q-sepharose® Fast Flow, using an increasing gradient of NaCl for the elution. Next, each obtained fraction was desalted on BioGel® P-10 resin, eluted in water with a flow rate of 12 mL/h. Thus, the fractions were finally separated according to chromatograms obtained through a refractive index detector connected at the end of the column and were analysed by ^{1}H NMR spectroscopy (data not shown). The proton spectra of the various fractions revealed that the cleanest fraction containing glycans was the one eluted with NaCl 10 mM NaCl. This product was obtained with a yield of 0.94% (0.32 mg : 34 mg of purified glycans/crude product) and further characterize by GC-MS and 2D NMR spectroscopy.

2.1.6. Capsular polysaccharides substitutional pattern analysis

Monosaccharide linkages were investigated by deriving the sample (0.2 mg) into partially acetylated and methylated alditols (AAPM), and injecting them into GC-MS instrument (De Castro, Parrilli, Holst, & Molinaro, 2010). As sample, it was used one of the fractions of the crude product obtained during the chromatographic purifications, less clean in respect to the last fraction characterized by NMR analysis. The chromatogram (Fig. 16) evidenced, in term of sugars, the presence of a 3-substituted hexofuranose (3-Hex*f*), 4-Hex*p*, 3-Hex*p*, and

two different 6-Hex*p*, while 16:0 and 18:0 refer to lipids. The other unmarked (and small) peaks are impurities.

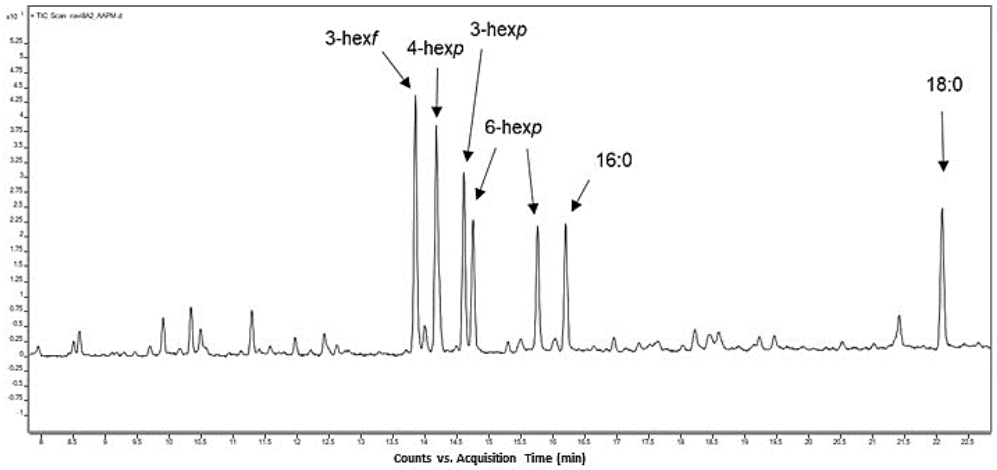

Figure 16. GC-MS substitution pattern analysis of a dirty fraction of *L. reuteri* sample, obtained during the various chromatographic purification procedures.

2.1.7. NMR analysis of the *L. reuteri* capsular polysaccharides

The structure of the *L. reuteri* CPSs was determined by analysing $^{1}H,^{1}H$ homo- and $^{1}H,^{13}C$ heteronuclear 2D NMR experiments, recorded by dissolving glycans in D_2O. $^{1}H,^{1}H$ COSY and $^{1}H,^{1}H$ TOCSY experiments were used to disclose the protons of each spin system, while carbon atoms were identified through $^{1}H,^{13}C$ HSQC and further confirmed by $^{1}H,^{13}C$ HSQC-TOCSY. Lastly, the primary sequence was inferred by analysis of inter-residue and long-range dipolar and scalar correlations from $^{1}H,^{1}H$ NOESY and $^{1}H,^{13}C$ HMBC spectra, respectively. The HSQC spectrum presents six anomeric signals between 5.3-4.5 ppm, that were labelled with a capital letter (A-F, Tab. 3, Fig. 17).

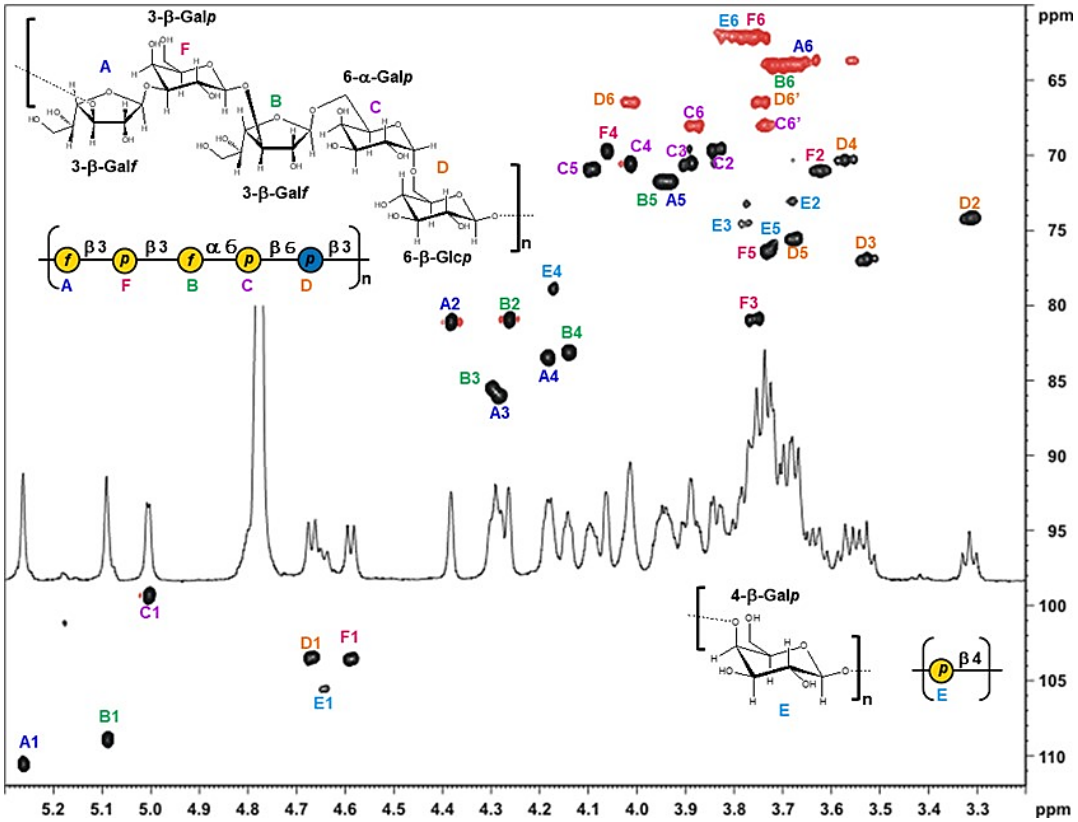

Figure 17. Expansion of HSQC spectrum (600 MHz, 298 K, D_2O) of *L. reuteri* capsular polysaccharides, with indication of their isolated structures. Red densities correspond to -CH_2 groups. Letters refer to carbohydrate residues as defined in Tab. 3, and drawn according to the SNFG. The letter "*p*" within the residues stands for pyran, while "*f*" stands for furan. Arabic numerals refer to the proton/carbon atoms in the respective residues.

Table 3. NMR chemical shifts of the *L. reuteri* CPSs, measured at 600 MHz, 298 K, in D_2O.

Residue	1	2	3	4	5	6
A	5.26	4.38	4.29	4.18	3.94	3.68 x 2
3-β-Gal*f*	*110.6*	*81.2*	*86.0*	*83.5*	*71.7*	*63.9*
B	5.09	4.26	4.30	4.14	3.96	3.70 x 2
3-β-Gal*f*	*108.9*	*80.9*	*85.6*	*83.2*	*71.7*	*63.9*
C	5.01	3.84	3.90	4.02	4.10	3.88;3.74
6-α-Gal*p*	*99.3*	*69.6*	*70.6*	*70.5*	*71.0*	*68.0*
D	4.67	3.31	3.53	3.57	3.68	4.02; 3.75
6-β-Glc*p*	*103.5*	*74.2*	*77.0*	*70.3*	*75.6*	*66.5*
E	4.64	3.68	3.78	4.17	3.70	3.78 x 2
4-β-Gal*p*	*105.5*	*73.0*	*74.6*	*78.9*	*75.9*	*62.1*
F	4.59	3.62	3.76	4.06	3.73	3.78 x 2
3-β-Gal*p*	*103.6*	*71.0*	*81.0*	*69.7*	*76.3*	*62.1*

NMR analysis started from residue A, whose anomeric proton (5.26 ppm) displays only three correlations in the TOCSY spectrum (Fig. 18b), typical of a galactose. Indeed, the comparison of the carbon chemical shift values read on the HSQC spectrum (Fig. 17) with those reported in literature, confirms that this residue is a 3-substituted galactofuranose β-configured at the anomeric centre (Speciale et al., 2022). The attribution of the proton and carbon atoms of the residue was completed by analysing the HMBC and the NOESY signals. In addition, these spectra also showed the linkage of the C-3 of A (86.0 ppm) to the C-1 of D and of the C-1 of A to the C-3 of F (81.0 ppm). Following the same approach, the residue B, C, E and F were identified as a 3-linked β-galactofuranose, 6-α-galactopyranose, 4-β-galactopyranose and a 3-β-galactopyranose, respectively. The anomeric configuration of the residues C, E, and F can also be counterchecked by their $^3J_{H1,H2}$ coupling constant values, that are 3.7, 7.8, and 7.5 Hz respectively. Moreover, the analysis of the HMBC and NOESY spectra reveals that: the residue B is linked in C-3 (85.6 ppm) with the C-1 of F (103.6 ppm) and at C-1 (108.9) to the C-6 of the unit C (68.0 ppm) ; the C-1 of the unit C (99.3 ppm) is linked to the C-6 of D (66.5 ppm), that is, in turn, linked to the C-3 of A (86.0 ppm). The anomeric proton of the residue D (4.67 ppm) displays five correlations in the TOCSY spectrum, because two of them overlap, while all the correlations between the other protons of the residue are clearly visible (Fig. 18b). This pattern is diagnostic of a *gluco*-configured sugar. Integration of the information of the TOCSY with those of the COSY spectrum led to the assignment of the chemical shifts of all the protons of this residue (Tab. 3). The comparison of the carbon chemical shift values read on the HSQC spectrum (Fig. 17) with those reported in literature confirms the unit D as a 6-linked glucose, β-galacto-configured at the anomeric center, as also confirmed by its $^3J_{H1,H2}$ coupling constant value, which is 7.9 Hz. The residue E is, instead, a separated glycan, named a β-1,4-galactopyranose, because in the NOESY spectrum (Fig. 18b) it is present the correlation $E_{1,4}$,

that is not possible appreciate in a single β-galactose molecule as H-1 and H-4 nuclei are not in the same orientation and, so, close in space. In addition, its anomeric signal in the protonic spectrum (4.64 ppm) has a lower intensity in respect to the rest of the anomeric signals present and it does not appear linked to any other characterized residue. So, the sample analysed contains a mixture of two different glycans, a glucogalactan and a galactan, respectively. By integration of the anomeric signals, it was possible to establish the relative proportions – in mols – between the two polysaccharides, that was 2:1, in favor of the glucogalactan. Moreover, by taking into account the MW of the repeating units of the two polysaccharides (810 g/mol for the glucogalactan, and 162 g/mol for the galactan), it has been possible to calculate the % by weight of each polymer in the mixture by using the following formula: % glucogalactan = [(810 x 2) / (810 x 2 + 162 x 1)] x 100 = 90.9. The spin system assignments of all residues and the sequence between the different residues was further confirmed by agree with the information from contained in the HSQC-TOCSY and NOESY spectra (Fig. 18a and 18b).

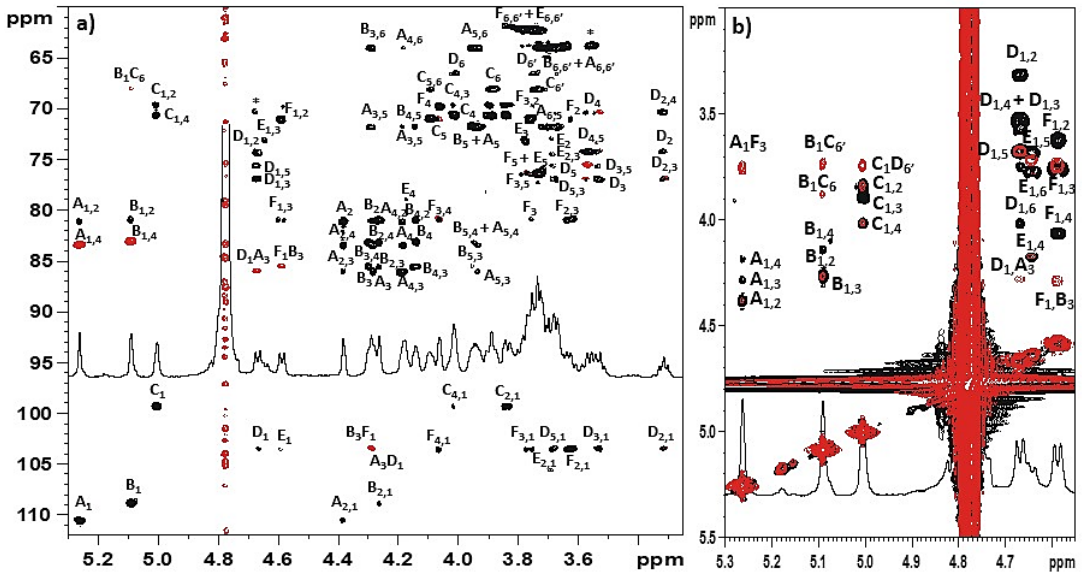

Figure 18. (600 MHz, 315 K, D_2O) a) Expansion of HMBC (red) and HSQC-TOCSY (black) of the *L. reuteri* CPSs. Signals marked with (*) are due to minor impurities. b) TOCSY spectrum in black overlapped to the NOESY spectrum in red of the CPSs produced by *L. reuteri*. In both panels, letters refer to carbohydrate residues as defined in Tab. 3, and arabic numerals to the atoms of the respective residues.

2.2. Structural characterization and immunomodulatory activity of *Lactobacillus rhamnosus* GG CPS

The growth of the bacterium, and the procedures of extraction, purification, structural characterization and MW evaluation of the CPS were done by myself, while the whole

immunomodulatory assays were performed by Prof. Canani's research team from CEINGE, respectively.

The powdered food supplement of *L. rhamnosus* GG (ATCC 53103) was resuspended in water and extracted by using n-butanol, a method conventionally adopted for the recovery of LTA, in case it is present (Vinogradov, Sadovskaya, Cornelissen, & van Sinderen, 2015a). Then cell debris was subjected to a harder extraction with trichloroacetic acid. After that, the crude product was purified by a combination of size-exclusion and ion-exchange chromatography, in order to separate CPS from WTA present in the same mixture. However, this procedure led to the isolation of CPS contaminated with starch, probably used as excipient in the commercial product. Thus, the bacterium was isolated from the commercial powder by centrifugation of the water suspension, and grown in MRS for 24 h. The biomass was recovered by centrifugation and then extracted heating the water suspension in autoclave (120 °C for 20'). The slurry was centrifuged giving an inactivated pellet and, in the supernatant, a crude polysaccharide (Fig. 19). Inactivation was verified by resuspending the pellet in MRS and adding it in different plates, at several decreasing concentration (starting from 10^{-1} to 10^{-7}). After 48 h at 37 °C, no bacterial growth was observed in any of the plates used. The "heat extraction" is a method generally adopted in this work to extract polysaccharides well anchored to the cellular membrane of Gram-positive bacteria. On the other hand, since the EPS are less anchored to the membrane and are released by bacteria into the external environment, the general practice to obtain them consists in precipitation from the growth medium with cold ethanol. Finally, the gained product was purified and characterized by NMR spectroscopy, through which we confirmed the structure already reported in literature (Landersjö, Yang, Huttunen, & Widmalm, 2002).

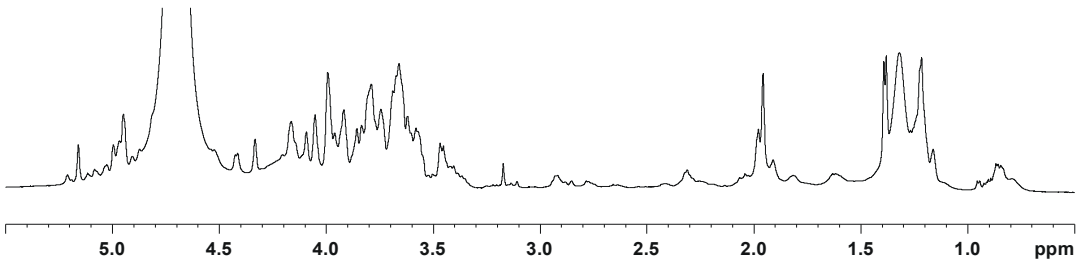

Figure 19. ^{1}H NMR profile (600 MHz, 298 K, D_2O) of the crude polysaccharide of *L. rhamnosus* obtained after autoclave heat treatment.

As for the immunomodulatory activity, it was observed that *L. rhamnosus* CPS is able to elicit a positive effect on differentiation and maturation of gut epithelium, increasing the expression of the main biomarkers, *lactase* and *Muc2,* respectively. Moreover, it was studied its interaction with peripheral blood mononuclear cells (PBMC) from children with a cow's milk allergy IgE-mediated (CMA children) and it was observed that this CPS was able to increase the expression of dendritic cell-associated (rDC) markers *Ifna2, Tgfb1 and Ptgs2*,

inducing the T-regs activation. This effect is consistent with a significant increase of the tolerogenic cytokine IL-10 and a decrease of the IL-4 and IL-3 production, resulting in a final reduction of the allergic response (Verma et al., 2018).

2.2.1 Purification of the CPS of *Lactobacillus rhamnosus* GG

CPS was purified by size-exclusion chromatography on Sephacryl® S-300 HR, eluted with NH_4CO_3 50 mM. The chromatographic profile was monitored by an on-line refractive index detector, and separated into four fractions (Fig. 20), all inspected by ^1H NMR spectroscopy (Fig. 21). The fraction eluted in the void volume (11/A) contained the capsule in pure form (yield 115 mg/$g_{dried\text{-}cells}$), while the spectra of the other fractions suggested the presence of complex mixtures of glycans with lipids and/or peptide-like molecules, hence they were not considered further.

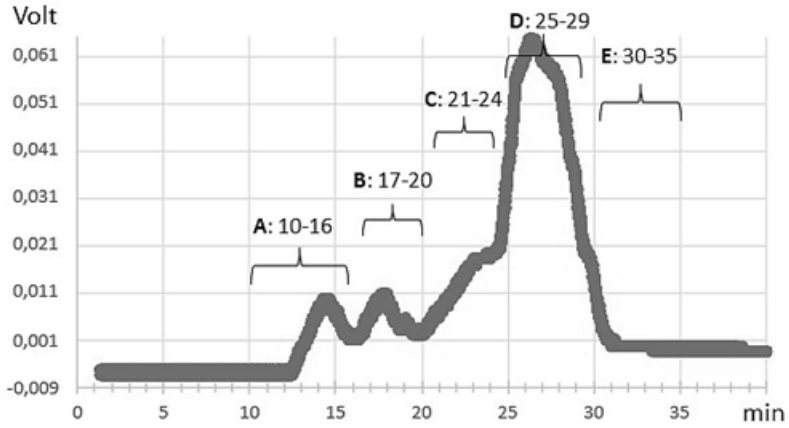

Figure 20. Chromatographic profile observed from size-exclusion chromatography via Sephacryl® S-300 HR. The flow rate was set to 14 mL/h, and the eluate was monitored by RID signal (sensibility=5xe-3). The above chromatogram reports how each fraction was collected.

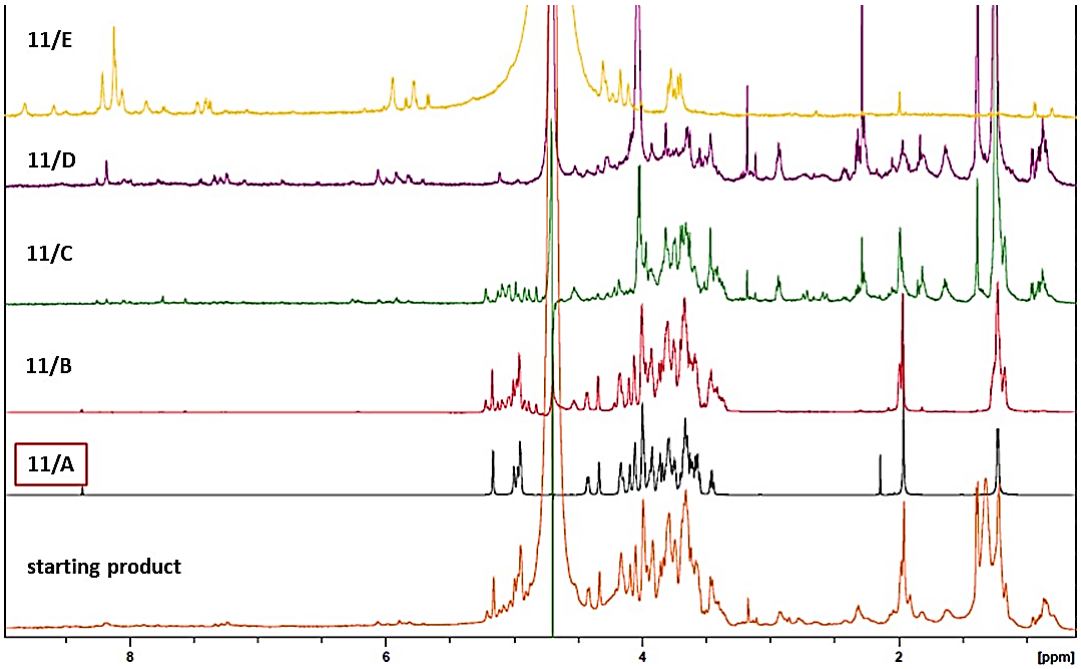

Figure 21. Proton spectra (600 MHz, 298 K, D_2O) of the fractions obtained after purification on Sephacryl® S-300 HR. The starting product is represented by the freeze-dried supernatant obtained after the heat treatment of the *L. rhamnosus* GG cells and centrifugation. The fraction 11/A contains the pure capsule, while the other fractions are a mixture of the CPS with impurities.

2.2.2 Structural characterization of *Lactobacillus rhamnosus* GG CPS

The polysaccharide structure was investigated by ^{1}H and $^{1}H,^{13}C$ HSQC (Fig. 22), where atoms chemical shifts have a tight match with those reported in literature (Landersjö et al., 2002). Hence, the repeating unit of this CPS consists of different units of galactose, both in the pyranose and furanose form, of a unit of glucosamine and another of rhamnose in the pyranose form (inset in Fig. 22).

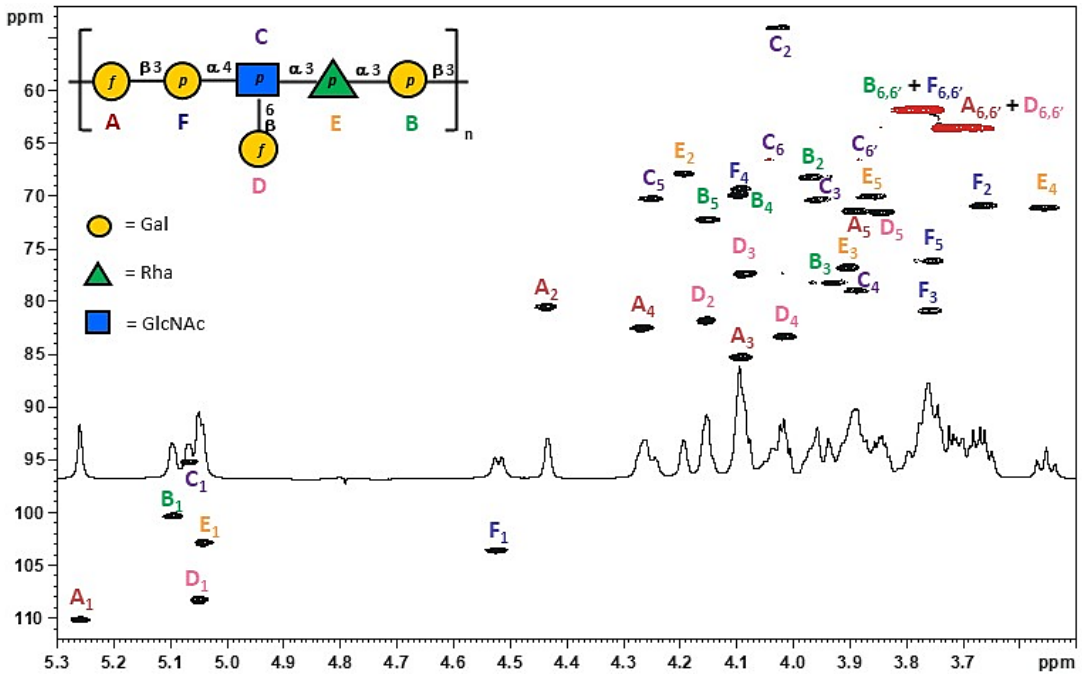

Figure 22. (600 MHz, 298 K, D_2O) HSQC spectrum of the capsular polysaccharide of *L. rhamnosus* along with its proton profile and structure. Letters refer to the carbohydrate residues as reported in figure, and drawn according to the SNFG. "*p*" and "*f*" stands for pyranosidic and furanosidic form, respectively. Arabic numerals refer to the proton/carbon atoms of the respective residue.

2.2.3 Molecular weight evaluation

The molecular weight determination was inferred by size-exclusion chromatography performed with TSK G-5000 PWXL, using NH_4HCO_3 50 mM as eluent (flow =0.8 mL/min) and monitoring the eluate with a refractive index detector, part of the HPLC system. The molecular weight of the samples reported in Tab. 4, was calculated based on the calibration parameters of the column (Fig. 23a), which gave the following equation: LogMW = -0,70Vr+11.1, with Vr = retention volume. The chromatographic profile of the compound consists on a single peak (Fig. 23b), denoting the purity of the obtained product.

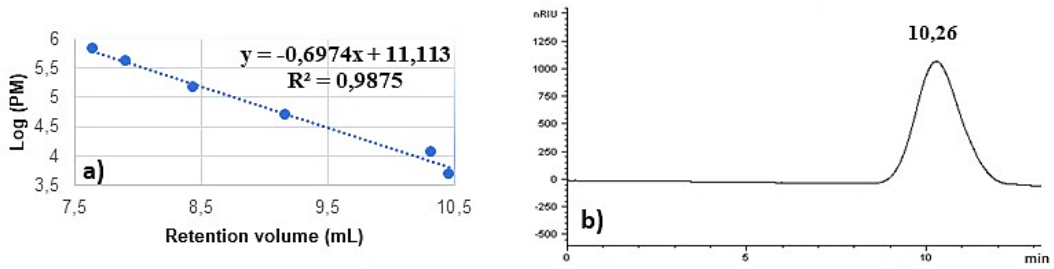

Figure 23. a) Calibration curve of TSK-GPW5000 column with different dextran standard of a known molecular weight, along with the line equation. R^2 indicates the degree of correspondence between the estimated values for the trend line and the actual values. A trendline is most accurate when its R^2 value is equal to 1. b) Chromatographic profile of *L. rhamnosus* CPS purified by size-exclusion chromatography.

Table 4. MW calculated for *L. rhamnosus* CPS.

Sample	tr (min)	Vr (mL)	Log (MW)	MW (Da)	MW (kDa)
LRGG/11/A	10,264	8,2112	5,38650912	243505,693	243,5

2.2.4 Effect on epithelial barrier

To evaluate the effects on human enterocytes differentiation, the gene expression levels of the main markers of mucus production (*Muc2*) and of enterocytes differentiation (*lactase*), were assessed. In this context, the activity of the inactivated *L. rhamnosus* (LGG), of its CPS and of ID35 were assessed. ID35 is a specific single-stranded oligodeoxynucleotides (ODNs) identified in the LGG genome (Iliev et al., 2005). Its activity is relevant in animal model of food allergy, because it promotes Th1 response and suppresses antigen-specific IgE production (Iliev et al., 2008). Thus, Caco-2 cells were incubated with CPS or ID35 or their combination or with inactivated LGG, for 48 h. After that, cells were processed for mRNA analysis by Real Time PCR and it was observed that the expression levels of *lactase* and *Muc2* were significantly increased (Fig. 24a and 24b). Moreover, it emerged that the combination of CPS + ID35 produced a better effect than using the component alone, for both gene expression.

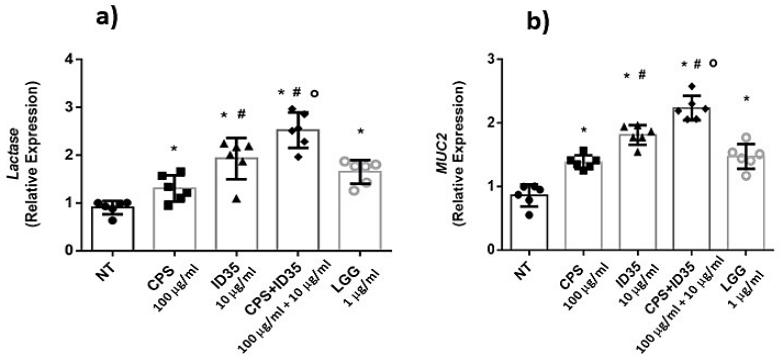

Figure 24. a) Influence of CPS (100 μg/ml), ID35 (10 μg/ml), CPS + ID35, and inactivated LGG (1 μg/ml) on lactase expression in human enterocytes. b) Influence of CPS, ID35, CPS + ID35, and inactivated LGG on Muc2 expression in human enterocytes. "NT" stands for "not-treated" cells. Real Time PCR analysis was performed using the comparative threshold cycle (CT) method. Gene expression was normalized against the expression of the reference gene glucuronidase beta (GUS-B). Data are expressed as means ± SD and were analyzed using paired t-test. *p<0.05 vs NT; #p<0.05 vs LGG; °p<0.05 vs CPS+ID35.

2.2.5 Effects of LGG components on Th2 cytokines response

To further assess the ability of CPS and ID35 in modulating immune tolerance, Th2 cytokines response, tolerogenic cytokine IL-10 production and the number of activated Tregs in PBMCs collected from four IgE-mediated CMA children were tested. The exposure of PBMCs to cow's milk allergen β-lactoglobulin (BLG) resulted in a significant increase of Th2 cytokine production: IL-4 (Fig. 25a), IL-13 (Fig. 25b) and IL-5 (Fig. 25c). The addition of CPS, ID35, their combination and of inactivated LGG, in the presence of BLG, significantly inhibited this increase (Fig. 25, panels a-c), resulting in an anti-inflammatory effect.

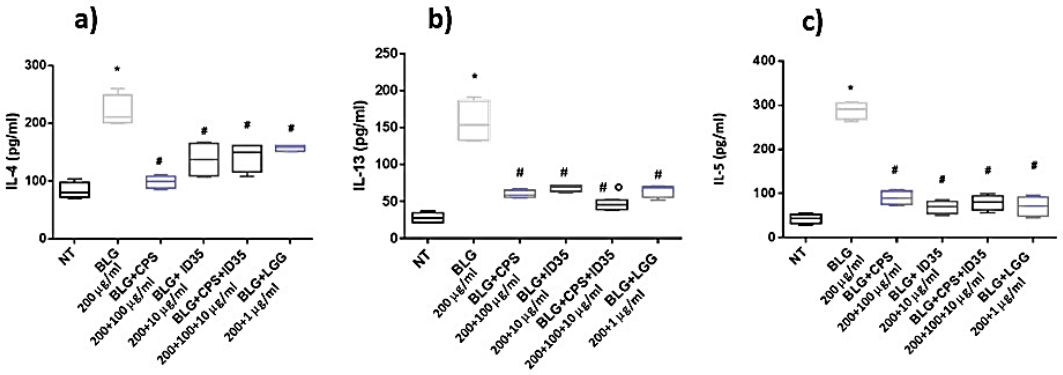

Figure 25. Effects of PBMCs stimulation with BLG (200 μg/ml), BLG + CPS (100 μg/ml), BLG + ID35 (10 μg/ml), BLG + CPS + ID35, and BLG + inactivated LGG (1 μg/ml) on Th2 cytokine production: a) IL-4; b) IL-13; c) IL-5. "NT" stands for "not-treated" cells. Data are expressed as means ± SD and were analyzed using paired t-test. *p<0.05 vs NT; #p<0.05 vs LGG.

2.2.6 Effects on tolerogenic mechanisms

Heat inactivated LGG, as well as ID35 or CPS or ID35+CPS are able to elicit an increase in IL-10 production by PBMCs collected from CMA children (Fig. 26a). This effect is associated with a significant increase of number of activated Tregs (Fig. 26b). Furthermore, the expression levels of regulatory dendritic cells (rDC)-associated markers Ifna2, Tgfb1, and Ptgs2 were evaluated. Finally, it was observed that heat inactivated LGG, as well as ID35 or CPS or ID35+CPS were able to enhance the expression levels of these factors (Fig. 27a, 27 b and 27 c), suggesting that Tregs induction was mediated by a dendritic cell–dependent mechanism.

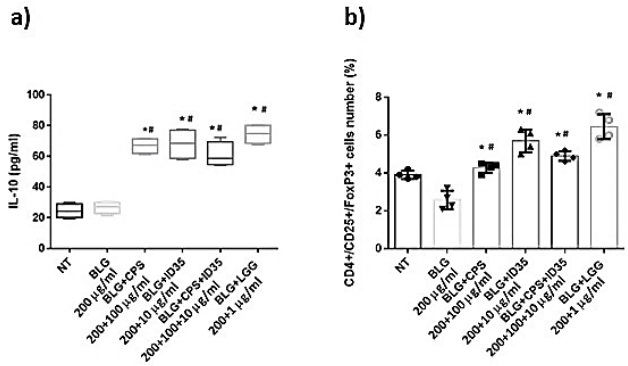

Figure 26. Effects of BLG (200 μg/ml), BLG + CPS (100 μg/ml), BLG + ID35 (10 μg/ml), BLG + CPS + ID35, and BLG + inactivated LGG (1 μg/ml) on tolerogenic mechanisms in human PBMCs from children affected by IgE-mediated CMA: a) effects on IL-10 production. b) increase of number of activated Tregs compared to PBMCs treated with BLG alone or with untreated cells. Data are expressed as means ± SD and were analyzed using paired t-test. *p<0.05 vs NT; #p<0.05 vs LGG.

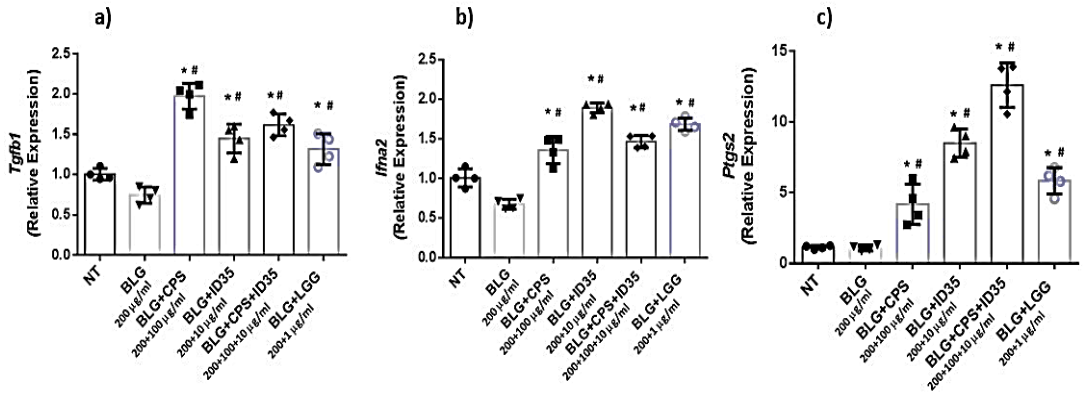

Figure 27. Effects of BLG (200 μg/ml), BLG + CPS (100 μg/ml), BLG + ID35 (10 μg/ml), BLG + CPS + ID35, and BLG + inactivated LGG (1 μg/ml) on the activation of Tregs DCs-mediated. CPS, ID35, their combination and inactivated LGG significantly enhanced the expression levels of: a) Tgfb1; b) Ifna2; c) Ptgs2. Data are expressed as means ± SD and were analyzed using paired t-test. *p<0.05 vs NT; #p<0.05 vs LGG.

2.3. Structural characterization of polysaccharides from *Lactobacillus paracasei* CBA L74

All the procedures involving the growth of the bacterium, the extraction and purification of its glycans and their structural characterization by NMR spectroscopy and GC-MS techniques were performed by myself, while I carried out the HR-MAS analysis on the bacterium cells in collaboration with Dr. Xavier Trivelli, from the CNRS of the University of Lille.

2.3.1 Polysaccharides extraction

Polysaccharides from *L. paracasei* CBA L74 were firstly isolated from a commercial cow's milk powder supplement for infants, fermented with this bacterium. Thus, the powder was first suspended in water and dialyzed to remove lactose and all the oligosaccharides present in the matrix, and centrifuged. Consequently, polysaccharides from the obtained pellet were tried to extract with different procedures, as with hydrofluoric acid. Unfortunately, these attempts only led to few mg of product, whose ^{1}H-^{13}C HSQC spectrum suggested the presence of a mixture of different polysaccharides, so difficult to analyse. Also, the SDS-PAGE displayed the presence of both polysaccharides and proteins (Fig. 28). All these pieces of evidence, along with the suspect that part of the material extracted could derive from milk, led us to restart the extraction by using the bacterium grown in a medium other than milk.

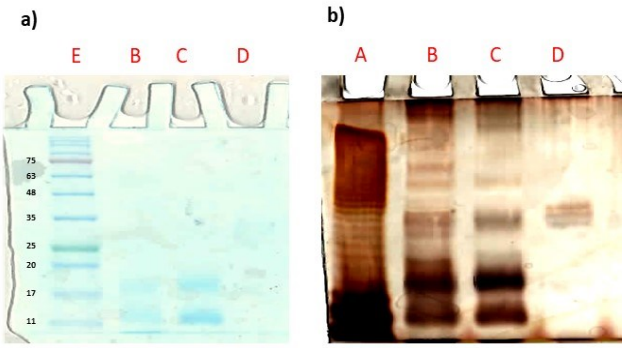

Figure 28. SDS-PAGE (12 μg sample) with: a) comassie blu brillante; b) silver staining. A. STD *E. coli* 0111:B4 LPS; B. aqueous phase of the extraction H_2O/ButOH; C. aqueous phase of the extraction with TCA; D. interphase of the extraction H_2O/ButOH; E. STD protein (blue eye protein).

Hence, the freeze-dried cells of *L. paracasei* were resuspended in water, centrifuged and the pellet grown in MRS medium. After 48 h, the pellet was collected, suspended again in water and extracted by heat treatment in autoclave (120 °C, 20'). Noteworthy, the crude product present in solution after centrifugation, was found to be the same previously isolated from the fermented milk matrix (Fig. 29a and 29b), suggesting that these glycans belong to the bacterium and not to the natural matrix from which they were isolated.

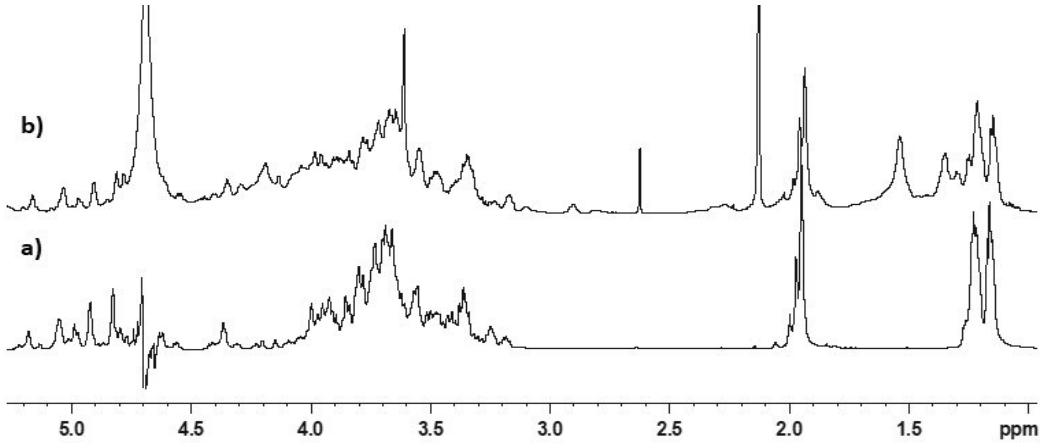

Figure 29. ^{1}H NMR (600 MHz) of *L. paracasei* glycans: a) from milk matrix, after HF treatment; b) from MRS, after heat treatment.

2.3.2 Polysaccharides purification

The supernatant resulting from the bacterium heat treatment and centrifugation underwent several steps of purification by size-exclusion and anion-exchange chromatography. Through size-exclusion chromatography on Sephacryl® S-300 HR, four

main fractions were separated (Fig. 30a), and their profiles were analysed by ^{1}H NMR spectroscopy (Fig. 30b), through which the two most important fractions containing polysaccharides were identified (RBC/16/A_0 and RBC/16/A). Note that RBC/16/A_0 was eluted from the size-exclusion chromatography in the flatline of the chromatogram, thus it represents the *L. paracasei* CPS (CPS-1) with a higher MW in respect to the fraction 16/A (CPS-2).

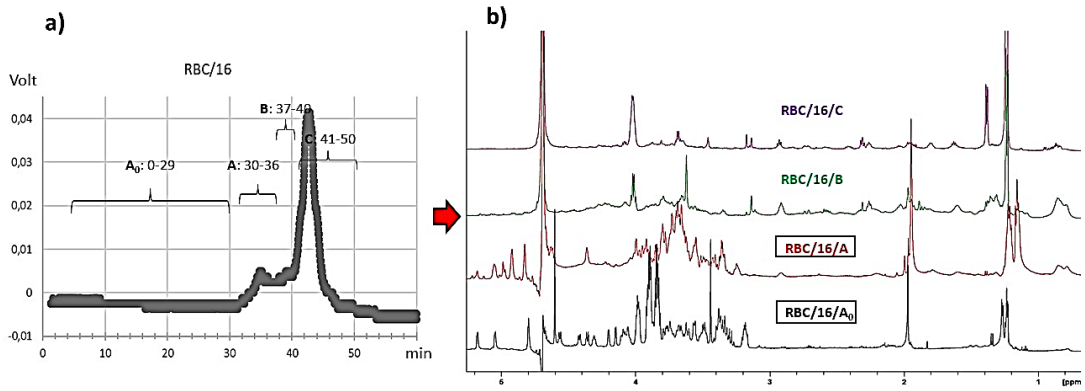

Figure 30. a) Chromatographic profile observed from size-exclusion chromatography via Sephacryl® S-300 HR. The flow rate was set to 15 mL/h, and the eluate was monitored by RID signal (sensibility=5xe-3). The above chromatogram reports how each fraction was collected. b) Proton spectra (600 MHz, 298 K, D_2O) of the fractions obtained after purification on Sephacryl® S-300 HR.

Hence, both fractions 16/A_0 and 16/A were further purified by anion-exchange chromatography on Q-sepharose® Fast-Flow resin, eluting with an increasing gradient of NaCl, and each obtained fraction was desalted on BioGel® P-10 resin, ran in water with a flow rate of 12 mL/h. Finally, from the fraction 16/A_0 were isolated two different polymers, a teichoic acid and a capsular polysaccharide (named CPS-1), respectively, while from the fraction 16/A was obtained another CPS (named CPS-2). Specifically, the teichoic acid was eluted with 700 mM of NaCl, with a final yield of 0.24 mg/$g_{dried\text{-}cells}$, while the CPS-1 and CPS-2 were eluted with 10 mM of NaCl, given a final yield of 8 mg/$g_{dried\text{-}cells}$ and 56 mg/$g_{dried\text{-}cells}$, respectively. Therefore, among the three glycans, the CPS-2 results to be the most abundant among the glycan components of the bacterium cell membrane.

2.3.3 GC-MS compositional analysis of the crude extract from *L. paracasei* cells

Monosaccharide analysis as acetylated O-methyl glycosides (MGA) was performed on the crude product obtained through the heat treatment of the *L. paracasei* pellet. Rhamnose and glucose were detected as the most abundant sugar components, while galactosamine, glucosamine, ribose, arabinose and glycerol were present in smaller percentages (Fig. 31). In particular, ribose, arabinose and glycerol derived from nucleic acids, culture medium and non-polysaccharide component of the cellular membrane, as demonstrated by following 2D NMR spectroscopic studies.

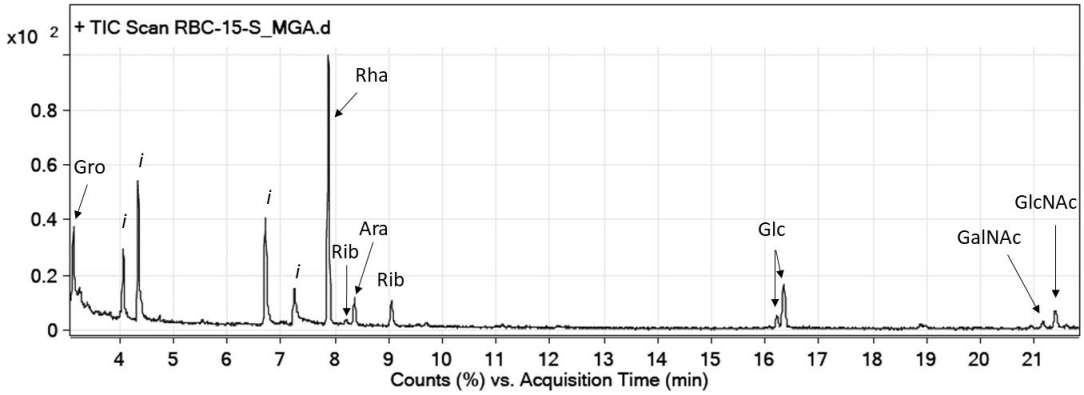

Figure 31. GC-MS compositional analysis of *L. paracasei* extract by hot water. "*i*" stands for impurities of a non-polysaccharide nature present on the sample.

2.3.4 Determination of the absolute configuration of *L. paracasei* glycans through GC-MS studies

The absolute configuration of the crude polysaccharides from *L. paracasei* extracted by hot water were inferred by deriving them into acetylated-octyl glycosides (AOG) by using an optically pure alcohol (2-(-)-octanol) (De Castro et al., 2010). Recognition of the diastereoisomers was performed by comparing their retention time with that of the reference compounds (Fig. 32b, 32c, 32d, 32e, 32f, 32g, 32l, and 32m). Hence, from this type of analysis it emerged that glucose (Fig. 32a), glucosamine and galactosamine (Fig. 32h) were D-configured, while rhamnose was L (Fig. 32i).

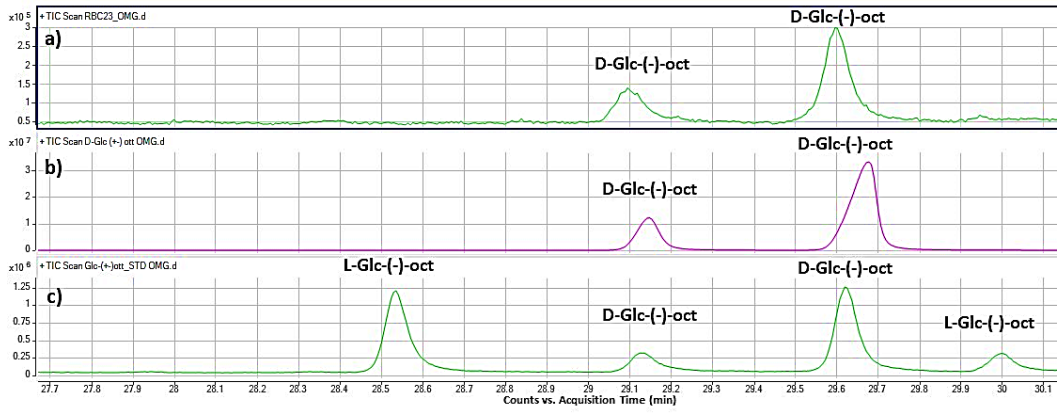

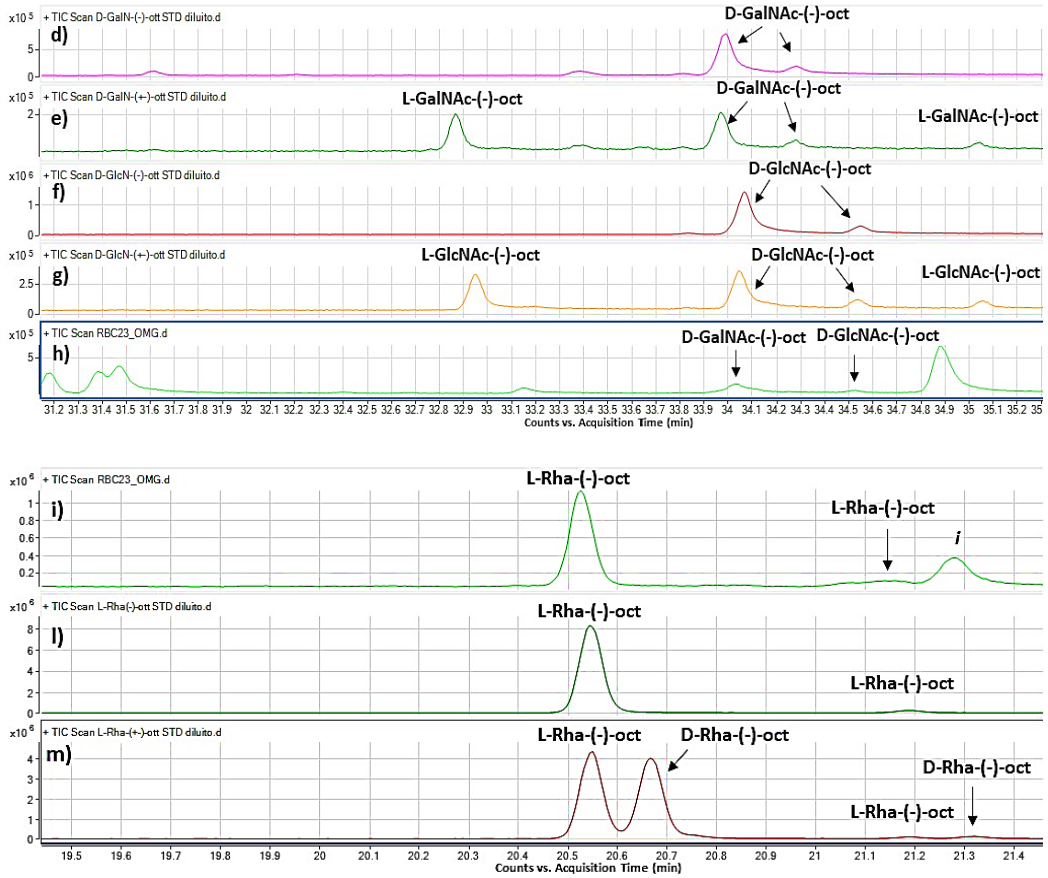

Figure 32. Absolute configuration of residues as determined by the O-octylglycoside derivatives method. In panels a), h), and i) are reported profiles obtained from monosaccharide derivatives of *L. paracasei* glycans. The term "*i*" stands for impurity. Panels b) and c) show the chromatographic standard profiles of Glc, as pure enantiomer and diastereoisomers, respectively. Panels d) and e) show the chromatographic standard profiles of GalNAc, as pure enantiomer and diastereoisomers, respectively. Panels f) and g) show the chromatographic standard profiles of GlcNAc, as pure enantiomer and diastereoisomers, respectively. Panels l) and m) show the chromatographic standard profiles of Rha, as pure enantiomer and diastereoisomers, respectively.

2.3.5 2D NMR structural analysis of CPS-1 and TA from *L. paracasei*

The structure of the *L. paracasei* glycans was determined by analysing $^{1}H,^{1}H$ homo- and $^{1}H,^{13}C$ heteronuclear 2D NMR experiments, recorded by dissolving glycans in D_2O. $^{1}H,^{1}H$ COSY and $^{1}H,^{1}H$ TOCSY experiments were used to disclose the protons of each spin system, while carbon atoms were identified through $^{1}H,^{13}C$ HSQC and further confirmed by $^{1}H,^{13}C$ HSQC-TOCSY. Lastly, the primary sequence was inferred by analysis of inter-residue and long-range dipolar and scalar correlations from $^{1}H,^{1}H$ NOESY and $^{1}H,^{13}C$ HMBC spectra, respectively.

Regarding with CPS-1 and TA, the total set of 2D NMR spectra was acquired on their mixture. Their purification by anion-exchange chromatography occurred later, and the comparison of the $^{1}H,^{13}C$ HSQC (Fig. 33) and the proton (Fig. 34b) spectra of the mixture with those of the pure glycans (Fig. 34a and 34c), confirmed the resolution of the mixture.

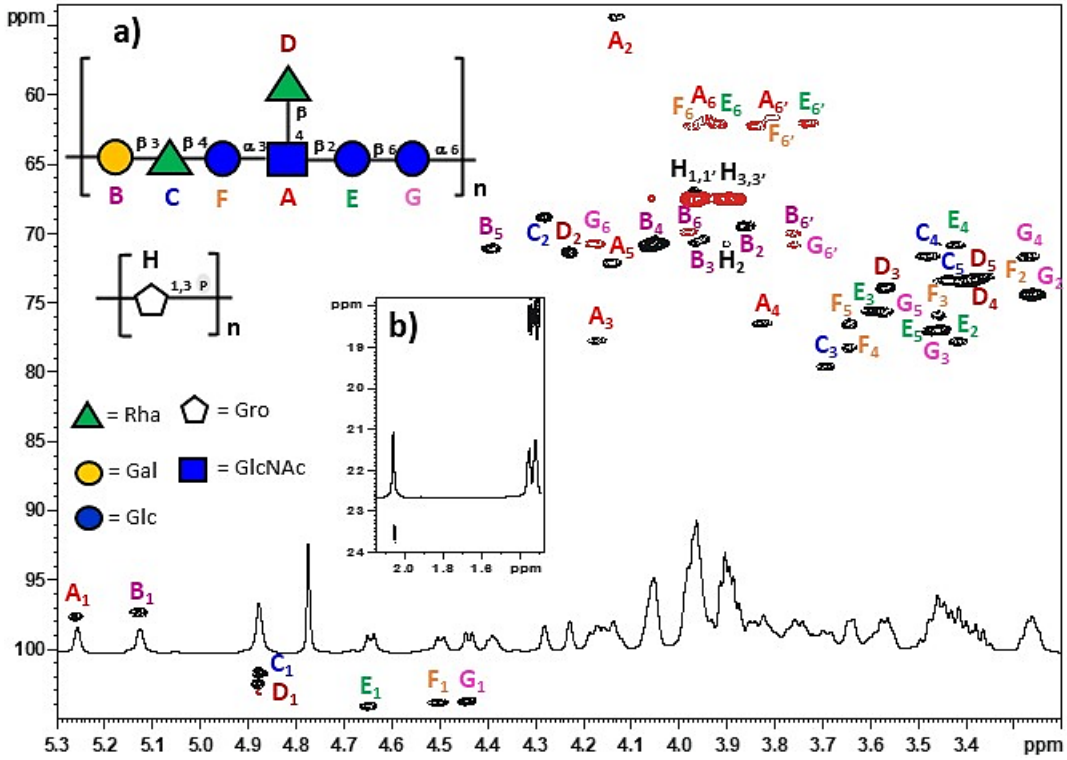

Figure 33. Expansion of the HSQC spectrum (600 MHz, 298 K, D_2O) of: a) the mixture of the CPS-1 + TA isolated from *L. paracasei*, along with the proton profile and the structures. Letters refer to the carbohydrate residues as reported in figure and drawn according to the symbolic nomenclature for glycans. All monosaccharides are in the pyranose form. Arabic numerals refer to the proton/carbon atoms of the respective residue; b) N-acetyl signal (2.05 ppm) of the glucosamine (residue A) plus methyl signals (1.35-1.30 ppm) of the rhamnoses units (C and D residues).

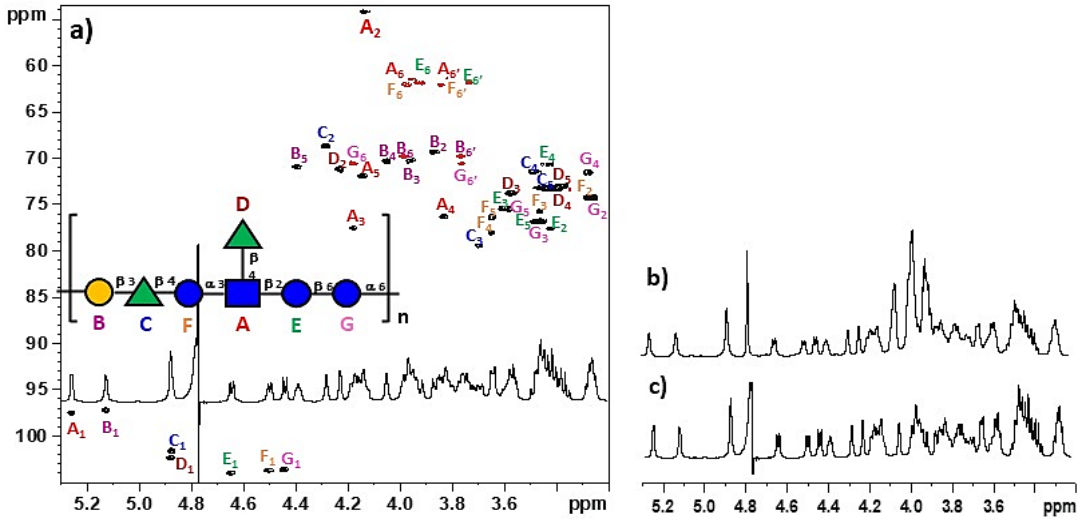

Figure 34. a) Expansion of the HSQC spectrum (600 MHz, 298 K, D2O) of the CPS-1 isolated from *L. paracasei*, along with the proton profile and the structure. Letters refer to the carbohydrate residues as reported in figure and drawn according to the Symbolic Nomenclature For Glycans. All monosaccharides are in the pyranose form. Arabic numerals refer to the proton/carbon atoms of the respective residue. b) ^{1}H NMR (600 MHz, D2O) of the mixture of CPS-1 + TA. c) ^{1}H NMR (600 MHz, D2O) of the pure CPS-1 alone.

Table 5. NMR chemical shifts of the *L. paracasei* CPS-1, measured at 600 MHz, 298 K, in D_2O.

Residue	1	2	3	4	5	6
A	5.26	4.13	4.17	3.83	4.14	3.95-3.82
3,4-α-L-Glc*p*NAc	*97.6*	*54.3*	*77.7*	*76.5*	*72.1*	*61.8*
B	5.13	3.86	3.97	4.05	4.40	3.98-3.74
6-α-D-Gal*p*	*97.5*	*69.4*	*70.5*	*70.9*	*71.2*	*69.9*
C	4.88	4.29	3.70	3.48	3.42	1.30
3-β-L-Rha*p*	*101.7*	*68.8*	*79.5*	*71.5*	*73.4*	*17.8*
D	4.88	4.22	3.56	3.38	3.42	1.30
t-β-L-Rha*p*	*102.5*	*71.3*	*73.9*	*73.3*	*73.4*	*17.8*
E	4.65	3.42	3.58	3.43	3.45	3.93-3.73
2-β-D-Glc*p*	*104.1*	*77.8*	*75.5*	*70.6*	*77.0*	*61.9*
F	4.50	3.25	3.45	3.65	3.65	3.97-3.84
4-β-D-Glc*p*	*104.0*	*74.3*	*75.9*	*78.2*	*76.5*	*62.2*
G	4.44	3.25	3.45	3.26	3.59	4.17-3.76
6-β-D-Glc*p*	*103.4*	*74.4*	*77.0*	*71.6*	*75.5*	*70.7*
H	3.96	3.89	3.89			
P*-Gro-*P	*67.4*	*70.6*	*67.4*			

The inter-residue correlations were identified through the study of the NOESY (Fig. 35a) and HMBC (Fig. 35b) spectra, which reveals that the C-1 of A is linked with the C-2 of the residue E, the C-3 is linked to the C-1 of F and the C-4 to the C-1 of D. A similar approach was adopted to also identified the residue E, F and G, all of which have five TOCSY correlations from the anomeric centres (104.1, 104.0 ppm, and 103.4, respectively). Thus, residue E, F and G were identified as β-glucose, -2, -4 and -6 linked, respectively. Indeed, all of them have a $^{3}J_{H1,H2}$ coupling constant value around 7.5 Hz, typical of a β-anomer with H2 in axial orientation (Speciale et al., 2022). Moreover, HMBC and NOESY spectra show the correlation between E1 and G6 (70.7 ppm), F4 (78.2 ppm) and C1 and between G1 and B6 (69.9 ppm). Moving further with the residue B, it shows only three TOCSY correlations from its anomeric position (97.5 ppm). This is typical of a galacto-configured sugar. The attribution of the other proton and carbon atoms of the residue was completed by analysing the HMBC and the NOESY spectra. The chemical shift values attributed to the carbon atoms of the residue matched with those reported in literature for a 6-linked α-galactose. In addition, in the NOESY spectrum is possible to clearly see the correlation of the C-1 of B with the C-3 (79.5 ppm) of C (Fig. 35a). Regarding with residue C and D, they have an only one TOCSY correlation from their C-1 (101.7 and 102.5 ppm, respectively), while it is possible to observe all the other ones from their C-2 (68.8 and 71.3 ppm, respectively), through which the attribution of the other proton and carbon atoms of the residue was completed. Thus, B and C are both rhamnose β-configured at their anomeric centre, as confirmed by the analogy with the chemical shift values reported in the literature for these sugars (Speciale et al., 2022). The assignments of all residues and the sequence between the different residues was further confirmed by the information from the NOESY and the HSQC-TOCSY spectra, respectively, yielding to the definition of the repeating unit of the CPS-1 (inset in Fig. 34a). Finally, the residue H was identified as a 1,3-polyglycerophosphate, according to the comparison of the carbon and proton chemical shift values read in the HSQC with the ones reported in literature (Kozlova et al., 1999).

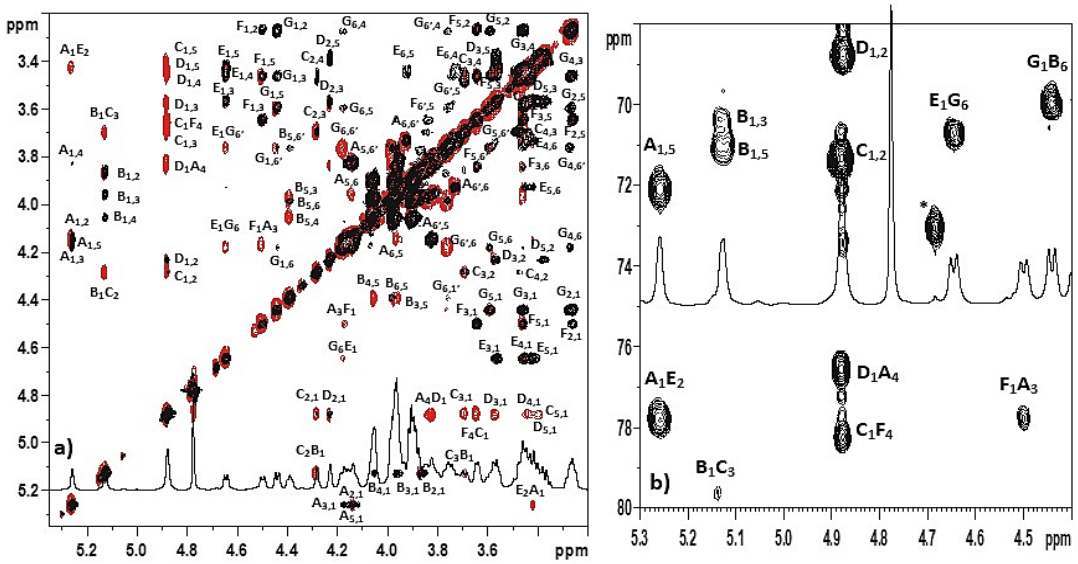

Figure 35. a) TOCSY spectrum in black overlapped to the NOESY spectrum in red (600 MHz, 298 K, D_2O) of the CPS-1 produced by *L. paracasei*. b) Expansion of the $^{1}H,^{13}C$ HMBC spectrum (600 MHz, 315 K, D_2O) of the CPS-1 produced by *L. paracasei*. Signal marked with (*) is due to a minor impurity. In both panels, letters refer to carbohydrate residues as defined in Tab. 5, and arabic numerals to the atoms of the respective residues.

2.3.6 2D NMR structural analysis of *L. paracasei* CPS-2

The structure was determined by analyzing the complete set of homo- and heteronuclear 2D NMR experiments (COSY, TOCSY, NOESY, ^{1}H-^{13}C HSQC, ^{1}H-^{13}C HMBC). The spin system of each residue was assigned by interpretation of the COSY and TOCSY spectra, while $^{1}H,^{13}C$ HSQC spectrum was used to assign the carbon chemical shift values. Attributions were counterchecked or completed using the other spectra recorded. During the analysis, by integrating the information of ^{13}C HSQC and ^{1}H NMR spectra (Fig. 36), it was possible to distinguish and identify fifteen majors anomeric signals between 5.3-4.6 ppm (Fig. 36b), a crowded carbinolic region (4.5-3.2 ppm, Fig. 36a), a group of acetyl signals between 2.1-1.9 ppm (Fig. 36c), and several methyl signals at ca. 1.3 ppm (Fig. 37b), attributed to the different rhamnose units. The anomeric signals were labeled with a capital letter (Fig. 36b, Tab. 6).

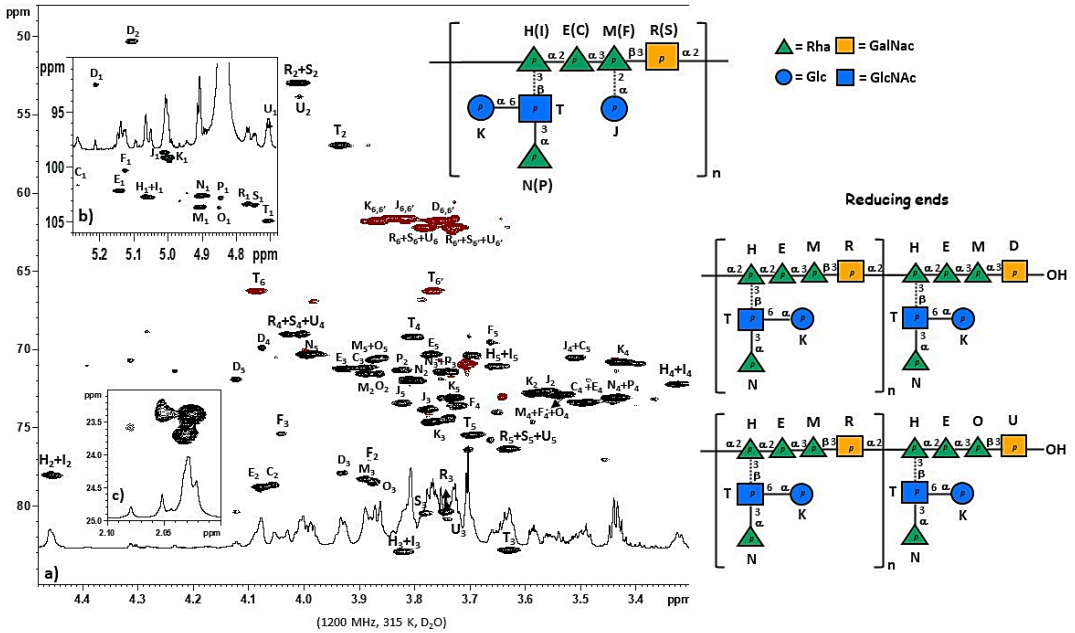

Figure 36. a) Expansion of the carbinolic region of the HSQC spectrum (1200 MHz, 293 K, D_2O) of the CPS-2 isolated from *L. paracasei*, along with the proton profile. Letters refer to the carbohydrate residues as reported in figure and drawn according to the SNFG. Arabic numerals refer to the proton/carbon atoms of the respective residue. In particular, when the substituent "J" is present and the dimer K→6T is absent, residues are called with the capital letters between brackets. Red densities are referred to –CH2 groups. Minor signals are not assigned. b) Expansion of the anomeric region of CPS-2. c) Expansion of the acetyl signals of the CPS-2.

Table 6. (1200 MHz, 293 K, D_2O) Proton (^1H) (plain text) and carbon (^{13}C) (italic) NMR chemical shifts of CPS-2 from *L. paracasei* CBA L74.

Residue	1	2	3	4	5	6
C	5.27	4.06	3.88	3.49	3.50	1.32
2-α-Rha*p*	*101.6*	*78.6*	*71.2*	*73.3*	*70.5*	*17.5*
D	5.20	4.30	3.93	4.07	4.11	3.74
3-α-Gal*p*NAc	*92.3*	*50.3*	*77.9*	*69.8*	*71.9*	*61.6*
E	5.15	4.07	3.92	3.49	3.76	1.30
2-α-Rha*p*	*102.0*	*78.6*	*71.1*	*73.3*	*70.3*	*17.6*
F	5.13	3.88	4.03	3.71	3.64	1.29
2,3-α-Rha*p*	*100.2*	*77.0*	*75.3*	*73.4*	*69.5*	*17.6*
H	5.07	4.46	3.82	3.32	3.65	1.24
2,3-α-Rha*p*	*102.7*	*78.0*	*82.8*	*72.2*	*69.9*	*17.6*
I	5.06	4.46	3.82	3.32	3.65	1.24
2,3-α-Rha*p*	*102.7*	*78.0*	*82.8*	*72.2*	*69.9*	*17.6*
J	5.00	3.55	3.77	3.50	3.81	3.84
t-α-Glc*p*	*98.5*	*72.6*	*74.6*	*70.5*	*73.4*	*61.6*
K	5.00	3.59	3.73	3.43	3.72	3.87
t-α-Glc*p*	*99.2*	*72.6*	*74.4*	*70.8*	*73.1*	*61.7*
M	4.91	3.89	3.89	3.53	3.87	1.29
3-α-Rha*p*	*103.6*	*71.4*	*78.3*	*73.0*	*70.6*	*17.6*
N	4.91	3.79	3.75	3.44	3.99	1.24
t-α-Rha*p*	*102.6*	*71.8*	*71.4*	*73.0*	*70.2*	*17.6*
O	4.85	3.86	4.06	3.53	3.87	1.29
3-α-Rha*p*	*103.6*	*71.4*	*78.5*	*73.0*	*70.6*	*17.6*
P	4.85	3.83	3.75	3.44	3.99	1.24
t-α-Rha*p*	*102.8*	*71.1*	*71.4*	*73.0*	*70.3*	*17.6*
R	4.77	4.00	3.73	4.02	3.62	3.78-3.72
3-β-Gal*p*NAc	*103.3*	*52.9*	*80.2*	*69.0*	*76.3*	*62.0*
S	4.75	4.00	3.77	4.02	3.62	3.78-3.72
3-β-Gal*p*NAc	*103.5*	*52.9*	*80.4*	*69.0*	*76.3*	*62.0*
T	4.69	3.94	3.62	3.81	3.69	4.08-3.77
3,6-β-Glc*p*NAc	*104.7*	*56.9*	*82.6*	*69.0*	*75.4*	*66.1*
U	4.69	4.00	3.73	4.02	3.62	3.78-3.72
3-β-Gal*p*NAc	*96.3*	*53.9*	*80.8*	*69.0*	*76.3*	*62.0*

NMR analysis started from residue C, whose anomeric proton (5.27 ppm) displayed only one correlation in the TOCSY spectrum (Fig. 38b), on the contrary, H-2 (4.05 ppm) correlated with other two protons of the unit, H-3 and H-4, whose sequence was inferred by analyzing the COSY correlations. Then, H-4 (3.47 ppm) led to the identification of H-5 (3.98 ppm), that in turn had a correlation with H-6, a methyl group at 1.32 ppm (Tab. 6, Fig. 37b). This pattern is diagnostic of a rhamnose residue, and integration with the carbon chemical shift values

determined from the HSQC spectrum identified this residue as α configured at the anomeric center because of the similarity between its C-5 value (70.1 ppm) with that reported for the reference glycoside (69.4 ppm) and 2-substituted due to the glycosylation shift at low fields detected for the corresponding carbon atoms.

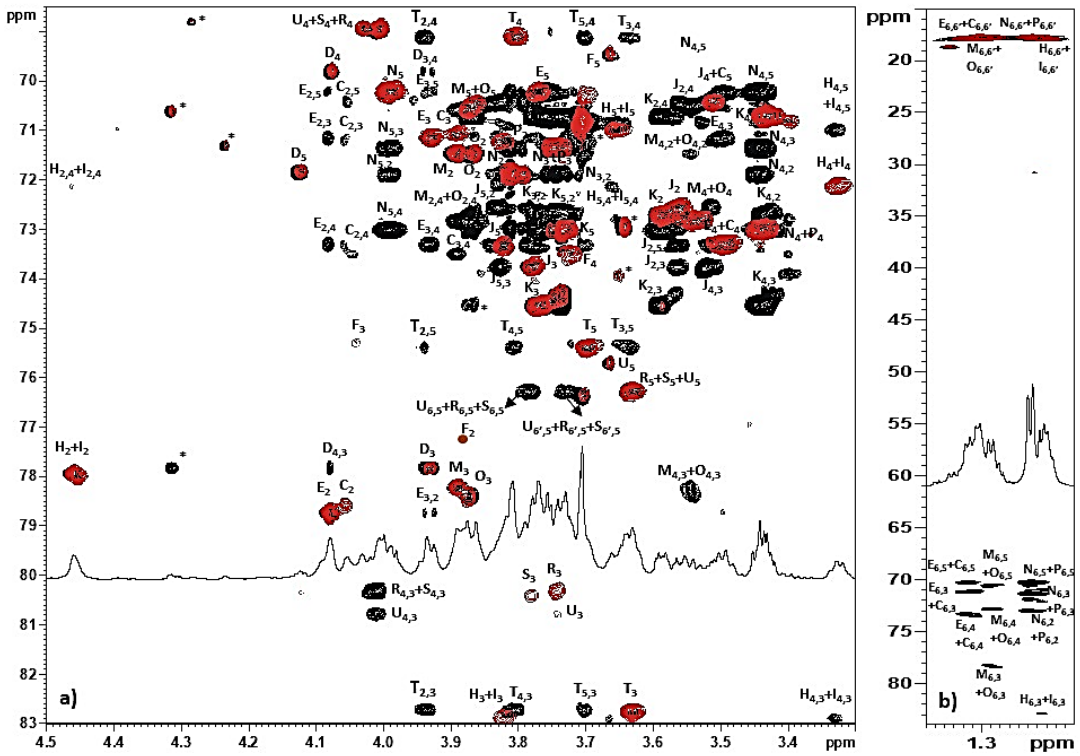

Figure 37. a) Expansion of the carbinolic region of the HSQC (in red) overlapped with HSQC-TOCSY (in black) spectrum (1200 MHz, 293 K, D_2O) of the CPS-2 from *L. paracasei*; b) expansion of the methyl groups region of the HSQC (in red) overlapped with HSQC-TOCSY (in black) spectrum (1200 MHz, 293 K, D_2O) of the CPS-2 from *L. paracasei*. Labels refer to Tab. 6 and arabic numerals refer to the proton/carbon atoms of the respective residue. Signals marked with (*) are not characterized.

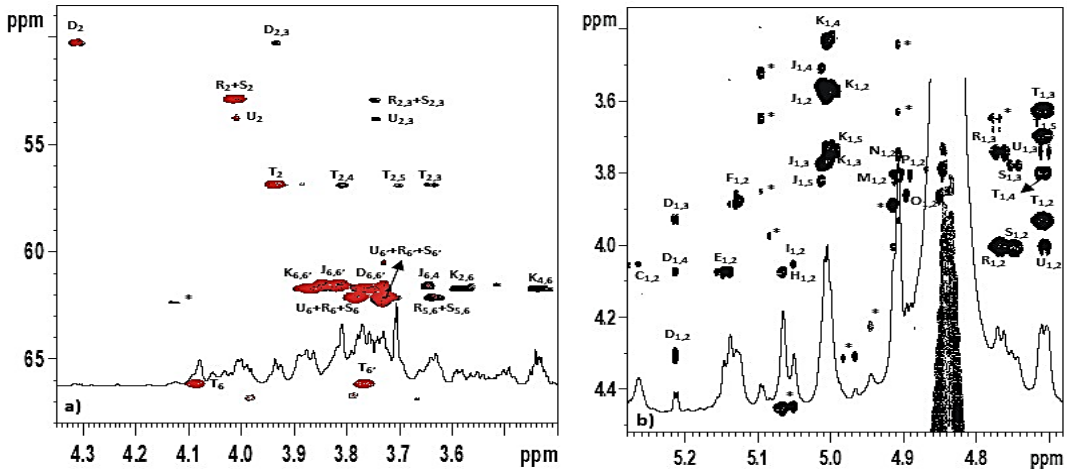

Figure 38. a) Expansion of the –CH_2 groups region of the HSQC (in red) overlapped with HSQC-TOCSY (in black) spectrum of the CPS-2 from *L. paracasei*; b) expansion of the anomeric region of the TOCSY spectrum of the CPS-2 from *L. paracasei* (1200 MHz, 293 K, D_2O). Labels refer to Tab. 6 and arabic numerals refer to the atoms of the respective residue. Signals marked with (*) are due to artifacts or are not attributed.

The analysis of NOESY (Fig. 39a) and HMBC (Fig. 39b) spectra showed that the residue C is linked in position C-1 (101.6 ppm) to the C-3 (75.4 ppm) of the residue F and in position C-2 (78.5 ppm) with the C-1 (102.7 ppm) of the residue I. Full attribution of the other rhamnoses, namely E, F, H, I, M, N and O chemical shifts was performed by using the same strategy discussed for C, and it was found that they were all α-rhamnose units, 2-linked in the case of E; 2,3-substituted in the case of F, H and I; 3-substituted in the case of M and O, and terminal in the case of the residue N (Tab. 6). Instead, the anomeric positions of residues J and K showed a TOCSY pattern (Fig. 38b) similar to that of a glucose. Indeed, by combining the analysis of the TOCSY and COSY with those of the HSQC spectrum, it was possible to determine that these residues were α-configured terminal glucose, in agreement with the carbon chemical shifts reported in literature for their respective methylglycoside (Speciale et al., 2022), and with their $^3J_{H1,H2}$ coupling constant value, which is 3.2 Hz. In addition, NOESY (Fig. 39a) and HMBC (Fig. 39b) spectra revealed the whole other inter-residues linkages, namely between:

-the positions C-1 (102.0 ppm) and C-2 (78.6 ppm) of the residue E with the C-3 (78.2 ppm) and C-1 (102.7 ppm) of the residues M and H, respectively;

-the positions C-1 (100.2 ppm) and C-2 (77.0 ppm) of F with the C-3 (80.4 ppm) and the C-1 (98.5 ppm) of the residues S and J, respectively;

-the position C-2 (78.0 ppm) of H with the C-1 (103.3 ppm) of the residue R;

-the position C-2 (78.0 ppm) of I with the C-1 (103.5 ppm) of S;

-the positions C-3 (both at 82.7 ppm) of the residues H and I with the C-1 (104.7 ppm) of T and the C-1 (96.3 ppm) of U, respectively;

-the position C-1 (99.2 ppm) of K with the C-6 (66.1 ppm) of T;

-the position C-1 (103.5 ppm) of M with the C-3 (80.4 ppm) of R;

-the position C-1 (102.6 ppm) of N with the C-3 (82.6 ppm) of the residue T.
Instead, regarding with the residue D, its anomeric proton (5.20 ppm) displays three correlations in the TOCSY spectrum (Fig. 38b), typical of a galactose. The attribution of the overall following proton and carbon atoms of the residue was completed by analysing HMBC and NOESY correlations. Moreover, the chemical shift value of D2 is at 50.2 ppm in the HSQC spectrum, suggesting the presence of an amino group in this position, and the comparison of the carbon chemical shift values read on the HSQC spectrum with those reported in literature, confirms that residue D is a 3-substituted galactosamine α-configured at the anomeric centre, as also confirmed by its $^{3}J_{H1,H2}$ coupling constant value of 3.5 Hz. By applying the same method of analysis, it was possible to fully identified also the residues R, S, and U as 3-substituted galactosamine, but β-configured at their anomeric center, as their ^{13}C chemical shifts matches with those reported in literature for the β-GalNAc (Speciale et al., 2022). Finally, as for the residue T, its anomeric proton (4.69 ppm) showed five correlation in the TOCSY spectrum (Fig. 38b), a pattern diagnostic of a glucose residue, and combining the analysis of the TOCSY and COSY spectra with those of the HSQC spectrum, it was possible to determine that T was a β configured N-acetylglucosamine, substituted in position O-3 and O-6, in agreement with the carbon chemical shifts reported in literature for its corresponding methylglycoside. The spin system assignments of all residues and the sequence between the different residues was further confirmed by agree with the information from contained in the HSQC-TOCSY (Fig. 37a and 37b and Fig. 38a) and NOESY spectra (Fig. 39a).

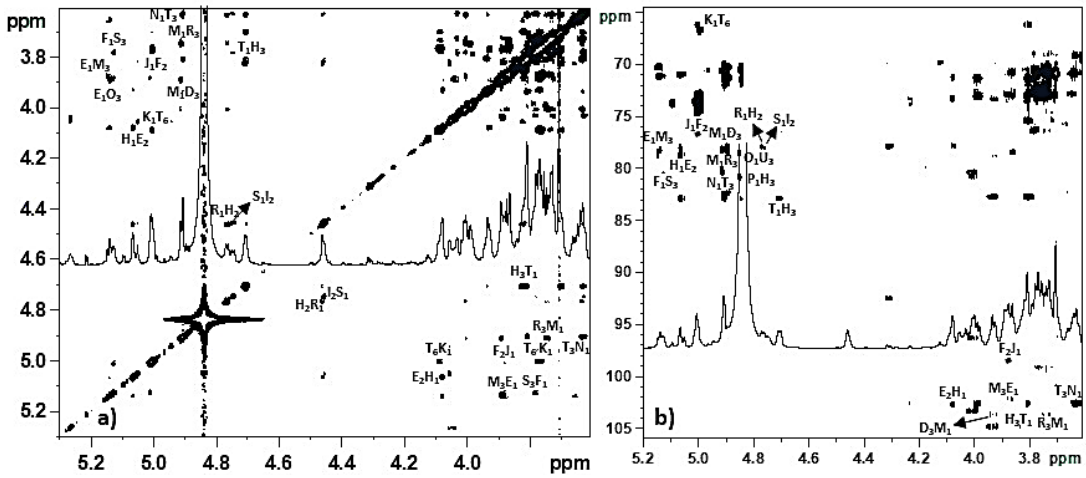

Figure 39. (1200 MHz, 293 K, D_2O) a) $^{1}H,^{1}H$ NOESY spectrum of the CPS-2 produced by *L. paracasei;* b) ^{1}H, ^{13}C HMBC spectrum of the CPS-2 produced by *L. paracasei*. In both panels, letters refer to carbohydrate residues as defined in Tab. 6, and arabic numerals to the atoms of the respective residues.

Although several signals overlap each other resulting in a single protonic signal, overall the signals in the anomeric region of the ^{1}H NMR spectrum are not at the same intensities between each other, suggesting that the polymer has a heterogeneous structure. This is due to the fact that the residues T (the β-GlcNAc) and J (the t-α-Glc*p*), are not stoichiometric substituents. Consequently, when the 3-α-Rha*p* (M) is substituted also in position 2 with the residue J, it becomes F, and when the branching portion K→6T is absent, the residue H becomes I, E becomes C, R becomes S, and the residue N becomes P, which is directly linked to the position C-3 of I. Moreover, the CPS-2 of *L. paracasei* is a small-sized polymer, as it is, among the whole glycans of *L. paracasei*, the most retained in the size-exclusion chromatography, and elutes with a time close to that of the salts (Fig. 30a). Therefore, by NMR spectroscopy it is possible to see also the reducing ends of the polymer. In particular, in NOESY (Fig. 39a) and HMBC (Fig. 39b) spectra it is possible to find the correlation between the C-1 of the residue M and the C-3 (77.9 ppm) of the terminal α-galactosamine, namely the residue D. The latter, due to the phenomenon of mutarotation of reducing sugars in solution, can switch its configuration at the anomeric center from α to β, resulting in residue called U. When it happens, the residue M becomes the residue O, and it is confirmed by the HMBC (Fig. 39b) correlation between the C-1 (101.6 ppm) of U and the C-3 (78.5 ppm) of O.

2.3.7 GC-MS substitutional pattern analysis of the CPS-2

Monosaccharide linkages were investigated by deriving the sample into partially acetylated and methylated alditols (AAPM), and injecting them into GC-MS instrument (De Castro et al., 2010). The chromatogram (Fig. 40) evidenced, in term of sugars, the presence of a terminal rhamnose, a 2-substituted, a 3-substituted and a 2,3-substituted rhamnose, of a terminal glucose, a 6-substituted and a 3,6-substituted glucosamine and of a 3-substituted galactosamine. The other unmarked (and small) peaks are impurities. Thus, the analysis confirms the structure of the major repeating unit hypothesized through 2D NMR spectroscopic studies.

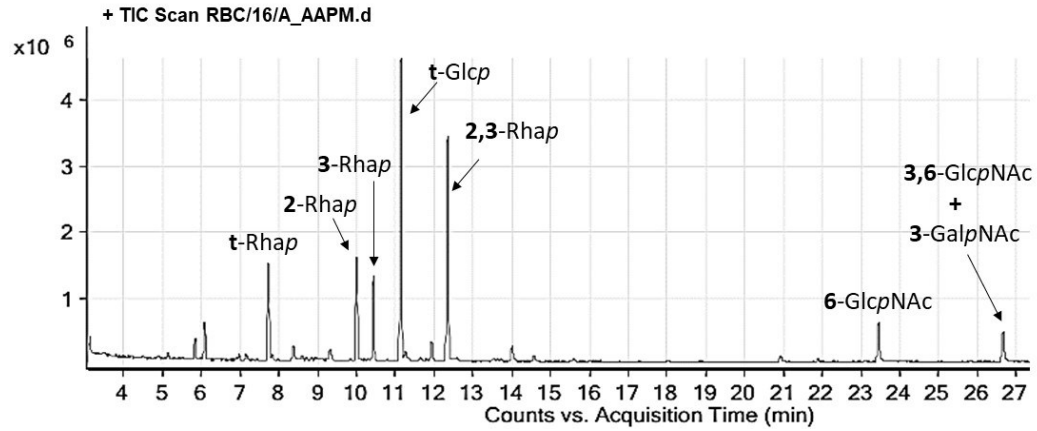

Figure 40. GC-MS substitution pattern analysis of the CPS-2 from *L. paracesei*, obtained after a combination of size-exclusion and anion-exchange chromatographic purification.

2.3.8 High-resolution magic-angle spinning NMR spectroscopy analysis of *L. paracasei* glycans

This technique was employed for a molecular examination of the surface cell glycan components. Briefly summarized, from *L. paracasei* CBA L74 they were identified a teichoic acid (TA) and two different CPSs (CPS-1 and CPS-2). Precisely, the TA is made up of a polyglycerol phosphate chain (Fig. 33a), and the CPS-1 is a polymer with a regular structure and a high MW, unlike CPS-2, which has an irregular repeating unit and a low MW. In particular, the CPS-1 has a linear chain made up of various sugars such as galactose, glucose, rhamnose and a glucosamine ramified in position 4 with a terminal β-rhamnose (Fig. 33a), while in CPS-2 we have a linear chain made up of a galactose and three rhamnoses, of which the first and the third are not stoichiometrically substituted with a dimer of a 6-β-glucosamine→α-glucose in position 3, and a terminal α-glucose in position 2, respectively (Fig. 36a). Thus, the surface expression of TA, CPS-1, and CPS-2 in both *L. paracasei* cells alive and after heat inactivation was further investigated by high-resolution magic-angle spinning (HR-MAS) NMR spectroscopy. In conclusion, the ^{1}H and $^{1}H,^{13}C$ HSQC spectrum of the cells after heat treatment was less rich in signals (Fig. 41a) in respect to that of the cells alive collected in their exponential (O.D.= 0.5) phase (Fig. 41b), suggesting that the adopted polysaccharide method of extraction was efficient.

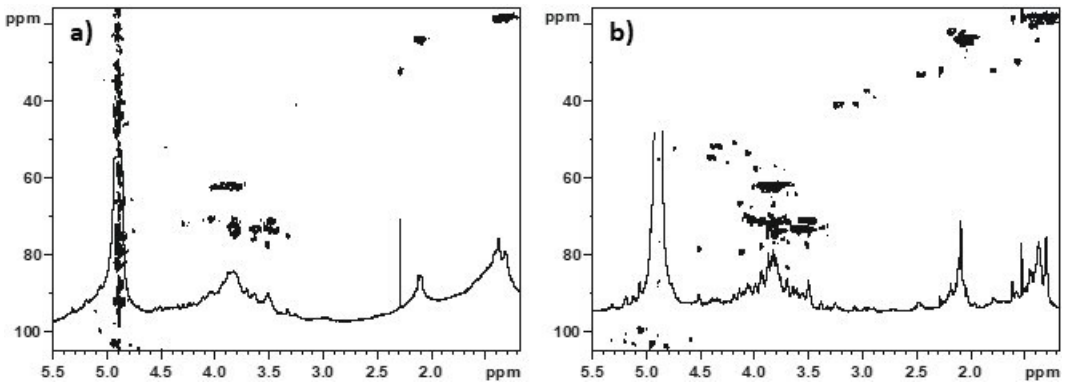

Figure 41. HR-MAS HSQC spectra (800 MHz, 293 K, D_2O) of *L. paracasei* cells: a) after heat-treatment; b) at their exponential growth phase.

Moreover, in order to see any difference in glycans expression during the different *L. paracasei* growth phases, the cells alive were harvested and analysed also in their lag (O.D.= 0.30) and stationary (O.D.= 3) phases. From the recorded spectra it emerged that *L. paracasei* polysaccharides were, generally, more expressed in the exponential phase (Fig. 42b), while the ^{1}H and $^{1}H,^{13}C$ HSQC sugar signals were fewer and with a lower intensity in the lag (Fig. 42a) and, especially, in the stationary phase (Fig. 42c).

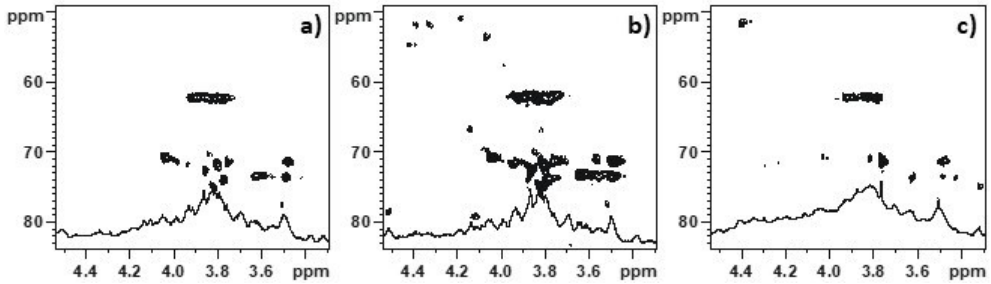

Figure 42 HR-MAS HSQC spectra (800 MHz, 293 K, D_2O) of *L. paracasei* cells at their: a) lag; b) exponential; c) stationary growth phase.

However, the low abundance of NMR signals in the lag and stationary growth phases could also be due to the shortening of glycans during these life stages of the bacterium. In particular, glycans can be shorter in the lag phase because the bacterial biosynthetic processes are not yet completed, while in the stationary phase their brevity can be attributed to some hydrolytic enzymes, such as glycosidases, which can exert their activity after the biosynthetic cellular processes are completed. In addition, HR-MAS $^{1}H,^{13}C$ HSQC signals of the CPS-1 are more visible in the inactivated cells (Fig. 43a and 43b), while signals of CPS-2 are more visible in the cells alive (Fig. 44a and 44b). This observation leads to assume that the CPS-2 is the polysaccharide component most flexible and most exposed on the bacterium cell surface, thus easier to extract and less anchored to the membrane in respect to the CPS-1. Finally, accordingly to the expected results, the $^{1}H,^{13}C$ HR-MAS NMR signals of the teichoic acid are not visible in the acquired spectra (Fig. 43 and 44), suggesting that it is an innermost and more fixed component of the cell membrane.

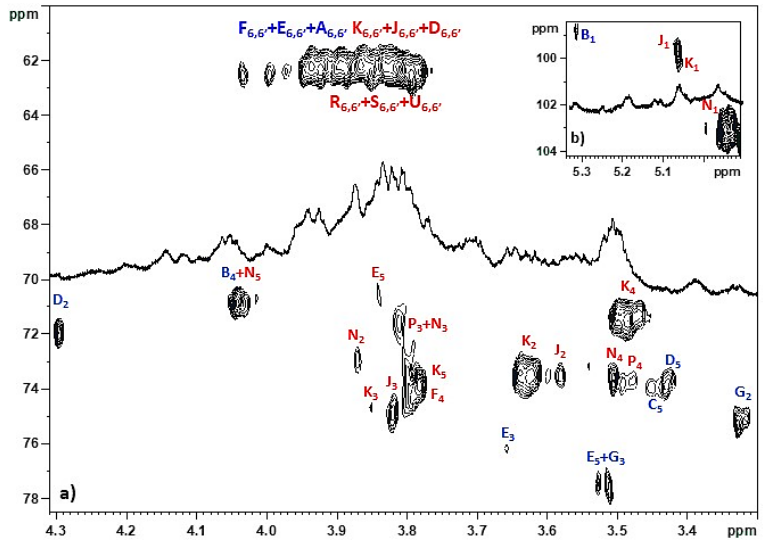

Figure 43. a) Expansion of the HR-MAS HSQC spectrum (800 MHz, 293 K, D_2O) of the heat treated *L. paracasei* cells, along with the proton profile; b) expansion of the anomeric region of the heat treated *L. paracasei* cells. Blue letters refer to the CPS-1 carbohydrate residues as reported in Tab. 5, while red letters refer to the carbohydrate residues of the CPS-2, as reported in Tab. 6. Arabic numerals refer to the proton/carbon atoms of the respective residue.

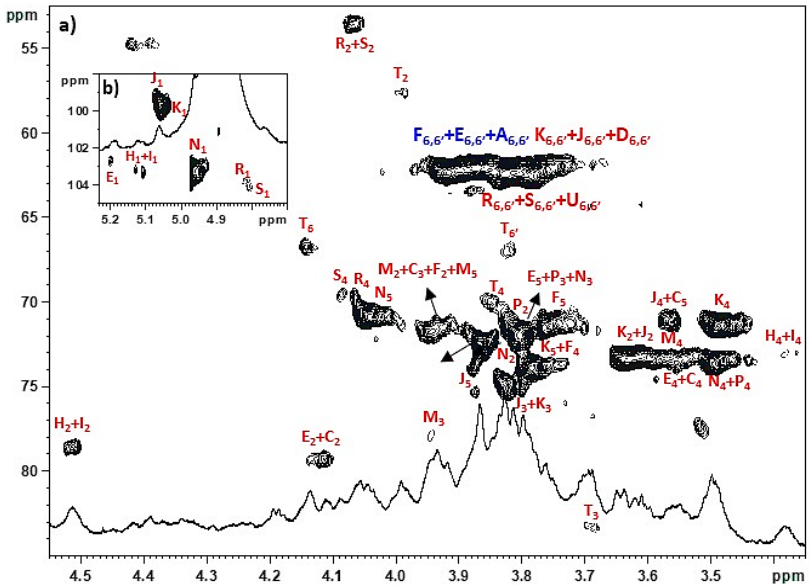

Figure 44. a) Expansion of the HR-MAS HSQC spectrum (800 MHz, 293 K, D_2O) of *L. paracasei* cells alive, along with the proton profile; b) expansion of the anomeric region of the *L. paracasei* cells alive. Blue letters refer to the CPS-1 carbohydrate residues as reported in Tab. 5, while red letters refer to the carbohydrate residues of the CPS-2, as reported in Tab. 6. Arabic numerals refer to the proton/carbon atoms of the respective residue.

2.4. Structural characterization and immunomodulatory activity of *Bacillus subtilis* 168 glycans

The crude glycans from *B. subtilis* 168 were firstly extracted by Prof. Volker's research team, from Georg-August University. Consequently, I purified and structurally characterized them to finally allow the Volker's team to evaluate their immunomodulatory activity, through specific leaf puncture assays.

2.4.1 Glycans extraction and purification

The pellet from *B. subtilis* 168 was resuspended in water and heat-extracted, boiling in autoclave at 120 °C for 20' and centrifuged. After that, the obtained supernatant was purified by a combination of size-exclusion and ion-exchange chromatography, and there were finally obtained two distinct glycans, further characterized by NMR analysis. The first one (glycan-1 = Leon/1/A) was a teichoic acid made of a polyglycerol-phosphate chain not-stoichiometrically substituted with a terminal α-Glc, and was achieved through a firstly size-exclusion chromatography on Sephacryl® S-300 HR of the autoclave supernatant, eluting with AMBIC 50 mM. The pure product (0.6 mg/54 $mg_{crude\text{-}extract}$) was isolated in the flat-line of the chromatogram (Fig. 45) resulting from a RID detector connected to the column.

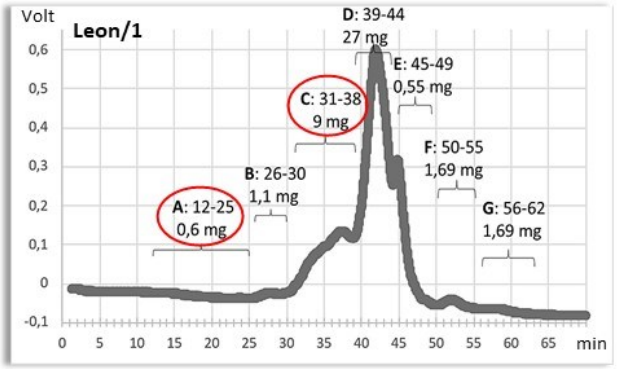

Figure 45. Chromatographic profile of heat-treated *B. subtilis* observed from size-exclusion chromatography via Sephacryl® S-300 HR. The flow rate was set to 15 mL/h, and the eluate was monitored by RID signal (sensibility=5xe-4). The above chromatogram reports how each fraction was collected.

The second pure glycan (glycan-2 = Leon/2/C1) was a capsular polysaccharide with a repeating unit made of a GalNAc and a Glc linked together through a phosphodiester bridge. It was obtained by a further purification of the third fraction isolated through size-exclusion chromatography (Fig. 45), with a final yield of 9 mg/54 $mg_{crude\text{-}extract}$. Thus, it underwent to an anion-exchange chromatography through resin Q-sepharose® Fast Flow, and a subsequent desalting on resin BioGel® P-10, ran in water with a flow rate of 12 mL/h. By ^{1}H NMR analysis (Fig. 46), the pure glycan-2 (Leon/2/C1) has been identified in the third fraction isolated by Q-sepharose, eluted with NaCl 200 mM. Fraction 2/D1 is almost a

mixture of glycan-1 and glycan-2 and the other ones are almost impurities of non-polysaccharidic nature.

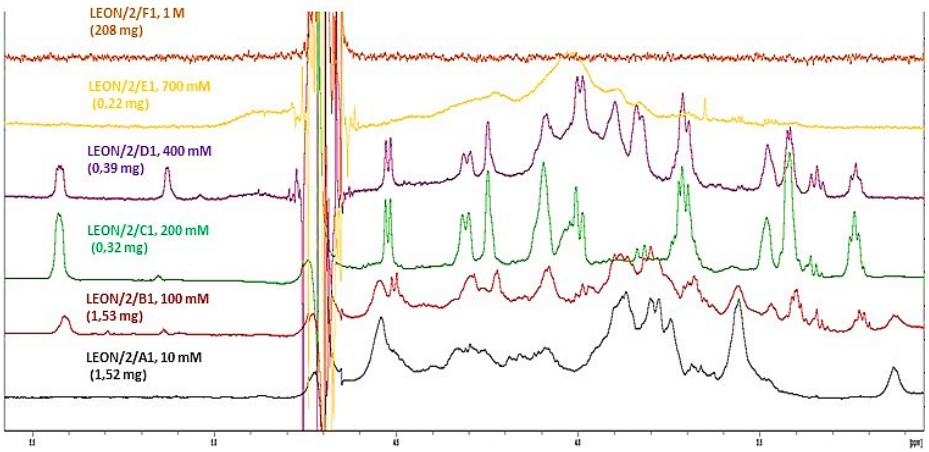

Figure 46. Proton spectra (600 MHz, 298 K, D_2O) of the main fractions collected by desalting the eluate of the ion exchange chromatography obtained with a specific ionic strength. The amount of each sample is indicated next to the profile.

2.4.2 2D NMR structural studies of *B. subtilis* glycan-1

The structure of the teichoic acids was determined by analysing $^{1}H,^{1}H$ homo- and $^{1}H,^{13}C$ heteronuclear 2D NMR experiments, recorded by dissolving glycans in D_2O. $^{1}H,^{1}H$ COSY and $^{1}H,^{1}H$ TOCSY experiments were used to disclose the protons of each spin system, while carbon atoms were identified through $^{1}H,^{13}C$ HSQC. The HSQC spectrum presents one anomeric signal at 5.19 ppm, that was labelled with the capital letter A (Fig. 47).

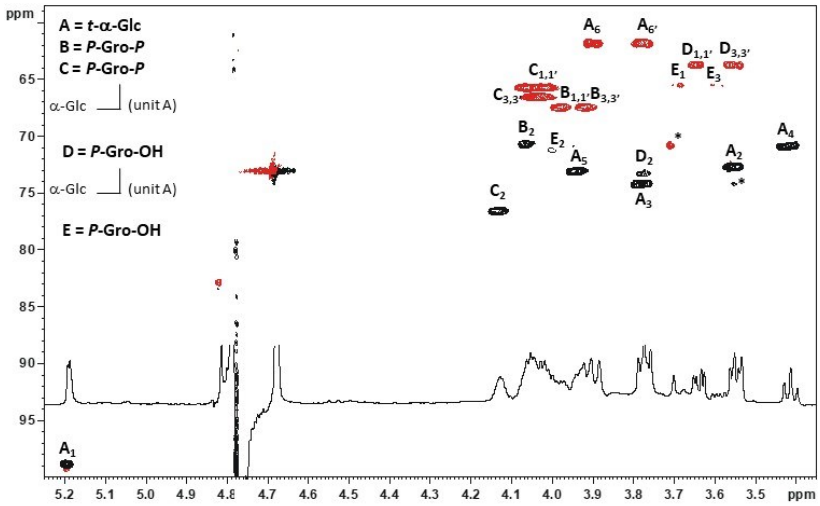

Figure 47. (600 MHz, 298 K, D2O) HSQC spectrum of the teichoic acid isolated from *B. subtilis*, along with the proton profile and the structure. Letters refer to the carbohydrate residues as reported in figure and arabic numerals refer to the proton/carbon atoms of the respective residue. Red densities represent the –CH2 groups. Signals marked with (*) are due to minor impurities.

Table 7. NMR chemical shifts of the *B. subtilis* glycan-1, measured at 600 MHz, 298 K, in D_2O.

Residue	**1**	**2**	**3**	**4**	**5**	**6**
A	5.19	3.55	3.78	3.42	3.94	3.90-3.78
t-α-Glc*p*	*99.03*	*72.8*	*74.19*	*70.89*	*73.14*	*61.8*
B	3.92	4.06	3.98			
P*-Gro-*P	*67.4*	*70.7*	*67.3*			
C	4.03	4.13	4.03			
P*-(Glc*p*)-Gro-*P	*66.5*	*76.6*	*65.7*			
D	3.65	3.77	3.54			
***P*-(Glc*p*)-Gro-OH**	65.5	73.3	63.7			
E	3.68	4.0	3.65			
***P*-Gro-OH**	65.5	71.2	63.7			

In the TOCSY spectrum (Fig. 48b) it has five correlations, with that at 3.55 ppm in common with the COSY spectrum. Hence, this density was assigned to H-2, and by a similar approach H-3 (3.78 ppm), H-4 (3.42 ppm), H-5 (3.95) and H-6,6' (3.90-3.78). This TOCSY pattern is typical of a gluco-configured sugar, and this information, along with the chemical shift values from literature (Speciale et al., 2022), led to identifying A as a terminal α-glucose. Finally, the study of the HMBC spectrum allows to identified residues B, C, D and E (Fig. 48a) as, respectively, a free linked 1,3-polyglycerol phosphate, a 2-linked 1,3-glycerol phosphate,

a 2-linked 1-phosphate terminal glycerol and a free 1-phosphate terminal glycerol. Chemical shift values of these residues (Tab. 7) matched with those reported in literature (De Boer et al., 1976) (Kozlova et al., 1999). Since the intensities of the signals relating to residues D and E are lower than those of the signals of B and C, they could represent chain terminators or fragments of chain hydrolyzed during the various extraction and purification procedures.

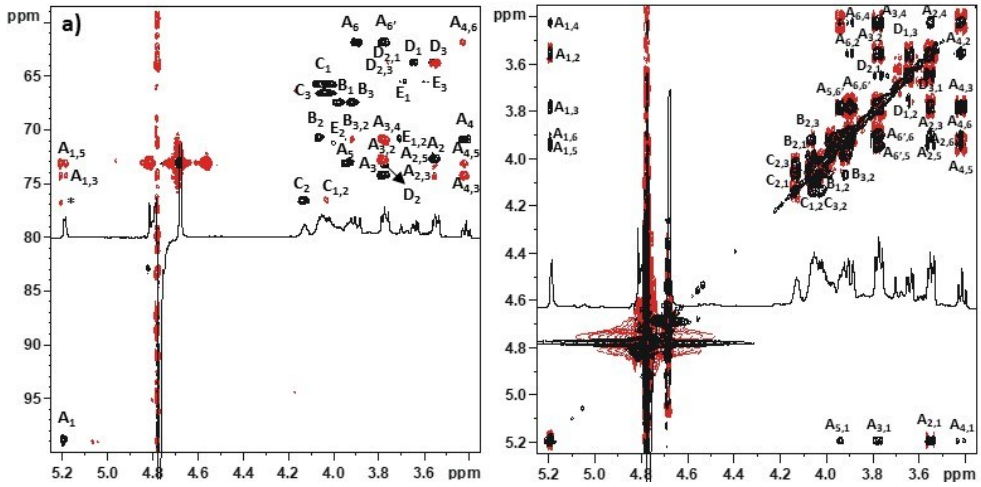

Figure 48. a) (600 MHz, 298 K, D_2O) $^1H,^{13}C$ HMBC spectrum in red and $^1H,^{13}C$ HSQC spectrum in black of the teichoic acid produced by *B. subtilis*. Signal marked with (*) is due to a minor impurity; b) (600 MHz, 298 K, D_2O) $^1H,^1H$ COSY spectrum in red and $^1H,^1H$ TOCSY spectrum in black of the teichoic acid produced by *B. subtilis*. In both panels, letters refer to carbohydrate residues as defined in Tab. 7, and arabic numerals to the atoms of the respective residues.

In conclusion, the main signals of the NMR spectra belong to the polygro-type polymer. The backbone of this polymer is made of polyglycerolphosphate, 1,3-linked (unit B and C); the position 2 of some of these Gro units is further substituted with a α-Glc (unit A). By integration of the B2 vs C2 densities in the HSQC spectrum (Fig. 47), it has been possible to evaluate the free-Gro vs the "linked Gro" ratio, that is 36%.

2.4.3 2D NMR structural studies of *B. subtilis* glycan-2

The structure of *B. subtilis* glycan-2 was determined by analysing $^1H,^1H$ homo- and $^1H,^{13}C$ heteronuclear 2D NMR experiments, recorded by dissolving glycans in D_2O. $^1H,^1H$ COSY and $^1H,^1H$ TOCSY experiments were used to disclose the protons of each spin system, while carbon atoms were identified through $^1H,^{13}C$ HSQC and further confirmed by $^1H,^{13}C$ HSQC-TOCSY. Lastly, the primary sequence was inferred by analysing the inter-residue and long-range dipolar and scalar correlations from $^1H,^1H$ T-ROESY and $^1H,^{13}C$ HMBC spectra, respectively.

The HSQC spectrum presents two main anomeric signals between 5.5-4.6 ppm, a crowded carbinolic region (4.4-3.3 ppm), and a N-acetyl signal at 2.05 ppm (Fig. 49b). The anomeric signals were labeled with a capital letter (A-B, Fig. 49, Tab. 8) and NMR analysis started from residue A, whose anomeric proton (5.49 ppm) displays three correlations in the TOCSY spectrum (Fig. 50), typical of a galactose. The attribution of the overall following proton and carbon atoms of the residue was completed by analysing COSY and HSQC-TOCSY correlations. Moreover, the chemical shift value of A2 is at 49.8 ppm in the HSQC spectrum, suggesting the presence of an amino group in this position, and the comparison of the carbon chemical shift values read on the HSQC spectrum with those reported in literature, confirms that residue A is a 3-substituted galactosamine α-configured at the anomeric centre, as also confirmed by its $^{3}J_{H1,H2}$ coupling constant value, which is 2.7 Hz. (Speciale et al., 2022).

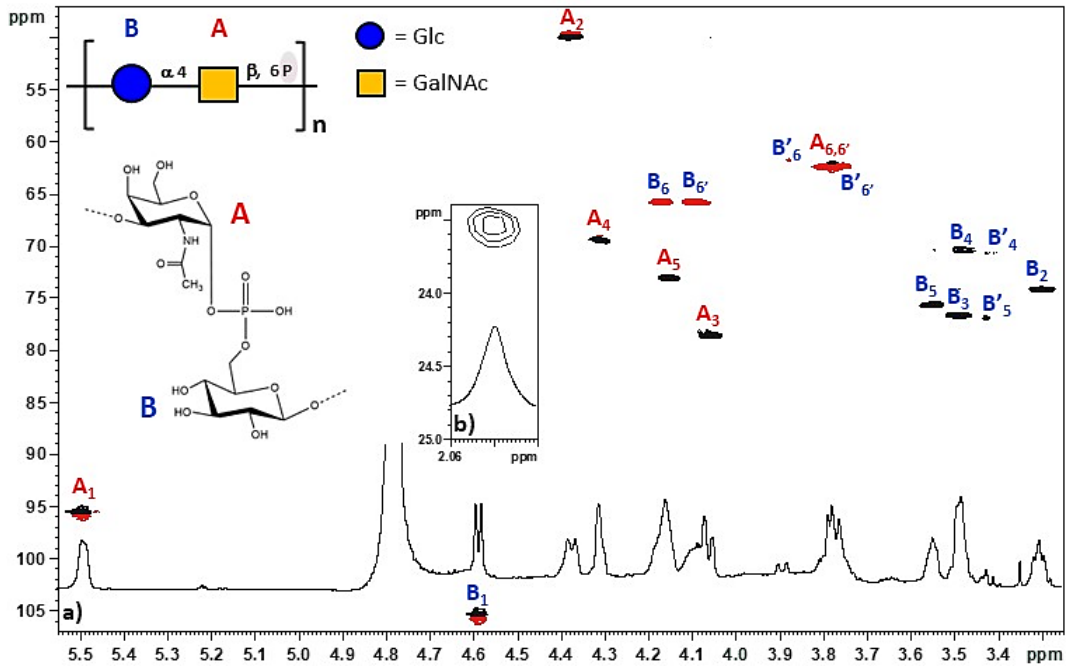

Figure 49. Expansion of the HSQC spectrum (600 MHz, 298 K, D_2O) of: a) glycan-2 isolated from *B. subtilis*, along with the proton profile and the structures. Red densities correspond to –CH2 carbons; b) N-acetyl signal (2.05 ppm) of the galactosamine (residue A). Letters refer to the carbohydrate residues as reported in figure and drawn according to the symbolic nomenclature for glycans. All monosaccharides are in the pyranose form. Arabic numerals refer to the proton/carbon atoms of the respective residue.

Table 8. NMR chemical shifts of the *B. subtilis* glycan-2, measured at 600 MHz, 298 K, in D_2O.

Residue	1	2	3	4	5	6
A	**5.50**	4.38	4.06	4.31	4.16	3.77 X 2
3-α-D-Gal*p*NAc-1*P*	*95.6*	*49.9*	*78.5*	*69.5*	*73.1*	*62.2*
B	4.58	3.30	3.47	3.44	3.57	4.09-4.17
6-β-D-Glc*p*	*105.5*	*74.2*	*76.7*	*70.8*	*75.6*	*65.7*
B'	4.58	3.30	3.47	3.42	3.43	3.73-3.88
6-β-D-Glc*p*-OH	*105.5*	*74.2*	*76.7*	*70.6*	*76.9*	*61.7*

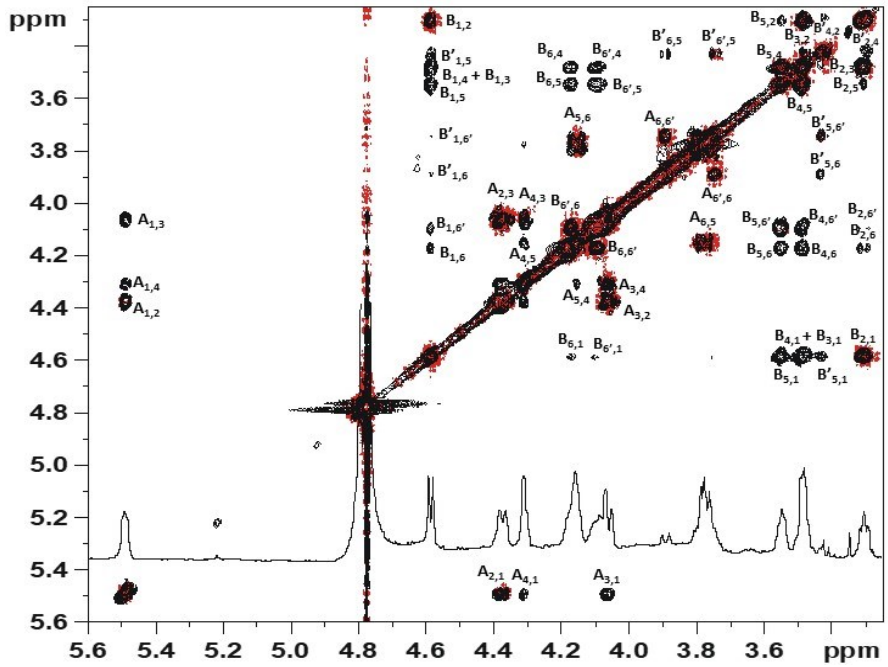

Figure 50. COSY (in red) overlapped with TOCSY (in black) spectrum (600 MHz, 298 K, D_2O) of the glycan-2 from *B. subtilis* 168. Labels refer to Tab. 8 and arabic numerals refer to the proton atoms of the respective residue.

Finally, the H-1 signal has a peculiarity: it appears like a double doublet, with an additional J of about 7 Hz. This is diagnostical of the presence of a phosphate as a substituent of the monosaccharide residue, scalarly coupled to the proton geminal to the site of attachment with a coupling constant $^3J_{P,H}$ ~ 5-7 Hz, as noted by the multiplicity observed for that proton. In agreement with this, C-1 of A (95.6 ppm) has a downfield shift of about 3 ppm with respect the value reported for the non-substituted glycoside (Speciale et al., 2022). Also the C-6 of the residue B has the almost same downfield shift in respect to the standard C-6

chemical shift values reported in literature for a free-linked glucose, suggesting that the position C-1 of A is linked to the position C-6 of B.

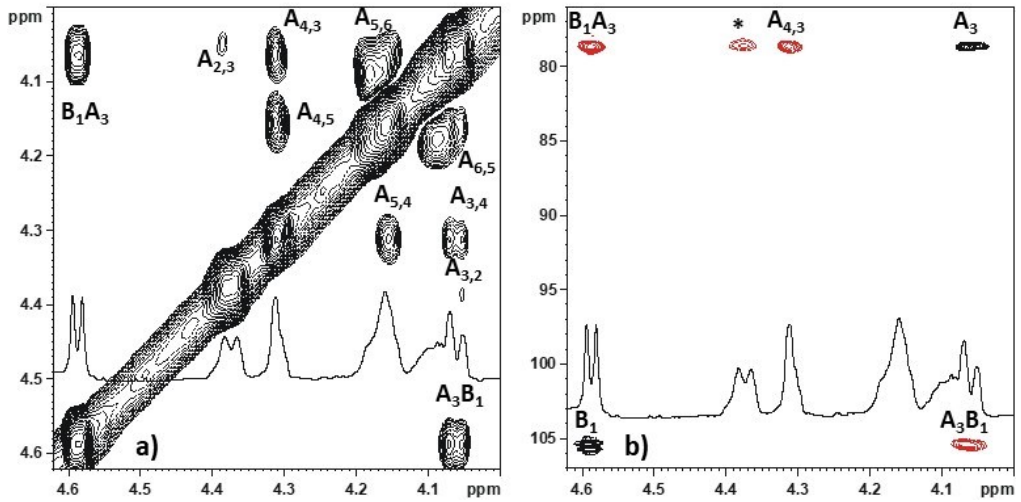

Figure 51. Expansion of: a) T-ROESY spectrum of the glycan-2 from *B. subtilis* 168 (600 MHz, 298 K, D_2O); b) HMBC spectrum (in red) plus HSQC spectrum (in black) of the glycan-2 from *B. subtilis* 168 (600 MHz, 298 K, D_2O). Signal marked with (*) is due to a COSY artifact. In both panels, labels refer to Tab. 8.

Moreover, the T-ROESY (Fig. 51a) and HMBC (Fig. 51b) spectra show the correlations between the C-3 of A (78.6 ppm) and the C-1 (105.5 ppm) of B. Full attribution of the chemical shifts of the residue B was performed by analysing COSY and TOCSY spectra. The anomeric proton (4.59 ppm) of B shows six TOCSY correlations, with that at 3.30 ppm in common with the COSY spectrum (Fig. 50). Hence, this density was assigned to H-2, and by a similar approach H-3 (3.49 ppm), H-4 (3.48 ppm), H-5 (3.56 ppm) and H-6,6' (4.09-4.17 ppm). This TOCSY pattern is typical of a gluco-configured sugar, and this information, along with the chemical shift values consistent with those reported in literature (Speciale, I., Notaro, A., et al. 2022), led to identifying B as a 6-substituted α-glucose, with a typical $^3J_{H1,H2}$ coupling constant value of 8.0 Hz. Finally, in the HSQC spectrum there are other four signals of minor intensities related to the C-4 (70,7 ppm), C-5 (76.9 ppm) and C-6 (61.7 ppm) of the unit B' (Fig. 49, Tab. 8), which would be the residue B not-substituted in position C-6. This unit can probably be seen by NMR spectroscopy because it is the chain terminator of a low molecular weight polysaccharide, namely of the glycan-2 (see next paragraph 2.4.5). The proton sequence of the unit B' was assigned by COSY and TOCSY spectra (Fig. 50), and confirmed by comparing chemical shift values with those reported in literature for the glucose methyl glycoside (Speciale et al., 2022). The assignments of all residues was further confirmed by the information from the T-ROESY (Fig. 51a) and the HSQC-TOCSY (Fig. 52)

spectra, respectively, yielding to the definition of the repeating unit of this capsular polysaccharide (inset in Fig. 49a).

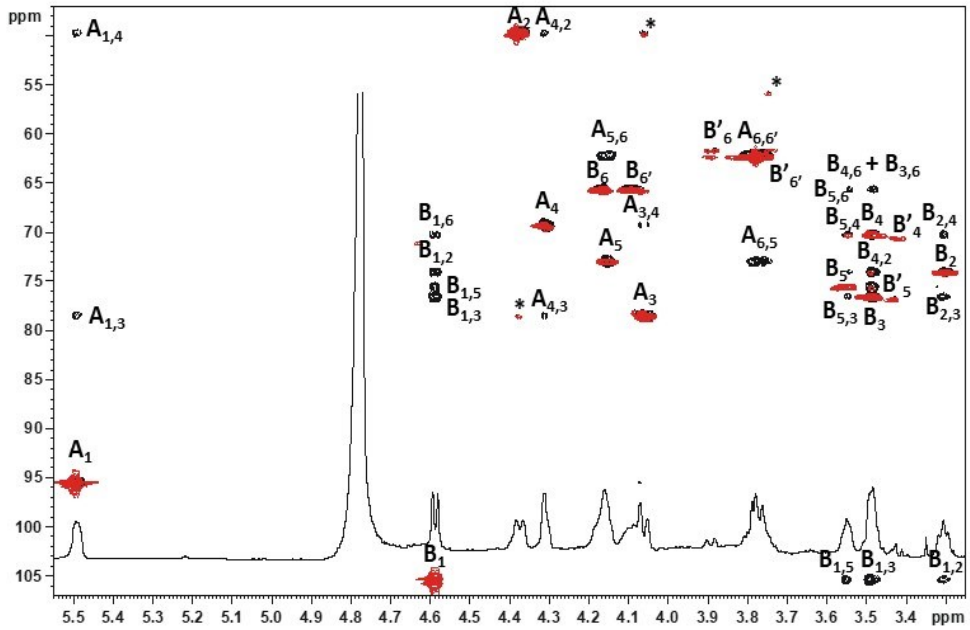

Figure 52. HSQC (in red) overlapped with HSQC-TOCSY (in black) spectrum (600 MHz, 298 K, D2O) of the glycan-2 from *B. subtilis* 168. Labels refer to Tab. 8 and arabic numerals refer to the proton/carbon atoms of the respective residue. HSQC signals marked with (*) are due to COSY artifacts or minor impurities.

2.4.4 Determination of the absolute configuration of *B. subtilis* glycan-2 through GC-MS studies

The absolute configuration of the residues belonging to the repeating unit of the glycan-2 (GalNAc and Glc), was inferred by deriving them into acetylated-octyl glycosides (OAG) by using an optically pure alcohol (2-(-)-octanol) (De Castro et al., 2010) and by comparing their retention time with that of the reference compounds (Fig. 53b and 53d). Hence, from this type of analysis it emerged that all sugars of the *B. subtilis* CPS (glycan-2) are D-configured (Fig. 53a and 53c).

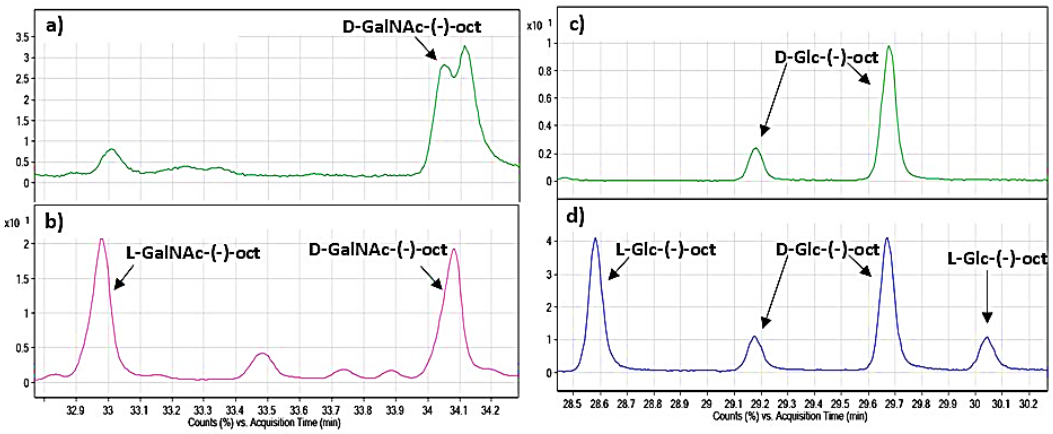

Figure 53. Absolute configuration of residues as determined by the O-octylglycoside derivatives method. In panels a) and c) are reported profiles obtained from monosaccharides of *B. subtilis* CPS; panels b) and d) show the chromatographic standard profiles of GalNAc and Glc, respectively.

2.4.5 Molecular weight evaluation of *B. subtilis* glycans

I performed the analysis by using the HPLC instrument equipped with a TSK-GPW5000 column, eluted in 50 mM ammonium bicarbonate at flow 0.8 mL/min. I calculated the molecular weight of the samples reported in Tab. 9, based on the calibration parameters of the column (Fig. 54a), which gave the following equation: LogMW = -0,71Vr+10.9, with Vr = retention volume. The chromatographic profile of the obtained compounds are reported in fig. 54b and 54c. Note that both chromatographic peaks (the one related to Leon/1/A, namely the *B. subtilis* CPS, and to Leon/2/C1, namely the *B. subtilis* TA) are not homogeneous, probably due to the presence of the acidic phosphate groups in the polymer chain, which can cause interference during elution.

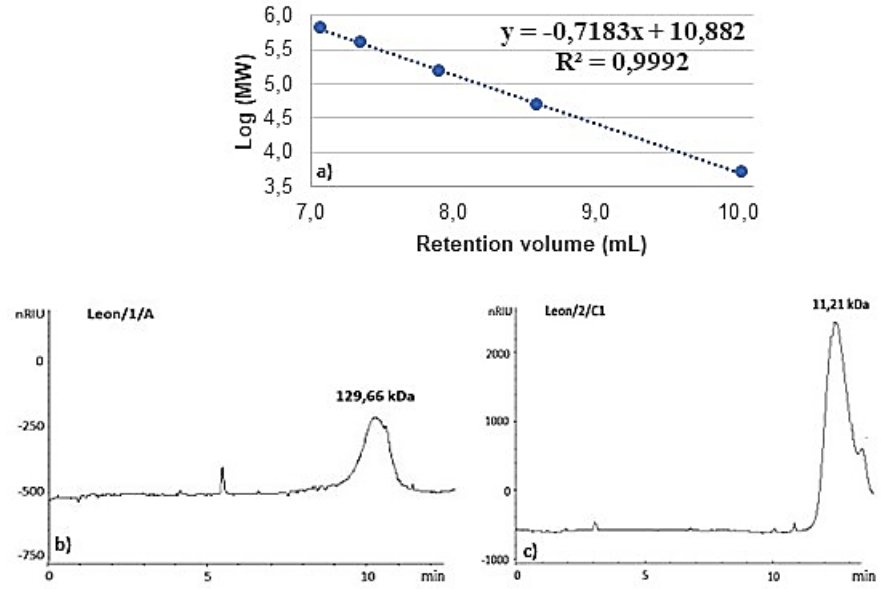

Figure 54. a) Calibration curve of TSK-GPW5000 column with different dextran standard of a known molecular weight, along with the line equation. R^2 indicates the degree of correspondence between the estimated values for the trend line and the actual values. A trendline is most accurate when its R^2 value is equal to 1. b) Chromatographic profile of *B. subtilis* teichoic acid (glycan-1, Leon/1/A); c) chromatographic profile of *B. subtilis* CPS (glycan-2, Leon/2/C1).

Table 9. MW calculated for *B. subtilis* glycans.

Sample	tr (min)	Vr (mL)	Log (MW)	MW (Da)	MW (kDa)
Teichoic acid	10,04	8,032	5,113	129662,503	130
Capsule	11,89	9,512	4,050	11213,220	11

2.4.6 Biological assays

Arabidopsis infiltration assays were performed by leaf puncture with *B. subtilis* glycans at different concentrations, in order to see if they could trigger any plant inflammatory response. The leaves were the whole living bacterium was injected were considered as positive control as wilting was observed in them (Fig. 55a), symptom of a hyperinflammatory response. As negative control was used a solution of 10 mM $MgCl_2$ (Fig. 55b). Finally, it was discovered that the teichoic acid (glycan-1) of *B. subtilis* 168, in a concentration range from 100 ng to 100 mg/mL, is able to cause a leaf wilting in the Arabidopsis plant (Fig. 55c). Instead, at lower concentrations (10-1 ng/mL), the compound does not cause any phenotype change in the leaf (Fig. 55c). On the other hand, as for the

bacterium capsular polysaccharide (glycan-2), it did not give any visible change in the Arabidopsis leaf in the total range of concentrations used (1 ng-100 mg/mL), (Fig. 55d).

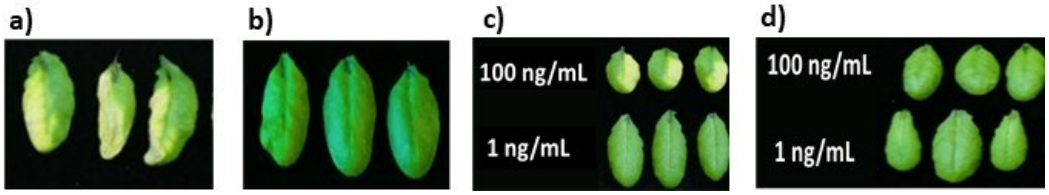

Figure 55. Arabidopsis infiltration assays. a) positive control: leaf wilting consequently to the injection on *B. subtilis* OD600=0.02; b) negative control: no leaf wilting consequently to the injection of a solution of $MgCl_2$ 10 mM; c) leaf wilting concentration dependent: not observed after the injection of a solution of 1 ng/mL of *B. subtilis* 168 teichoic acid, while it was observed at 100 ng/mL; d) no leaf wilting observed, at any concentration of *B. subtilis* 168 capsular polysaccharide used (1-100 ng/mL).

Therefore, the ability of *B. subtilis* to activate plant immune defenses can be attributed to its teichoic acid, which can be considered as a pathogen-associated molecular pattern molecule (PAMP), recognized by the cell surface plant related receptors (PRR). This interaction could activate a whole series of cascading signaling events within the plant cell that would result in a final inflammatory response. However, this effect appears to be dose-dependent, suggesting that at low concentrations pure teichoic acid isolated from the bacterium could be used to activate the plant's defenses against the invasion of pathogens, with a consequent advantage for agricultural production.

2.5. Structural characterization and immunomodulatory activity of *Ruminococcus gnavus* glycans

R. gnavus type strain ATCC 29149 harbours an EPS, glucorhamnan-I (Fig. 56c), previously reported to be secreted in the growth medium (Henke et al., 2019). In this study, by following several procedures of extraction, purification, and structural characterization, I have shown that a different EPS, named glucorhamnan-II, is instead produced by other two *R. gnavus* strains, ATCC 35913 and E1. Both these two types of EPS have a rhamnan backbone (Fig. 56a and 56b), but of different length: three rhamnose units in that of the type strain and four in that of ATCC 35913 and E1. Moreover, both EPSs present a rhamnose unit 2,3-linked with a branch placed onto O-2, which for the type strain is a α-D-Glc-(→6)-α-D-Glc disaccharide (Fig. 56c) (Henke et al., 2019), while in ATCC 35913 (Fig. 56b) and E1 (Fig. 56a) it is a terminal β-Glc unit. From the structural point of view, the EPS from *R. gnavus* 35913 and E1 present a novel structure, not previously reported in the CSDB database.
Finally, Prof. Nathalie Juge's research team from Quadram Institute Bioscience carried out biological assays on these three different *R. gnavus* strains and their EPS, with the aim to evaluate their immunological activity. The obtained data show that it may vary depending on the considered strain and its related cell surface glycans.

2.5.1. Polysaccharides extraction

To avoid any contamination from the growth medium components, the isolation of EPS from the type (ATCC 29149) and from the ATCC 35913 and E1 strains started from the cells, by assuming that EPS is loosely bound on the bacterial surface, likely through a phosphodiester linkage. Accordingly, the LTA was first removed from the biomass by treatment with *n*-butanol (Vinogradov et al., 2015a), and then the resulting pellet was suspended in aqueous HF to break selectively the phosphodiester linkage. The comparison of the three ^{1}H NMR profiles denoted that the EPS from E1 and 35913 (glucorhamnan-II) strains is different from that of the type strain 29149 (glucorhamnan-I, Fig. 56c). Further structural investigation was done on EPS from the strain 35913 since, although equal to the profile of the EPS of the strain E1, it was cleaner, especially in the regions of the acetyl (about 2.0 ppm) and methyl (about 1.o ppm) groups of the protonic spectrum.

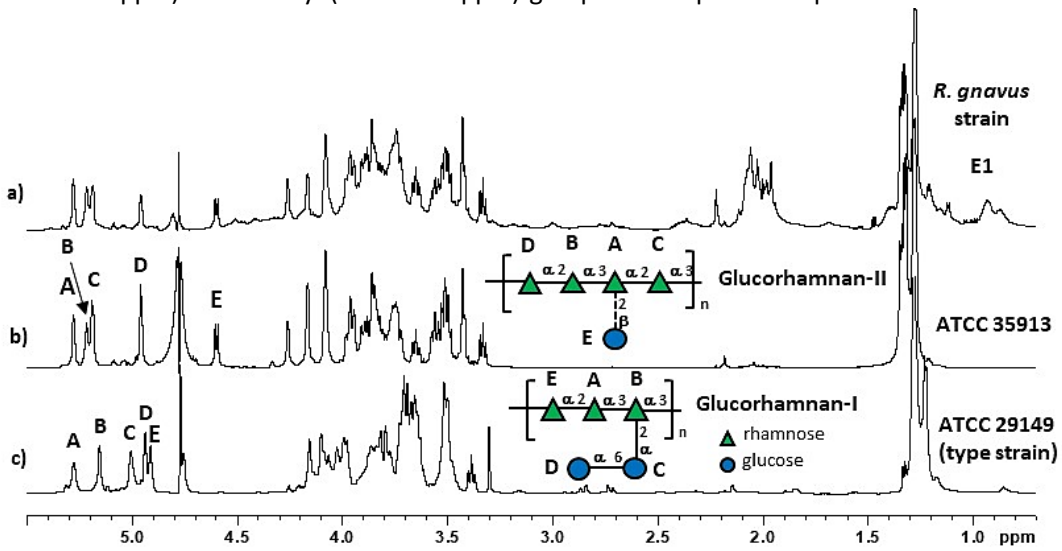

Figure 56. (600 MHz, 298 K, D_2O) ^{1}H NMR spectra of the EPS isolated by HF treatment of the bacterial cells from *R. gnavus*: a) strain E1, b) ATCC 35913, and c) ATCC 29149. The structures of the EPS of *R. gnavus* type strain or glucorhamnan-I, and of ATCC 35913 (glucorhamnan-II) are reported above the corresponding proton spectra. For glucorhamnan-II, letters refer to carbohydrate residues as defined in Tab. 10, while for glucorhamnan-I are used to indicate the different anomeric protons. All monosaccharides are in the pyranose form.

2.5.2. NMR structural characterization of the EPS from *R. gnavus* ATCC 35913

The structure was determined by analyzing the complete set of homo- and heteronuclear 2D NMR experiments (COSY, TOCSY, NOESY, ^{1}H-^{13}C HSQC, ^{1}H-^{13}C HMBC). The spin system of each residue was assigned by interpretation of the COSY and TOCSY spectra, while ^{1}H,^{13}C HSQC spectrum was used to assign the carbon chemical shift values. Attributions were counterchecked or completed using the other spectra recorded. The ^{1}H,^{13}C HSQC spectrum (Fig. 57) presented five main anomeric signals at 5.3 - 4.5 ppm, a crowded carbinolic region

(4.3-3.3 ppm) and a group of methyl signals at ca. 1.3 ppm, attributed to the different rhamnose units. The five anomeric signals were labeled with a capital letter (A-E, Fig. 57, Tab. 10) and NMR analysis started from residue A, whose anomeric proton (5.28 ppm) displayed only one correlation in the TOCSY spectrum (Fig. 58), on the contrary, H-2 (4.26 ppm) correlated with other two protons of the unit, H-3 and H-4, whose sequence was inferred by analyzing the COSY correlations. Then, H-4 (3.65 ppm) led to the identification of H-5 (3.77 ppm), that in turn had a correlation with H-6, a methyl group at 1.31 ppm (Tab. 10, Fig. 56b). This pattern is diagnostic of a rhamnose residue, and integration with the carbon chemical shift values determined from the HSQC spectrum identified this residue as α configured at the anomeric center because of the similarity between its C-5 value (70.6 ppm) with that reported for the reference glycoside (69.4 ppm) and 2,3-substituted due to the glycosylation shift at low fields detected for the corresponding carbon atoms.

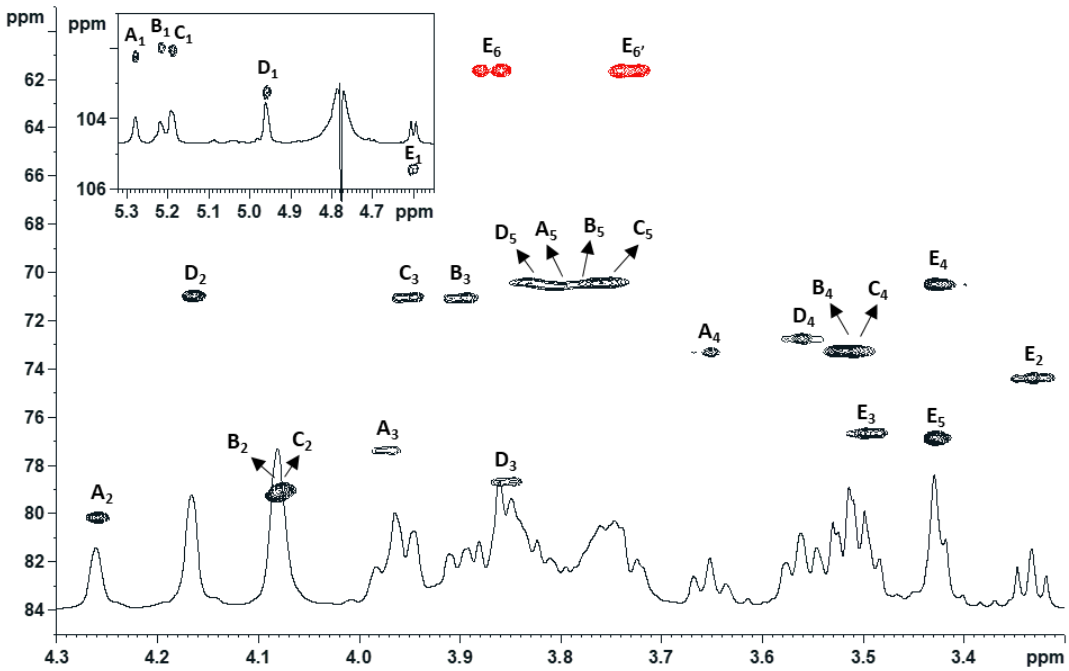

Figure 57. (600 MHz, 298 K, D_2O) HSQC spectrum of the EPS produced by *R. gnavus* strain. Letters refer to carbohydrate residues as defined in Tab. 10, and the arabic numerals to the protons in the respective residues.

Table 10. (600 MHz, 298 K, D_2O) Proton (^1H) (plain text) and carbon (^{13}C) (italic) NMR chemical shifts of the EPS from *R. gnavus* ATCC 35913 strain.

Residue	1	2	3	4	5	6
A	5.28	4.26	3.98	3.65	3.77	1.28
2,3-α-L-Rha*p*	*102.4*	*80.3*	*77.6*	*73.5*	*70.6*	*17.7*
B	5.22	4.07	3.90	3.52	3.81	1.35
2-α-L-Rha*p*	*102.1*	*79.1*	*71.2*	*73.4*	*70.7*	*17.7*
C	5.19	4.08	3.96	3.52	3.84	1.32
2-α-L-Rha*p*	*102.2*	*79.3*	*71.2*	*73.4*	*70.6*	*17.7*
D	4.96	4.17	3.86	3.56	3.76	1.28
3-α-L-Rha*p*	*103.4*	*71.1*	*78.8*	*72.9*	*70.6*	*17.7*
E	4.60	3.33	3.50	3.42	3.43	3.87-3.73
t-β-D-Glc*p*	*105.6*	*74.6*	*76.8*	*70.7*	*77.0*	*61.8*

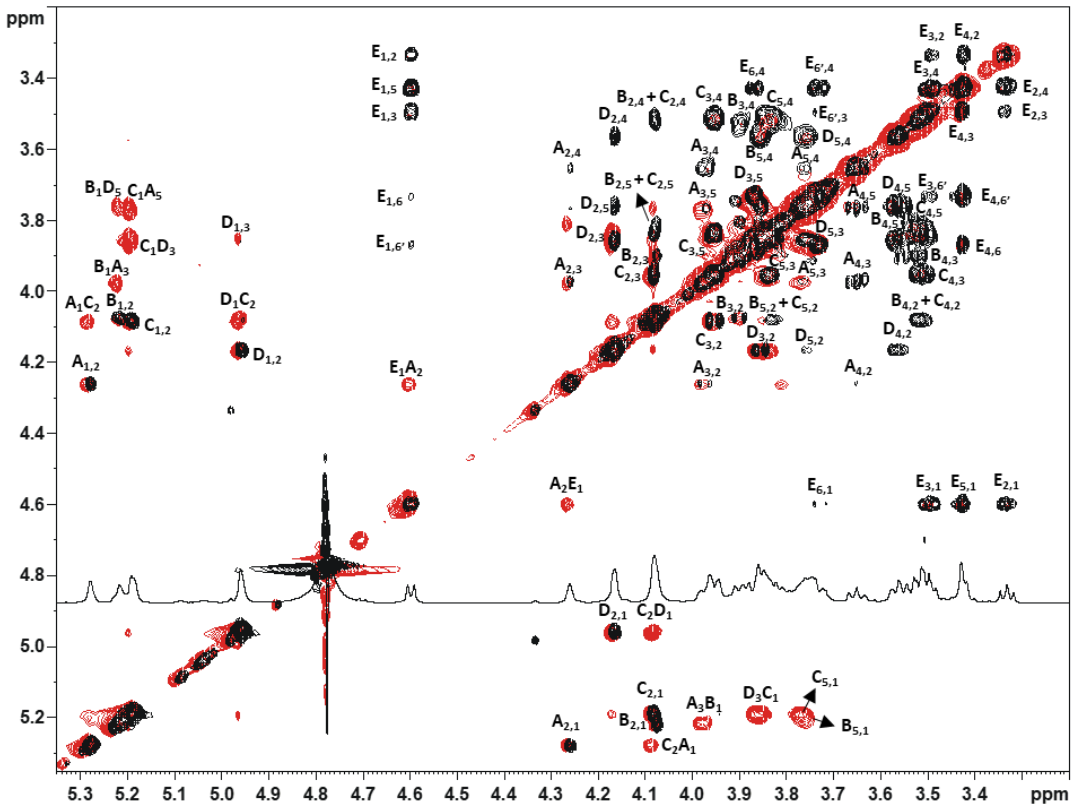

Figure 58. (600 MHz, 298 K, D_2O) Expansion of the TOCSY (black) and NOESY (red) spectra of the EPS produced by *R. gnavus* ATCC 35913. Letters refer to carbohydrate residues, as defined in Tab. 10, and the arabic numerals to the protons in the respective residues.

The analysis of the HMBC spectrum (Fig. 59) showed three connections for the anomeric proton of A, two *intra*-residual correlation with A-3 (77.6 ppm) and A-5 (70.6 ppm), and an *inter*-residual correlation with a signal at 79.3 ppm, later identified as C-2 of C.

Full attribution of B, C and D chemical shifts was performed by using the same strategy discussed for A, and it was found that they were all α rhamnose units (with a $^{3}J_{H1,H2}$ coupling constant value around 3 Hz), 2-linked in the case of B and C, and 3-substituted in the case of D (Tab. 10). The analysis of the HMBC spectrum (Fig. 59) showed that the anomeric proton of B had two *intra*-residue correlations, namely with its own H-3 (71.2 ppm) and B-5 (70.7 ppm) and one with a signal at 77.6 ppm, identified as C-3 of A.

Identification of the substituent linked to O-2 of B was possible by analyzing the HMBC spectrum, which connected C-2 of B with C-1 of D (Fig. 59). As for the residue C, the HMBC spectrum displayed the correlation of the anomeric proton with the position C-3 (78.8 ppm) of the residue D.

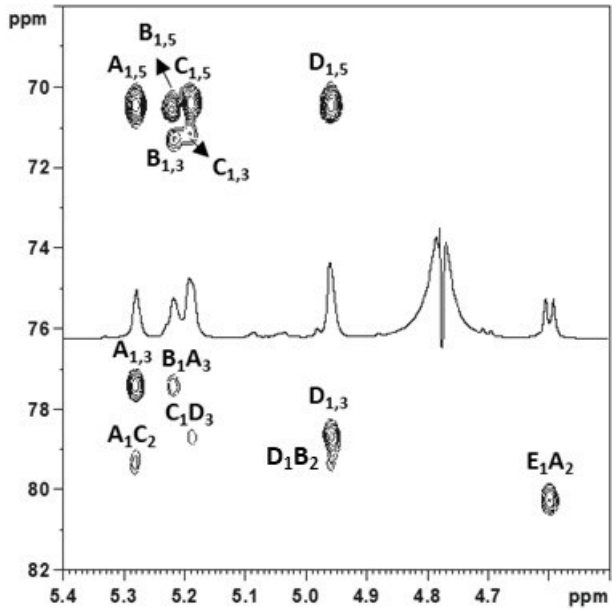

Figure 59. (600 MHz, 298 K, D_2O) expansion of the $^{1}H,^{13}C$ HMBC spectrum of the EPS produced by *R. gnavus* ATCC 35913. Letters refer to carbohydrate residues as defined in Tab. 10, and the arabic numerals to the protons in the respective residues.

The anomeric proton of E (4.60 ppm) displayed several correlations in the TOCSY spectrum (Fig. 58), a pattern diagnostic of a glucose residue, and combining the analysis of the TOCSY and COSY spectra with those of the HSQC spectrum, it was possible to determine that E was a β configured terminal glucose, in agreement with the carbon chemical shifts reported in literature for the methylglycoside, and with its $^{3}J_{H1,H2}$ coupling constant value of 8.1 Hz.

Finally, the HMBC spectrum indicated that E was linked to O-2 (^{13}C at 80.3 ppm) of the residue A, as confirmed by the equivalent correlation in the NOESY spectrum (Fig. 58).
Taken together, the NMR data disclosed that the repeating unit of the EPS from *R. gnavus* ATCC 35913 is a branched glucorhamnan comprising a rhamnan backbone, with residue A carrying the terminal glucose unit (Fig. 56b). This glucorhamnan is termed glucorhamnan-II, to differentiate it by that produced by the type strain *R. gnavus* ATCC 29149 (Fig. 56c).
However, the integration of the anomeric signals of glucorhamnan-II from *R. gnavus* ATCC 35913 revealed that the five anomeric signals were not in a 1:1 ratio, as expected for a regular structure, while the same integration performed on the glucorhamnan from E1 returned the values expected for a regular polymer (Fig. 56a).
This discrepancy was explained by assuming that glucose was a non-stoichiometric substituent and based on this evaluation, an improved model of the structure of glucorhamnan-II was elaborated (Fig. 60c). This model assembles together two different repeats, each with four rhamnose units in the backbone and named G(+) and G(-) depending on the presence or the absence of the Glc unit, respectively, so that the G(+) repeat comprises the residues A-E, and when the Glc unit is absent, it turns into G(-). According this model, the 2,3-linked rhamnose unit (A) of G(+) becomes 3-linked in G(-) and it appears equivalent to the D residue in the NMR spectra. Regarding with the B unit in G(+), it becomes equivalent to C in the G(-) motif. Thus, when Glc is missing, the net effect in the proton NMR spectrum is an increase in the C and D units (Fig. 60a).
The integration of the anomeric signals has furnished the proportion of G(-) versus G(+), expressed as “m”, a value given by half the difference between the A and D, since two D units compose G(-) repeat. As for E1, “m” was nearly zero, meaning that the polysaccharide has a regular structure made entirely of the G(+) motif. On the contrary, the proportion between G(+) and G(-) motifs in ATCC 35913 was 1 : 0.29, which transformed in percentage indicated the 77.5% occurrence of G(+) motifs or that 77.5% the idoneous rhamnose units were glucosylated.

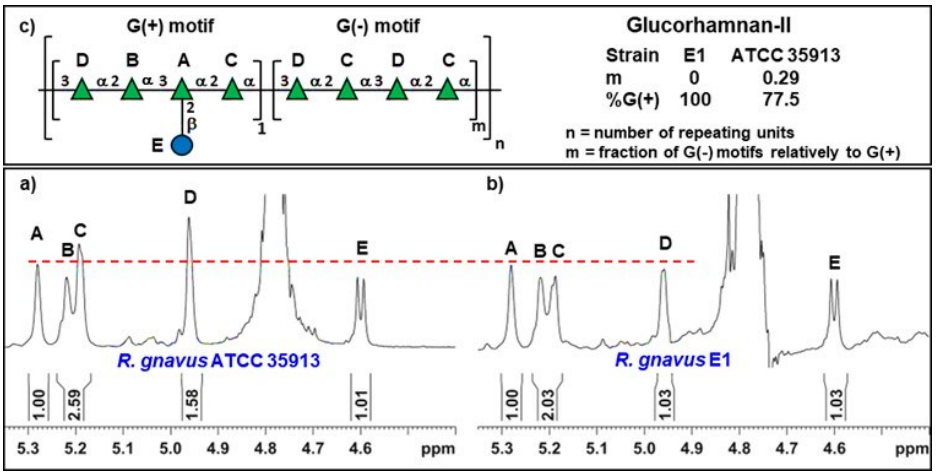

Figure 60. Integration of the anomeric region of the glucorhamnan isolated by *R. gnavus* a) ATCC 35913 and b) E1. The intensity of each spectrum is adjusted to facilitate the comparison between homologue couples of signals. In particular, a red dotted lines is place on the top of A, so that the differences between C and D units are better appreciated. Integration values are reported above the spectra scale. c) structural model elaborated for glucorhamnan-II: the relative ratio between G(-) and G(+) is expressed with the letter "m" which in turn is given by half the difference between D and A integration values.

2.5.3. GC-MS analysis on glucorhamnan-II from *R. gnavus* ATCC 35913

As for the glucorhamnan-II, monosaccharide chemical analysis detected rhamnose and glucose as main constituents, along with traces of glycerol, galactose and mannose (Fig. 61a). The linkage analysis (Fig. 61b) and the absolute configuration of the two main residues (Fig. 62a), inferred that rhamnose was linked at O-2, O-3, and both O-2 and O-3, and L-configured, while glucose was terminal and D-configured.

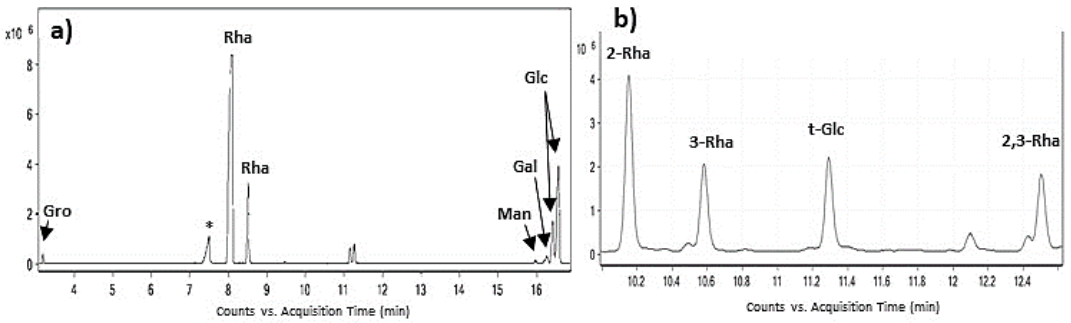

Figure 61. GC-MS chromatogram of: a) monosaccharide composition of *R. gnavus* ATCC 35913 EPS, as established by the acetylated O-methyl glycoside derivatives method. * impurity deriving by the reactives used; b) partially methylated and acetylated alditols obtained from *R. gnavus* ATCC 35913 EPS.

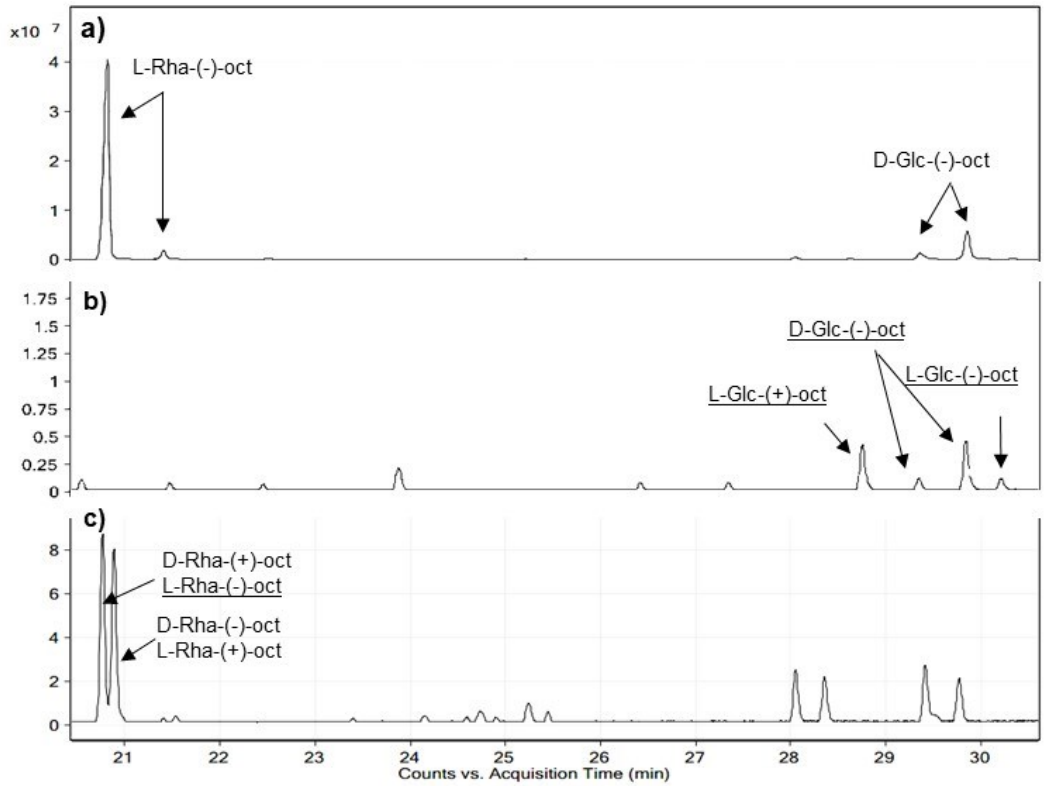

Figure 62. Absolute configuration of Rha and Glc as determined by the O-octylglycoside derivatives method. a) Profile obtained from *R. gnavus* ATCC 35913 EPS acetylated octylglycosides prepared with pure 2-(-)-octanol; b) Glc fully acetylated octylglycoside profile prepared with racemic 2-(±)-octanol; c) Rha acetylated octylglycoside profile prepared with racemic 2-(±)-octanol.

2.5.4. Molecular weight evaluation of the EPS from *R. gnavus* strains

The analysis was performed by using the HPLC instrument equipped with a TSK-GPW5000 column, eluted in 50 mM ammonium bicarbonate at flow 0.8 mL/min. The molecular weight of the samples reported in Tab. 11, was calculated based on the calibration parameters of the column (Fig. 63a), which gave the following equation: LogMW = -0,70Vr+10.71, with Vr = retention volume. The chromatographic profiles of the obtained compounds show a symmetrical peak for *R. gnavus* ATCC 35913 EPS (Fig. 63 b1), in contrast with that observed for E1 EPS (Fig. 63 b2), confirming that the glucorhamnan-II is more pure in respect to the glucorhamnan-I (as previously discussed and showed in Fig. 56)

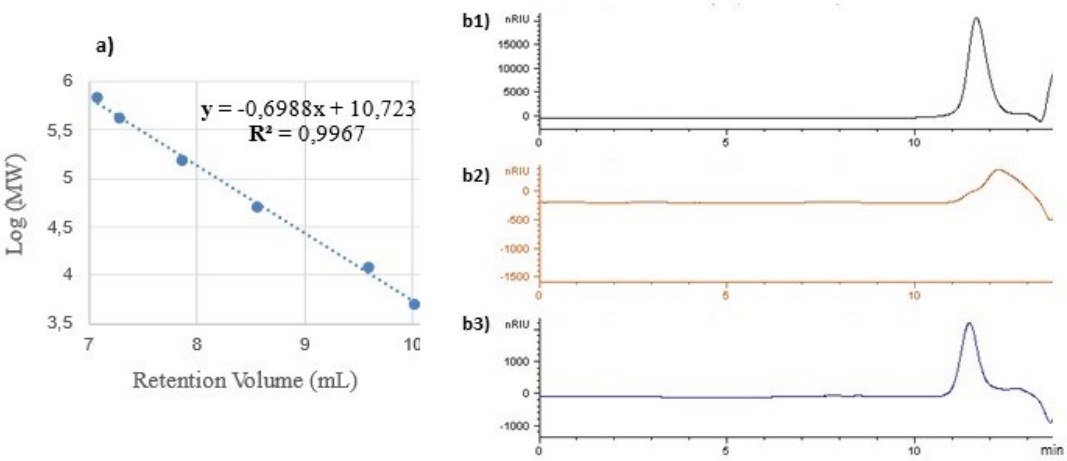

Figure 63. a) calibration curve of the column perfomed by using pullulan standards of known molecular weight (5, 12, 50, 150, 410 and 670 kDa), along with the line equation. R^2 indicates the degree of correspondence between the estimated values for the trend line and the actual values. A trendline is most accurate when its R^2 value is equal to 1. b1) HPLC chromatogram recorded for *R. gnavus* ATCC 35193 EPS; b2) HPLC chromatogram recorded for *R. gnavus* E1 EPS; b3) HPLC chromatogram recorded for *R. gnavus* type strain (ATCC 29149) EPS. In both b1), b2) and b3) panels, the distortion of the baseline after 13 min. is not reported and it is due to the spike of the solvent.

Table 11. MW calculated for EPS of *R. gnavus* strains.

Sample	tr (min)	Vr (mL)	Log (MW)	MW (Da)	MW (kDa)
***R. gnavus* ATCC 35913**	11,616	9,293	4,229	16939,97	17
***R. gnavus* E1**	12,199	9,758	3,903	7997,94	8
***R. gnavus* ATCC 29149**	11,426	9,141	4,335	21633,89	22

2.5.5. Effect of *R. gnavus* and glucorhamnan on cytokine production

The immunomodulatory properties of *R. gnavus* E1, ATCC 29149 and ATCC 35913 strains and their respective purified glucorhamnans were assessed *in vitro* by monitoring cytokine production in mBMDCs (bone marrow-derived dendritic cells). mBMDCs were incubated with *R. gnavus* ATCC 29149, ATCC 35913 or E1 strains at a MOI of 50:1 or with purified glucorhamnan (200 µg/ml) from these strains for 18 h. Thus, the production of six pro-inflammatory cytokines (TNF-α, IL-1β, IL-6, IL-12p40, CCL2 and CXCL1) was quantified by multiplex ELISA. As shown in Fig. 64, *R. gnavus* ATCC 35913 enhanced significantly more production of several pro-inflammatory cytokines in mBMDCs than the two other strains tested. On the other hand, *R. gnavus* ATCC 29149 showed 12% higher induction of CCL2 than E1, while a decreased expression of CXCL1 was observed with E1 and ATCC 29149 in

comparison with the negative control (by 13% and 14%, respectively). The purified glucorhamnans also showed strain-specific effects on cytokine production in mBMDCs. Here, the glucorhamnan from *R. gnavus* ATCC 29149 induced more production of TNF-α (by 35%), IL-6 (by 38%), CXCL1 (by 13%) and IL-12p40 (by 60%) than the glucorhamnan from ATCC 35913 and induced more production of IL-6 than the glucorhamnan from E1, while the glucorhamnan from *R. gnavus* E1 induced more production of TNF-α (by 30%), IL-6 (by 38%) and IL-12p40 (by 49%) than the glucorhamnan from ATCC 35913.

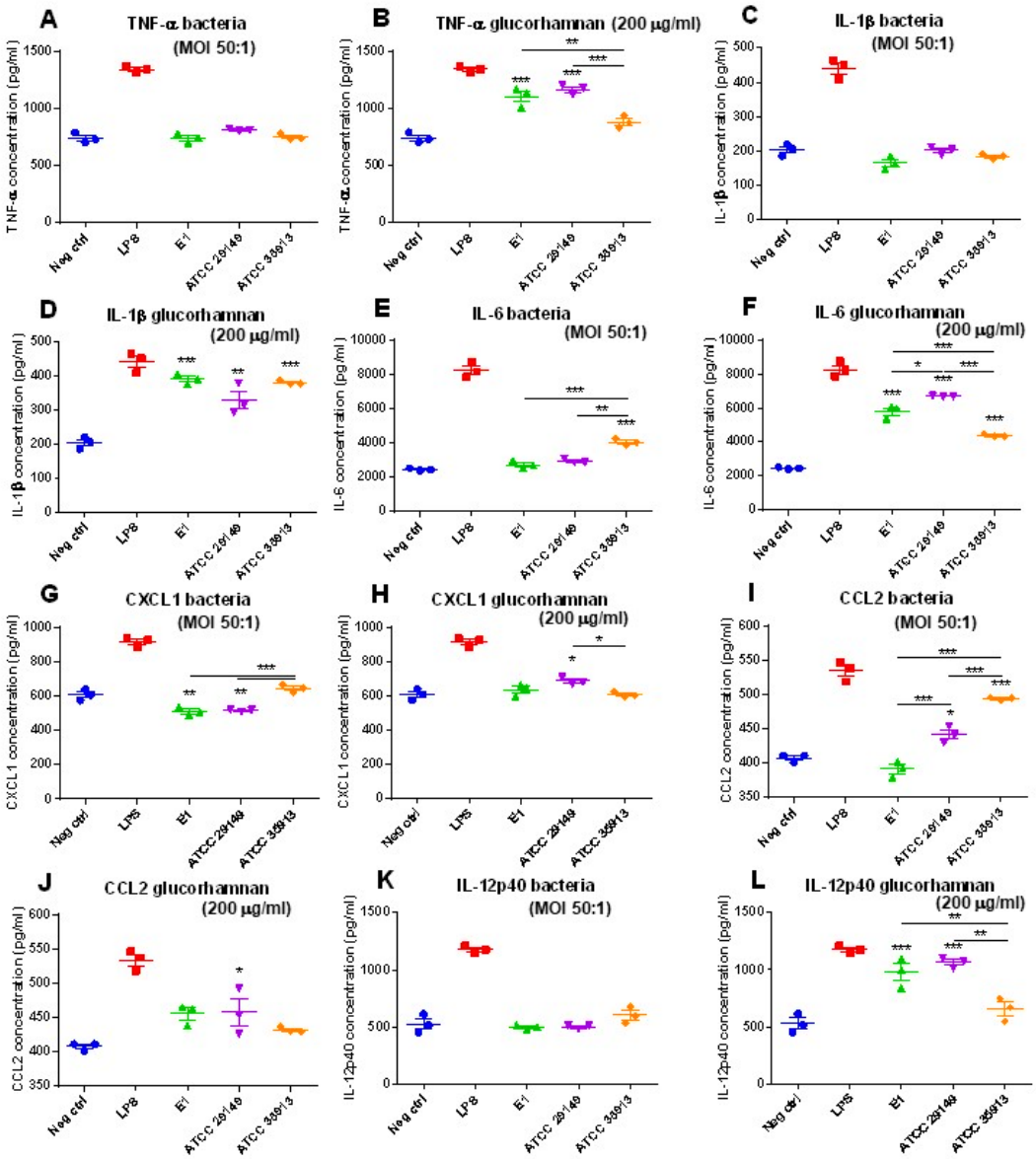

Figure 64. Production levels of: A) TNF-α following treatment with whole bacteria; B) their glucorhamnans; C) IL-1β following treatment with whole bacteria; D) their glucorhamnans; E) IL-6 following treatment with whole bacteria; F) their glucorhamnans; G) CXCL1 following treatment with whole bacteria; H) their glucorhamnans; I) CCL2 following treatment with whole bacteria; J) their glucorhamnans; K) IL-12p40 following treatment with whole bacteria; L) their glucorhamnans. Neg ctrl refers to mBMDCs cultured without bacteria or glucorhamnan. LPS from *E. coli* O111:B4 at 100 µg/ml was used as a positive control. The experiment was reproduced in 3 biological replicates. One way ANOVA was used for comparison with the negative control (* for $p<0.05$, ** for $p<0.01$, *** for $p<0.001$).

In addition, mBMDCs were incubated with *R. gnavus* ATCC 29149, ATCC 35913 or E1 strains (at MOI of 50:1) and with purified glucorhamnan (200 µg/ml) from these strains for 18 h, to see their effect on anti-inflammatory cytokine IL-10 production. This type of cytokine was, in turn, quantified by ELISA. All treatments led to IL-10 induction compared to the negative control but *R. gnavus* ATCC 35913 showing the highest induction level (Fig. 65A, 40% more than E1 and 47% more than ATCC 29149) while all glucorhamnans provided a similar level of induction compared to the strain origin (fig. 65B).

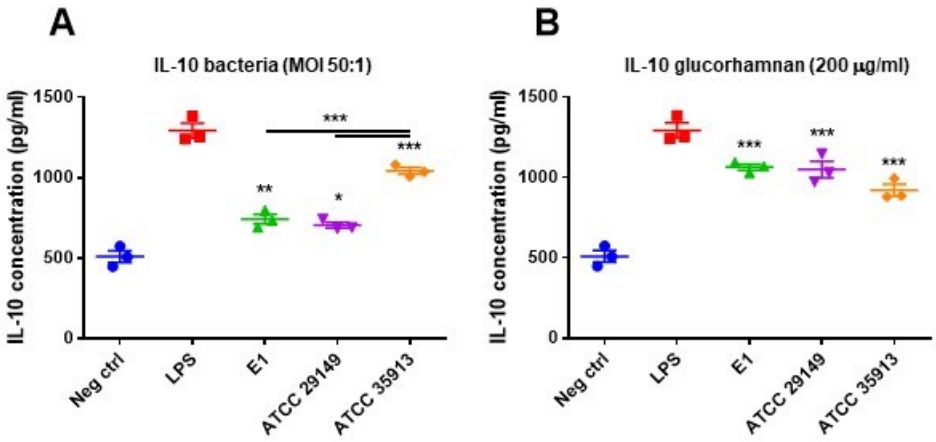

Figure 65. A) IL-10 levels after incubation with *R. gnavus* different strains. B) IL-10 levels after incubation with purified glucorhamnan from these strains. LPS from *E. coli* O111:B4 at 100 µg/ml was used as a positive control. The experiment was reproduced in 3 biological replicates. One way ANOVA was used for comparison with the negative control (* for $p<0.05$, ** for $p<0.01$, *** for $p<0.001$).

2.5.6. Role of NF-κB activation and TLR4 pathways in the interaction between *R. gnavus* and immune cells

Here, human THP1-Blue™ reporter cells were used to determine the effect of *R. gnavus* strains and associated glucorhamnans on the NF-κB signal transduction pathway. This cell line is derived from the human THP-1 monocyte cell line by stable integration of an NF-κB-inducible SEAP (secreted embryonic alkaline phosphatase) reporter construct. As a result, THP1-Blue™ NF-κB cells allow the monitoring of NF-κB activation by determining the activity of SEAP in the cell culture supernatant which can be monitored by spectrophotometry at 610 nm using QUANTI-Blue™, a SEAP detection reagent. THP1-Blue™ NF-κB cells were incubated with *R. gnavus* ATCC 29149, ATCC 35913 or E1 strains at MOI of 50:1 and with their associated glucorhamnans (100 µg/ml), for 18 h.

The results showed that *R. gnavus* ATCC 35913 strain induced the highest response in THP1-Blue™ NF-κB cells among the three *R. gnavus* strains tested (Fig. 66A). In addition, the

purified glucorhamnans from all three strains were shown to activate the NF-κB pathway in a strain-dependent manner. The glucorhamnan derived from *R. gnavus* E1 and ATCC 35913, which share the same structure, showed the same levels of activation which were significantly higher than the response generated with the glucorhamnan from ATCC 29149 (Fig. 66B).

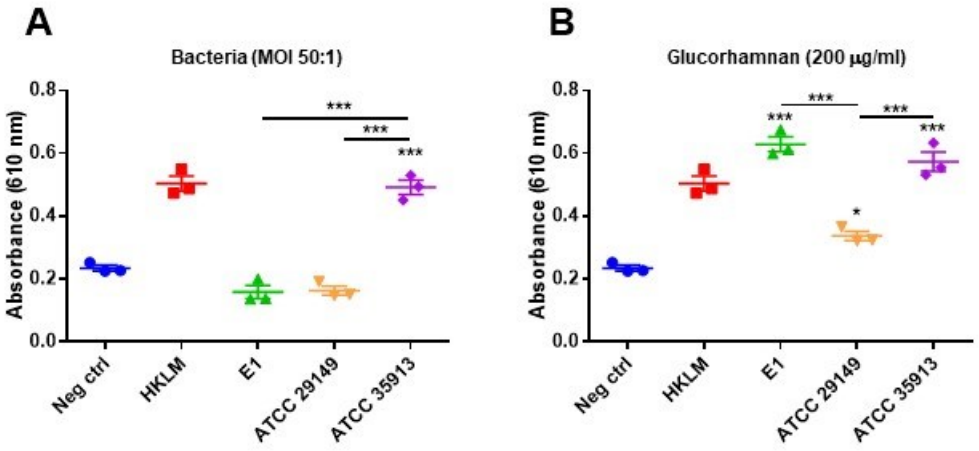

Figure 66. A) NF-κB activation after THP1-Blue™ NF-κB cells incubation with: A) *R. gnavus* ATCC 29149, ATCC 35913 or E1 strains; B) their associated glucorhamnans. HKLM (heat-killed *Listeria monocytogenes*) was used as positive control. The experiment was reproduced in 3 biological replicates. One-way ANOVA was operated in comparison with negative control (* for $p<0.05$, ** for $p<0.01$, *** for $p<0.001$).

Hence, among the three *R. gnavus* strains tested, *R. gnavus* ATCC 35913 strain and its glucorhamnan have the highest capacity to induce a NF-κB-associated immune response in monocytes, indicating, here again, that *R. gnavus* ATCC 35913 is the most immunogenic strain. The NF-κB signalling pathway in these reporter cells is dependent on *R. gnavus* interaction with PRRs (pathogen-related receptors), such as TLR4, which is known to be expressed in this cell line. Indeed, *R. gnavus* ATCC 29149 glucorhamnan induction of TNF-α and IL-6 was abrogated using mBMDCs isolated from TLR4 knockout mice (Haynie et al., 2021) (Henke et al., 2019). Since the glucorhamnans of *R. gnavus* E1 and ATCC 29149 strains induced a NF-κB response but not the whole bacteria, it may be that other compounds on *R. gnavus* cell surface of these two strains may be masking or inhibiting the interaction of glucorhamnans and PRRs.

2.6. Structural characterization and immunomodulatory activity of *Enterococcus faecium* U0317 capsular polysaccharide

I received the *E. faecium* U0317 pure CPS by Dr. Romero Saavedra's research group from Ludwig Maximilians University. Then, I structurally characterized it by GC-MS and NMR analysis, and the Saavedra's team went ahead with the glycoconjugate development and the evaluation of its immunogenic potential.

2.6.1. Identification of the strain and of its related capsular polysaccharide

Encapsulated *E. faecalis* strains are able to evade opsonophagocytosis thanks to a heteroglycan which prevents the binding of LTA-directed antibodies to their LTA (Huebner et al., 1999) (Huebner, Quaas, Krueger, Goldmann, & Pier, 2000). Employing an analogous approach, namely by targeting *E. faecalis* LTA for the capsular serotyping, the selection of the *E. faecium* specific strain and of its relative immunogenic capsular polysaccharide was performed through opsonophagocytic assays (OPA). To this end, different strains of this bacterium were tested, to see if some of them could be able to resist opsonophagocytosis meditated by antibodies that target LTA from *E. faecalis* 12030. These types of antibodies were chosen because they have been previously shown to mediate the killing of non-encapsulated enterococcal strains. Finally, among the whole strain tested, *E. faecium* U0317 showed the highest opsonophagocytic killing activity when exposed to its corresponding anti-*E. faecium* strain serum (Fig. 67a). After that, the opsonophagocytic inhibition assay was used to investigate whether the serum raised against the *E. faecium* U0317 (anti-U0317) mediated opsonophagocytosis due to antibodies directed to protein and/or polysaccharide antigens. Thus, *E. faecium* U0317 cells were pre-treated with heat, or proteinase K, or sodium metaperiodate to be subsequently used as inhibitors in an opsonophagocytic inhibition assay (OPIA). Among these treatments, only the serum treated with sodium metaperiodate-treated cells did not hinder the opsonophagocytic killing activity of the anti-U0317 serum (Fig. 67b). Sodium meta-periodate cleaves bonds between adjacent carbon atoms that contain hydroxyl groups (cis-glycols), creating two aldehyde groups and breaking the polysaccharidic chain. Therefore, these findings suggest that the primary target of antibodies in the anti-U0317 serum were polysaccharide antigens, making these antibodies valuable tools for the identification of immunogenic capsular polysaccharides.

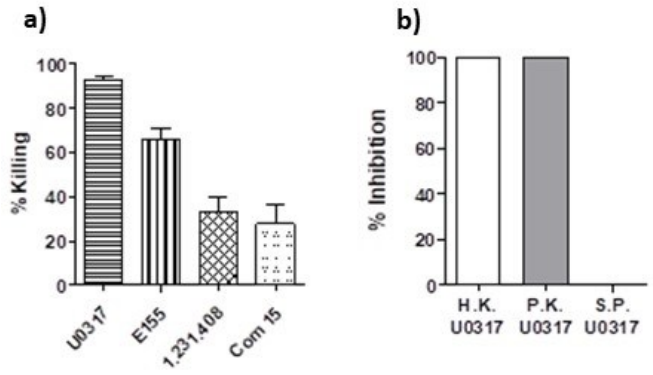

Figure 67. a) The antibodies directed to each *E. faecium* strain, shown in the x-axis, were used at 1:100 dilution. Bars represent the mean of at least three independent results and the error bars represent the standard error of the mean. b) Opsonophagocytic killing activity of anti-U0317 serum at 1:100 dilution evaluated for its ability to bind specifically cells of *E. faecium* U0317 treated with heat (H.K.), or proteinase K (P.K) or sodium metaperiodate (S.P.).

2.6.2. Polysaccharide extraction and purification

The crude cell wall polysaccharides of the *E. faecium* U0317 were obtained through enzymatic digestion of the peptidoglycan, followed by a treatment of the cell's debris with nucleases and proteinase K. The crude extract was purified through a size-exclusion and a following anion-exchange chromatography. The pooling was based on colorimetric assays and a phenol-sulfuric assay (Fig. 68a). Additionally, the immunoreactivity of each collected fractions against the anti-U0317 serum was tested to identify the immunogenic polysaccharide (Fig. 68b and 69b). Finally, it was identified in the fraction eluted with NaCl 230 mM (Fig. 69a), named L22, which was obtained with a yield of 3.9 mg/41.15 $g_{wet\text{-}pellet}$.

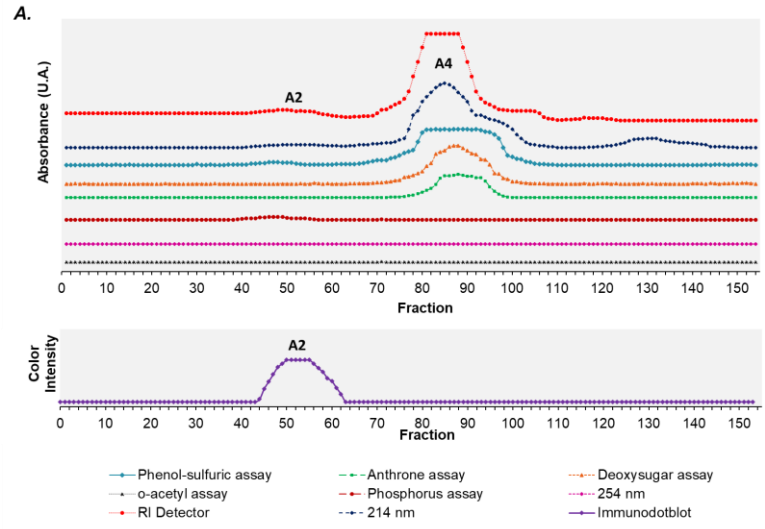

Figure 68. a) Elution profile of crude cell wall polysaccharides from *E. faecium* U0317 purified by a size-exclusion chromatography; b) immunodotblot analysis of the eluted fractions with anti-U0317 serum.

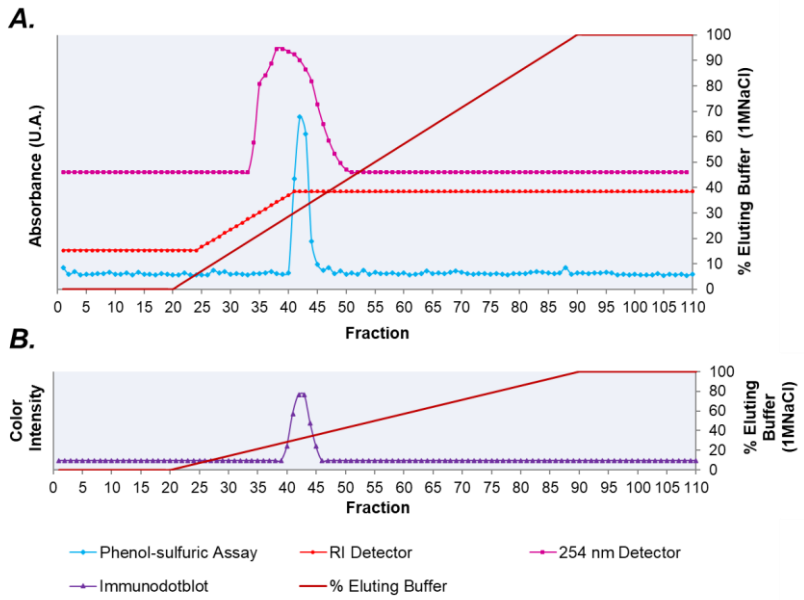

Figure 69. a) Elution profile of the fraction A2 (derived from the size-exclusion chromatography) from *E. faecium* U0317, over the ion-exchange chromatography using a two-step linear gradient elution mode; b) immunodotblot analysis of the eluted fractions with anti-U0317 serum.

2.6.3. GC-MS analysis of the immunogenic capsular polysaccharide from *E. faecium* U0317

L22 monosaccharide compositional analysis as acetylated O-methyl glycosides showed the presence of glycerol, galactose, glucose and glucosamine as main constituents (Fig. 70). Moreover, deriving these hexoses onto O-octylglycosides and comparing them with the respective standards, the absolute configuration of these residues inferred that all are D-configured (Fig. 71a). Regarding the glycerol unit, the absolute configuration was afforded by oxidizing its free primary alcoholic function at C-3 to carboxylic acid, and the resulting glyceric acid was released from the polysaccharide by HF treatment, reacted with 2-(-)-octanol and acetylated. This approach returned a L-configured glyceric acid (Fig. 71e), but since its carbon atom numbering was reversed with respect to that of the original molecule, it was deduced that the phosphoglycerol moiety possessed the D-absolute configuration.

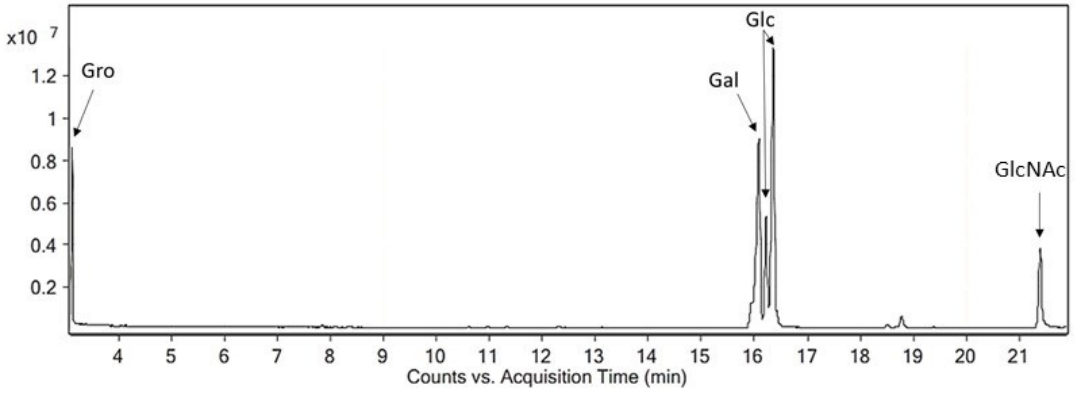

Figure 70. Monosaccharide composition of *E. faecium* capsule as established by the acetylated O-methyl glycoside derivatives method.

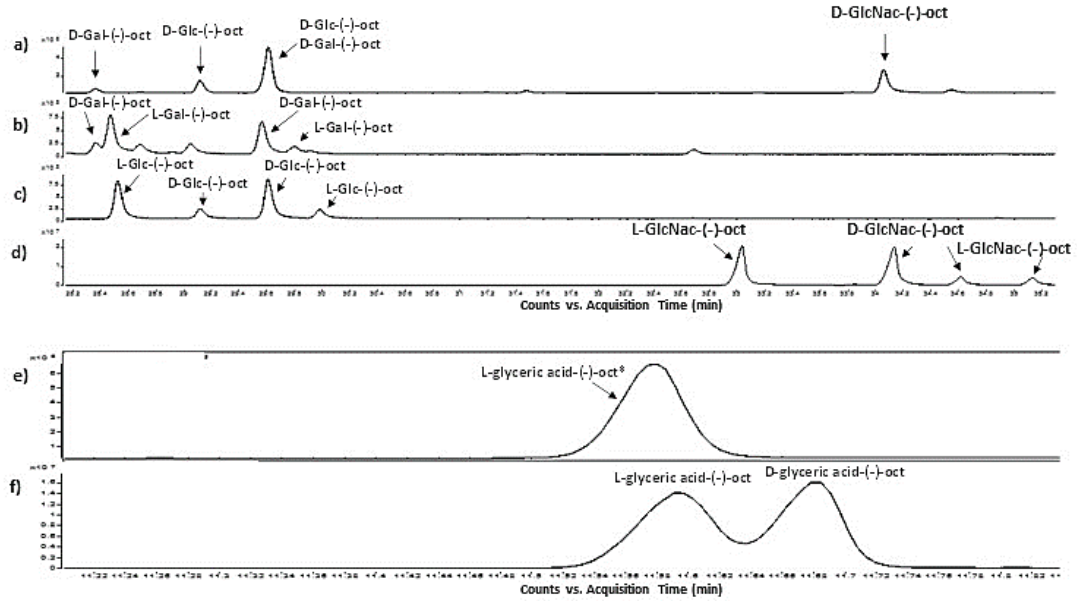

Figure 71. Absolute configuration of residues as determined by the O-octylglycoside derivatives method. a) profile obtained from monosaccharides of *E. faecium* L22; b) Gal standard profile; c) Glc standard profile; d) GlcNAc standard profile; e) profile obtained from the glycerol moiety of *E. faecium* L22 derived into glyceric acid; f) glyceric acid standard profile.

2.6.4. NMR structural analysis on *E. faecium* U0317 L22

The structure of the capsular polysaccharide was determined by analyzing the complete set of homo- and heteronuclear 2D NMR experiments (COSY, TOCSY, NOESY, ^{1}H,^{13}C HSQC, ^{1}H,^{13}C HMBC). The spin system of each residue was assigned by interpretation of the COSY and TOCSY spectra, while ^{1}H,^{13}C HSQC spectrum was used to assign the carbon chemical shift values. Attributions were counterchecked or completed using the other spectra recorded.

The ^{1}H NMR spectrum presented five main anomeric signals (two peaks named C and D overlap each other, resulting in a single protonic signal) at 5.4-4.4 ppm, a crowded carbinolic region (4.3-3.4 ppm) and the acetyl signal of the N-acetyl glucosamine unit at 2.03 ppm (Fig. 72B). The five anomeric signals were labelled with a capital letter (A-E, Fig. 72A, Tab. 11) and NMR analysis started from residue A, whose anomeric proton (5.40 ppm) displayed four correlations in the TOCSY spectrum (Fig. 73a), while all the correlations between the other protons of the residue are clearly visible. This pattern is diagnostic of a *gluco* configured residue. Indeed, the carbon chemical shift values read on the HSQC spectrum and compared with those reported in literature, confirmed this unit as α configured at the anomeric center (Speciale et al., 2022). Finally, integration of the information of the TOCSY with those of the COSY spectrum led to the assignment of the chemical shifts of all the protons of this residue (Tab. 11).

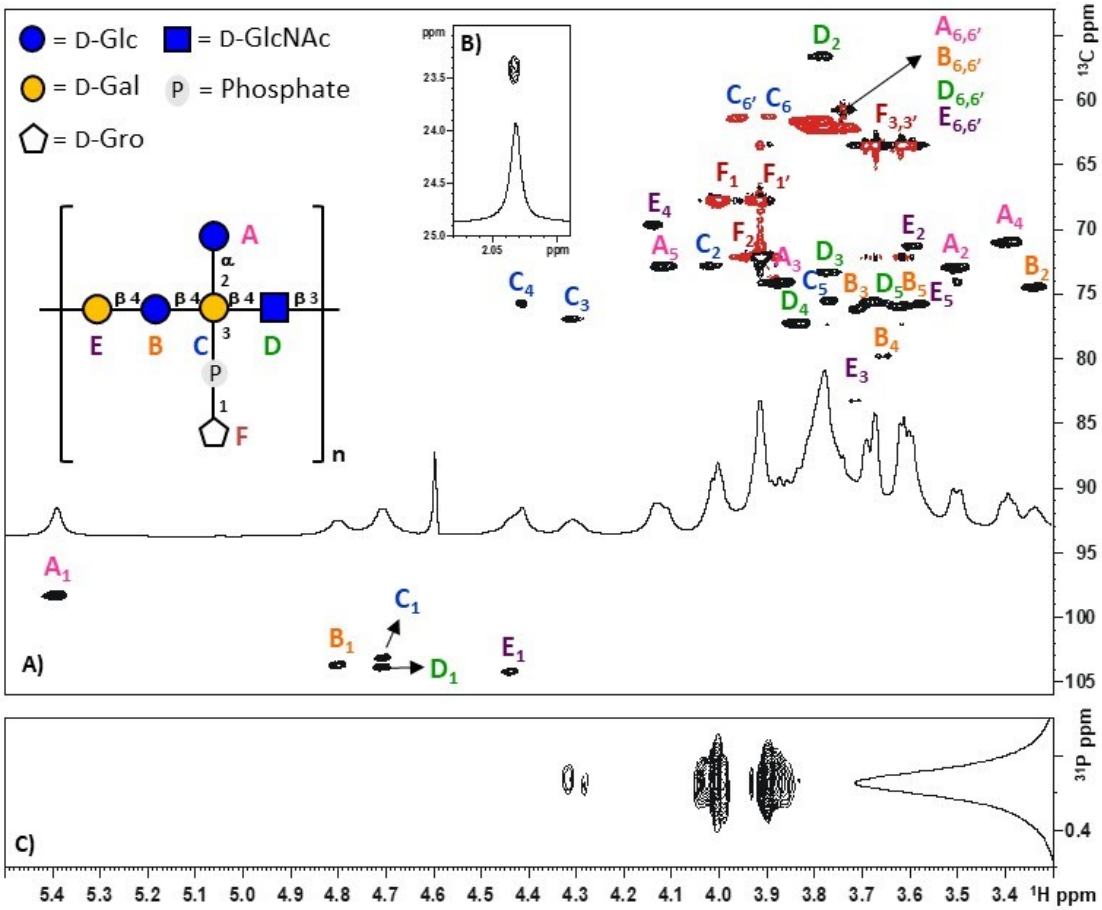

Figure 72. A) HSQC spectrum of the capsular polysaccharide I22 along with the proton profile and the structure of the capsular polysaccharide isolated from *E. faecium* (600 MHz, 315 K). B) Expansion of the ^{1}H,^{13}C NMR spectrum containing the acetyl group (2.03; 23.4 ppm). C) Expansion of the ^{1}H,^{31}P HSQC spectrum (400 MHz, 298 K) of the phosphodiester group connecting O-3 of **C** to O-1 of the glycerol moiety (**F**). Letters refer to the carbohydrate residues as reported in figure and drawn according to the Symbolic Nomenclature For Glycans. All monosaccharides are in the pyranose form. Arabic numerals refer to the proton/carbon atoms of the respective residue.

Table 12. (600 MHz, 315 K, D_2O) Proton (^1H) (plain text) and carbon (^{13}C) (italic) NMR chemical shifts of L22 from *E. faecium* U0317.

Residue	1	2	3	4	5	6
A	5.40	3.50	3.87	3.40	4.11	3.81
α-D-Glc*p*	*98.3*	*73.0*	*74.1*	*71.0*	*72.9*	*61.6*
B	4.80	3.34	3.68	3.66	3.58	3.78
4-β-D-Glc*p*	*103.7*	*74.4*	*75.7*	*79.7*	*75.8*	*62.0*
C	4.71	4.01	4.30	3.42	3.77	3.95-3.90
2,3,4-β-D-Gal*p*	*103.1*	*72.8*	*77.0*	*75.8*	*75.6*	*61.4*
D	4.71	3.79	3.76	3.84	3.62	3.77
4-β-D-Glc*p*NAc	*103.7*	*56.7*	*73.3*	*77.2*	*75.8*	*61.9*
E	4.44	3.60	3.70	4.14	3.71	3.77
3-β-D-Gal*p*	*104.1*	*71.3*	*83.1*	*69.6*	*76.0*	*61.9*
F	4.00-3.91	3.92	3.67-3.61			
***P*-D-Gro**	*67.8*	*72.0*	*63.5*			

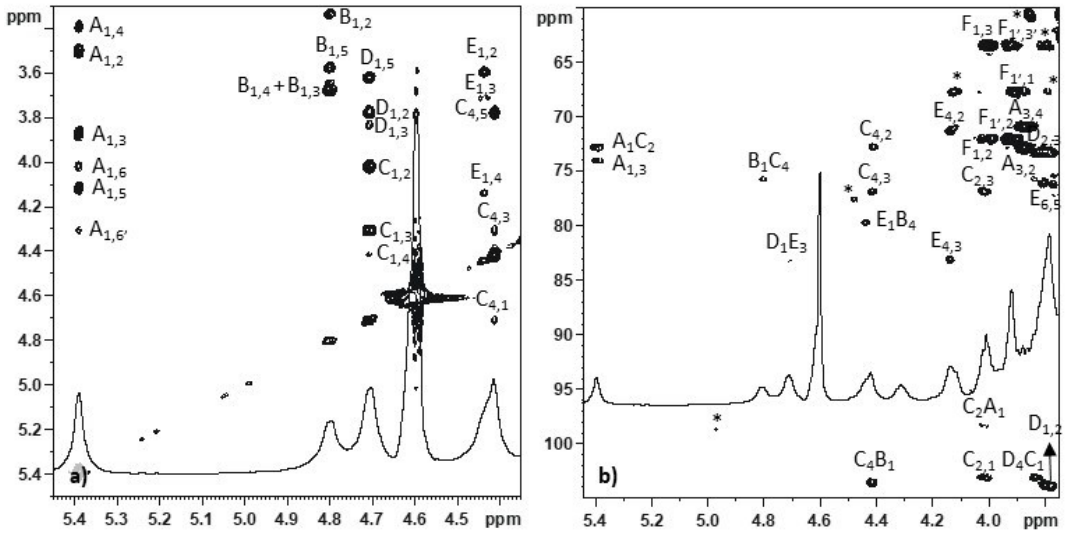

Figure 73. a) TOCSY spectrum (600 MHz, 315 K, D_2O) of L22 produced by *E. faecium* U0317 strain. b) Expansion of the ^1H,^{13}C HMBC spectrum (600 MHz, 315 K, D_2O) of the capsular polysaccharide produced by *E. faecium* U0317. Letters refer to carbohydrate residues as defined in Tab. 11, and arabic numerals to the protons in the respective residues. Signals marked with (*) are due to minor impurities and/or sequence artifacts.

The analysis of the HMBC spectrum (Fig. 73b) showed the connection of the anomeric proton of A with the signal at 72.8 ppm, identified as carbon 2 of the residue C. Full attribution of B chemical shifts was performed by the same strategy used for A, which in this case defined this residue as a β configured glucose (all the correlations from the

anomeric proton at 4.80 ppm are visible in the TOCSY spectrum), 4-substituted. The analysis of the HMBC spectrum showed that the C-4 of B (79.7 ppm) had a correlation with a signal at 104.1 ppm, identified as C-1 of the residue E. Moreover, the HMBC spectrum shows another correlation, namely that of the C-1 of B (74.4 ppm) with a signal at 75.8 ppm, assigned at the C-4 of the residue C. By following the COSY signals and the TOCSY pattern, this latter residue was identified as a galactose, β configured comparing its carbon chemical shifts shown in the HSQC spectrum with those reported in literature. Moreover, the HMBC spectrum shows the correlation of the C-1 of C with the C-4 of D (77.2 ppm). Of note, H-3 of **C** (4.30 ppm) appeared like a broad triplet with a *J* of about 7 Hz. Typically, H-3 proton of a *galacto* configured unit appear as double-doublet, or more often as a broad doublet, due to the coupling with H-2 (~ 10 Hz) and H-4 (~ 2 Hz) and not as a triplet, therefore the multiplicity of this proton along with the shift at low fields observed, suggested the presence of a phosphate, scalarly coupled to the proton geminal to the site of attachment with a coupling constant $^{3}J_{P,H} \sim 7$ Hz. In agreement with this hypothesis, C-3 of **C** had a downfield shift of about 3 ppm when compared to the value reported for non-substituted glycoside (Speciale et al., 2022). On the other hand, the combined analysis of the HSQC and HMBC spectra led to the identification of a glycerol unit, with one of its primary carbons, labeled as $\mathbf{F_1}$ (Fig. 72A) downfield shifted at 67.8 ppm, a value consistent with the presence of a phosphate. These two findings led to hypothesize that O-1 of F and O-3 of C were connected by a phosphodiester bridge, as confirmed by acquiring the ^{1}H-^{31}P HSQC spectrum (Fig. 72C).

Full attribution of the chemical shifts of D was performed by the same strategy used for B, which defined this residue as a β configured 2-N-acetyl-glucosamine. The analysis of the HMBC spectrum showed that the anomeric proton of D has a correlation with a signal at 83.1 ppm, identified as C-3 of E. Lastly, the residue E was identified as a α galactose due to the typical TOCSY pattern which shows only three correlations from the anomeric proton (Fig. 73a) and by comparing the carbons chemical shifts with those reported in literature. The attribution of the other proton and carbon atoms of the residue was completed by analysing the HMBC and the NOESY signals. In addition, these spectra also showed the linkage of C-1 of E to C-4 of the residue B (79.7 ppm). The assignments of all residues and the sequence between the different residues was further confirmed by the information from the NOESY (Fig. 74a) and the HSQC-TOCSY (Fig. 74b) spectra, respectively, yielding to the definition of the repeating unit of this capsular polysaccharide (inset in Fig. 72A). This polysaccharide is quite unique in its chemical structure, it has indeed a large repeating unit (a tetrasaccharide motif) which is disubstituted at the same residue with one of the substituents being Gro-*P*, clearly a reminiscence of teichoic acids structure.

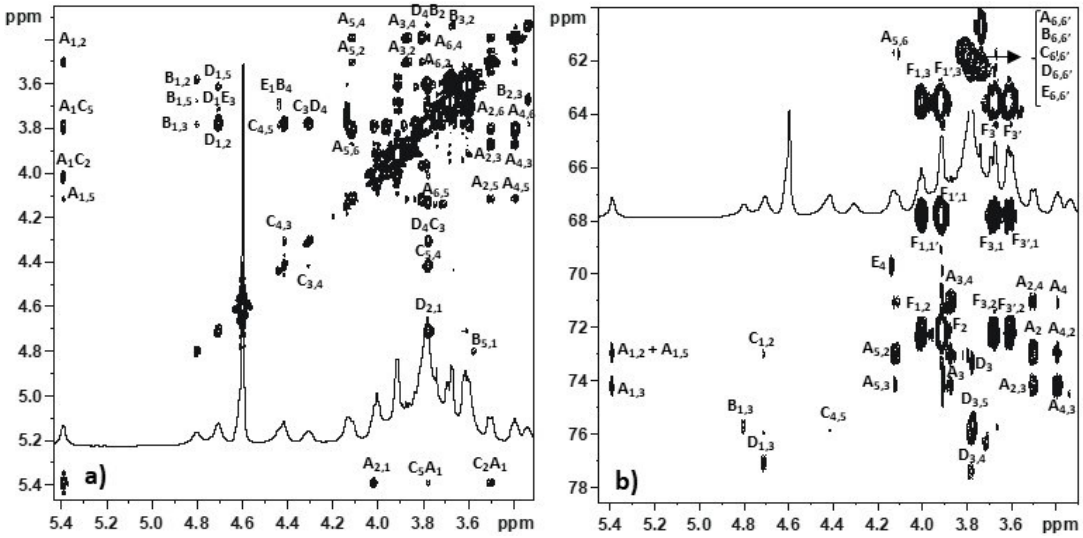

Figure 74. a) NOESY spectrum (600 MHz, 315 K, D_2O) of L22 produced by *E. faecium* U0317 strain. b) $^{1}H,^{13}C$ HSQC-TOCSY spectrum (600 MHz, 315 K, D_2O) of L22 produced by *E. faecium* U0317. Letters refer to carbohydrate residues as defined in Tab. 11, and arabic numerals to the protons in the respective residues.

2.6.5. Glycoconjugation of the *E. faecium* U0317 CPS with BSA

L22 from *E. faecium* U0317 was linked to BSA, used as a carrier protein. This type of protein was chosen since it is highly stable, namely easy to manage. The glycoconjugate was developed because polysaccharide antigens typically have low immunogenicity for active immunization while, when linked to a protein, they can elicit T-cell dependent responses providing an effective immune response and B-cell memory (Micoli, Adamo, & Costantino, 2018). The optimal ratio for conjugating the aforementioned L22 to BSA was found to be 1:3 (weight/weight). The correctness of the conjugation process was assessed using SDS-PAGE, and the cleanup procedure involved diafiltration with a 100 kDa membrane cut-off. The glycoconjugates exhibited broad bands at a higher molecular weight cut-off (MWCO) compared to the unconjugated polysaccharide, confirming the successful conjugation (Fig. 75a). As previously described (Romero-Saavedra et al., 2019), the sugar and protein content was quantified through the Dubois phenol-sulfuric acid assay and Bradford assay, respectively, to determine the amount of glycoconjugate required for mice immunization (Fig. 75b). The analysis confirmed the ratio utilized during the reaction.

a)

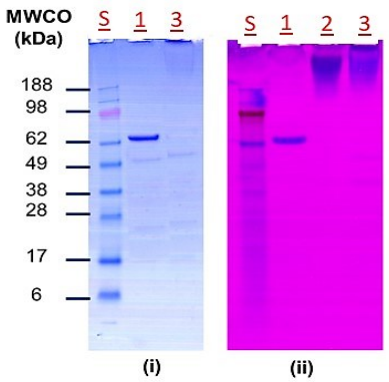

b)

	L22-BSA 1:3 100 kDa
Polysaccharide	59.8 μg/mL
Protein	176.9 μg/mL
Final concentration	242.5 μg/mL
Final ratio Polysaccharide-Protein (weight)	1:2.9

Figure 75. a) SDS-PAGE gels of glycoconjugates stained with Coomassie (i) and Stains All (ii). The glycoconjugates were compared to the unconjugated protein and/or *E. faecium* U0317 polysaccharide to confirm the conjugation procedure. S. See-blue prestained standard, 1. BSA, 2. L22, 3. Glycoconjugate; b) determination of sugar and protein content in glycoconjugate preparations.

2.6.6. Biological assays

The purification of the immunogenic *E. faecium* U0317 CPS was successfully targeted by employing the serum generated against the whole heat-killed bacterium, which specifically recognized capsular antigens. After that, it was tested if the observed immunoreactivity of L22 with the anti-U0317 serum during the purification process may also be translated to the opsonic activity of the serum. To this end, it has been evaluated the polysaccharide ability to inhibit killing activity of the anti-U0317 serum by an opsonophagocytic inhibition assay (OPIA). The fraction A4 obtained by size-exclusion chromatography, which was not immunogenic but was the most abundant polysaccharide among the fractions collected during the purification process, was used as a negative control. Afterwards, L22 and fraction A4 at different concentrations (100, 20, 4 and 0.8 μg/mL) were pre-incubated with anti-U0317 antibodies at 1:200 dilution for 1 hour at 4°C prior OPIA. Finally, it was observed that L22 inhibited the opsonic killing activity of anti-U0317, whereas pool A4 showed no activity (Fig. 76a). These results indicate that the opsonic antibodies induced by immunization with heat-killed *E. faecium* U0317 primarily target the newly purified and structurally

characterized L22. To confirm this finding, the polysaccharide was conjugated with a carrier protein, the mice were immunized with BSA, L22 and with the glycoconjugate L22-BSA and the final blood sample obtained post-immunization was assessed in an opsonophagocytic assay, to determine their capacity to induce opsonic killing antibodies against the parental strain *E. faecium* U0317. The positive control, anti-U0317 serum, was tested at a final dilution of 1:200 using the parental strain *E. faecium* U0317, while polyclonal mouse sera generated against different glycoconjugates and unconjugated components were tested at a 1:10 dilution. Opsonic killing activity was evident in the sera generated against the glycoconjugate L22-BSA, while minimal opsonic activity was observed for the unconjugated components, BSA, and L22. Normal mouse serum (NMS) showed almost no opsonophagocytic killing activity and was used as the negative control in the experiment (Fig. 76b).

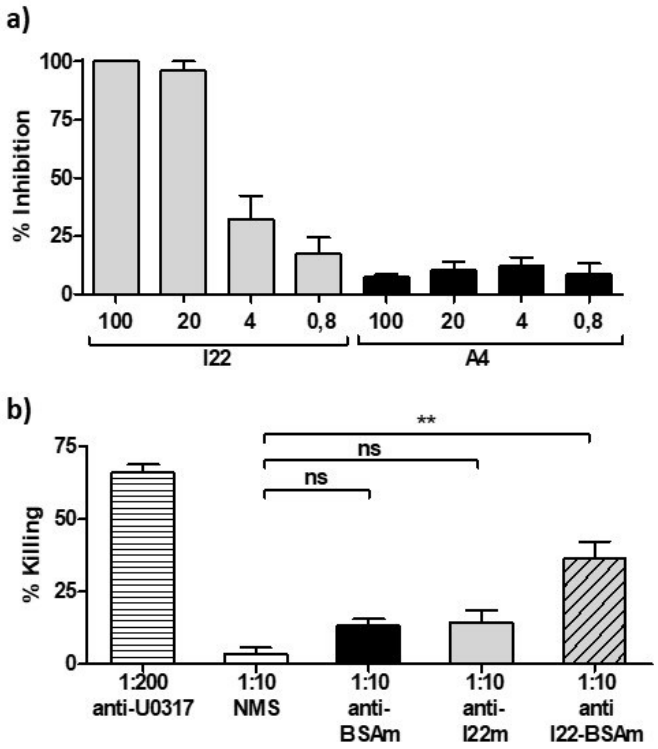

Figure 76. a). Opsonophagocytic inhibition assay using the *E. faecium* U0317 CPS and fraction A4 obtained after size-exclusion chromatography, as negative control; b) opsonophagocytic assay of mouse sera generated against the glycoconjugate I22-BSA and unconjugated components. The bars represent the mean of the data, and the error bars represent the standard error of the mean. ns ≥ 0.5, *P ≤ 0.05, **P < 0.01.

However, the killing activity of the anti-L22-BSA serum was lower when compared to the anti-U0317. This difference can be attributed to the extensive diversity of antigenic determinants present in the serum generated against the entire bacterium, as opposed to the antigenic determinant (L22) alone, located in the core of the same bacterium. Nonetheless, the anti-glycoconjugate sera exhibited notable opsonic killing activity of more than 40% against the parental strain, illustrating the feasibility of selectively purifying antigenic and immunogenic determinants from pathogenic bacteria based on their functional properties.

Chapter 3

General conclusions

The main focus of this Ph.D. thesis is to isolate and investigate the structure (in terms of sugar composition, sequence, and molecular mass) of polysaccharides from Gram-positive bacteria belonging to the human and plant microbiota. This in turn aims to evaluate their immunological activity for possible applications as postbiotic compounds or vaccines in the biomedical field, or as antimicrobials in agriculture. This second objective has been (or will be) developed in collaboration with other research groups. More in details, the polysaccharides analysed came from: *Lactobacillus reuteri; Lactobacillus rhamnosus* GG ATCC 53103*; Lacticaseibacillus paracasei* CBA L74*; Bacillus subtilis* 168*; Ruminococcus gnavus* ATCC 35913*; Enterococcus faecium* U0317.

As for ***L. reuteri***, there were been identified: a wall- and a lipo-teichoic (WTA and LTA, respectively) acids, and two capsular polysaccharides (Fig. 77). Regarding with the teichoic acids, they had the same type of polyglycerol phosphate backbone decorated with a α-glucose unit in a not stoichiometric ratio. They could be differentiated by the different molecular weight, lower for LTA. Moreover, in this sample it was possible to identify the primer oligosaccharide unit (CBF motif, Fig. 9b). Meanwhile, the capsular polysaccharides are a mixture of a glucogalactan-galactan, in a 9:1 ratio. A possible immunoregulatory activity of these characterized glycans is waiting to be evaluated by the research group of Prof. Sin Hyeog Im from Pohang University of Science and Technology.

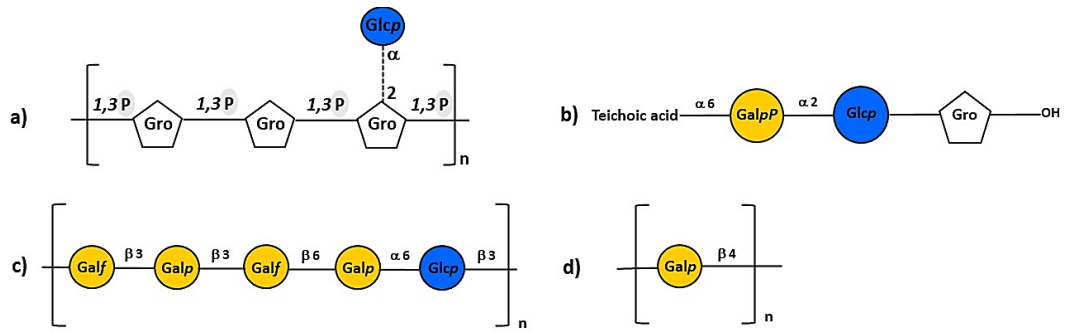

Figure 77. Chemical structures of *L. reuteri*: a) teichoic acids; b) primer oligosaccharide unit of LTA; c) glucogalactan capsular polysaccharide; d) galactan capsular polysaccharide. All structures are reported according to the Symbolic Nomenclature for Glycans (SNFG).

As for ***L. rhamnosus*** **GG (ATCC 53103)**, its CPS was at first isolated from the corresponding commercial powder of the bacterium, sold on market as lactic ferment. However, this procedure led to the isolation of the product contaminated with starch, probably used as excipient in the commercial formula. For this reason, the pure CPS was subsequently obtained directly from the *L. rhamnosus* cells, by isolating the bacterium from the food supplement and growing it in MRS medium. After that, the bacterium was heat-treated and its pure CPS was extracted and isolated. Finally, it was characterized by NMR spectroscopy, confirming the structure already reported in literature (Landersjö et al., 2002) (Fig. 78a).

Regarding with the polysaccharide biological activity, this was evaluated by Prof. Roberto Canani's research group, from CEINGE-Biotecnologie Avanzate of Naples. Specifically, it was assessed the influence on the differentiation and integrity of the intestinal epithelium by real time PCR, and on the modulation of the host immune system, by ELISA and flow cytometry experiments. Through the first mentioned technique, it was observed that the combination of the LGG CPS and the ID35 (a specific LGG genome sequence that suppress inflammatory responses in animal model of food allergy) was the best solution to increase the expression levels of *Muc2* (Fig. 78b) and *lactase* (Fig. 78c), namely the enzymatic markers of a healthy intestinal barrier. In addition, ELISA tests and flow cytometry on PBMC treated with LGG, as well as ID35 or CPS or ID35+CPS, revealed a decrease of Th2 pro-inflammatory cytokine production (Fig. 78d is provided as a single example, more in details in Fig. 27) and an increase of Tregs DCs-mediated expression levels (Fig. 78e), respectively. All together, these data suggest that the tolerogenic action elicited by *L. rhamnosus* in children with CMA could be exerted by its heat inactivated cells, and that these effects are modulated at least by the activities of two LGG derived postbiotic compounds: the CPS and the ID35. Though taking *L. rhamnosus* provides various benefits, the treatment with live probiotic bacteria could be not safe, increasing the risk for microbial translocation from the gut lumen to blood, of infections and prevent potential detrimental effects shown by probiotics within a pro-inflammatory context. In this context, the use of cell components and metabolites defined as postbiotics, represents a safe method to improve host health, bypassing the problem of acquiring antibiotic resistance genes and virulence factors, which may occur when probiotics are used. Therefore, the aforementioned CPS isolated from *L. rhamnosus* could be a potential postbiotic candidate for the treatment of cow's milk allergy in childhood.

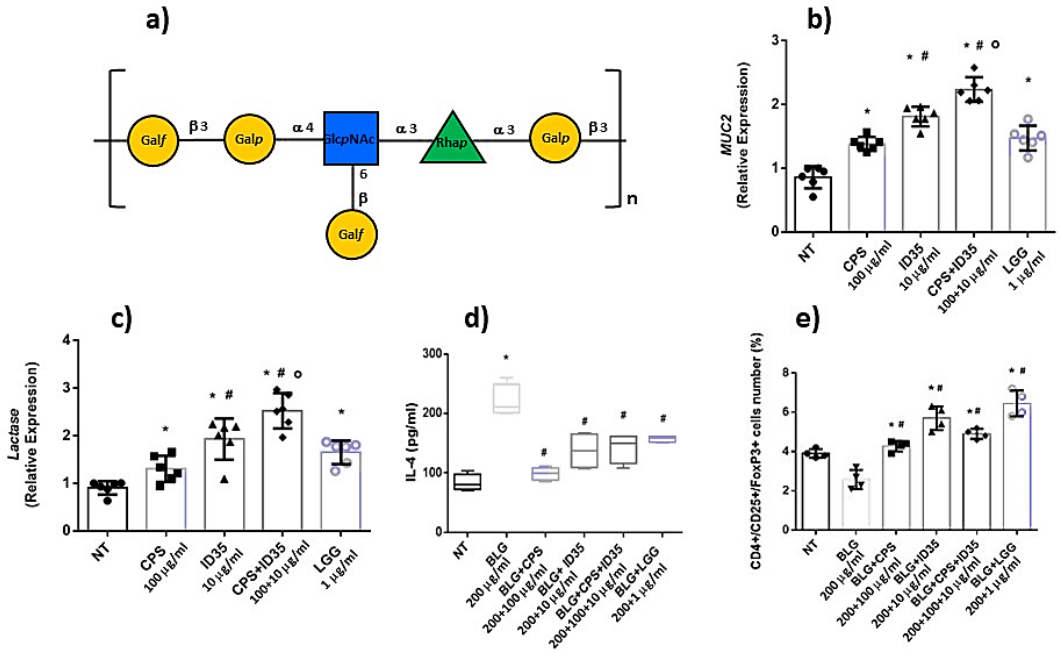

Figure 78. a) Chemical structures of the CPS from *L. rhamnosus* GG, reported according to the Symbolic Nomenclature for Glycans (SNFG); b) influence of CPS, ID35 and inactivated LGG on *Muc2* expression in human enterocytes; c) influence of CPS, ID35 and inactivated LGG on *lactase* expression in human enterocytes; d) influence of CPS, ID35 and inactivated LGG on Th2 production of IL-4 in PBMC; e) influence of CPS, ID35 and inactivated LGG on number of activated Tregs in PBMC.

As for ***L. paracasei* CBA L74**, its polysaccharides were initially extracted from commercial cow's milk powder supplements for infants, fermented with the bacterium. However, the final yield was very low and the proton spectrum suggested the presence of a mixture of different polysaccharides (Fig. 29), so difficult to analyse. Also, the SDS-PAGE displayed the presence of both polysaccharides and proteins (Fig. 28). For this reason, the polysaccharides extraction was subsequently performed from the freeze-dried *L. paracasei* cells cultured in a medium other than milk, namely in MRS. Finally, the isolated crude product presented, as regards the sugar component, the same ^{1}H NMR profile as that of the glycans previously isolated from the fermented milk matrix (Fig. 29a), confirming their belonging to the bacterium rather than to the culture medium. Therefore, from *L. paracasei* they were isolated and structurally characterized a teichoic acid (Fig. 79b) and two capsular polysaccharides (CPS-1 and CPS-2). The CPS-2 was isolated from the other two compounds through a size-exclusion chromatography, from which it eluted with a longer retention time with respect to the other two (Fig. 30a) suggesting that, among the *L. paracasei* isolated glycans, it was the compound with the lowest molecular weight. Furthermore, by using the same procedures of extraction, the CPS-2 was obtained with the highest yield compared to CPS-1 and TA. Finally, while the NMR spectra of the TA and the CPS-1 revealed that these

two compounds had a homogeneous and well-defined structure, the NMR spectra recorded for the CPS-2 were rich of signals in a not-stoichiometric ratio between each other, suggesting the presence of a rather heterogeneous and complex chemical structure. Going deeper, while the structure of the *L. paracasei* TA, made of a polyglycerol phosphate chain, is one of the most typical structure among those of teichoic acids of Gram-positive bacteria (S. Brown, Santa Maria, & Walker, 2013), the CPS-1 structure is not yet reported in literature, and it consists of different units of glucose, rhamnose and of a unit of galactose and another of a branched glucosamine (Fig. 79a). As for the CPS-1, also the *L. paracasei* CPS-2 structure represents a total novelty in carbohydrate database. Specifically, it is a heterogeneous polymer, with the linear portion of the repetitive unit consisting of three L-rhamnoses and a single D-galactosamine (Fig. 79c). The heterogeneity is given by the dimer K→6T and the residue J, which are not stoichiometric branches of the linear polysaccharide chain. Consequently, the chemical around of all the other residues changes along with their chemical shift. Precisely, when the dimer K→6T is absent the residue N becomes P and appears to be directly linked to the position 3 of the residue H, and when the residue J is present the residues H, E, M and R become the residues I, C, F, and S, respectively (Fig. 79c). This explains why in the CPS-2 proton spectrum there are so much signals similar to each other, and in non-stoichiometric proportions (Fig. 36b). Moreover, the heterogeneity of the NMR signals is also increased by the fact that, since this glycan is a small polymer, it is also possible to see its reducing end in the NMR spectra, namely with the D-galactosamine in the reducing form. Therefore, having the anomeric position free, this galactosamine in solution exists in the two α and β configurations, identified respectively in the D and U units (Tab. 6, Fig. 36a). Therefore, when it is α configured, the galactosamine binds the residue M while, when it is β, the residue bound to it becomes O (Fig. 36a).

Moreover, the surface glycan components of the *L. paracasei* cells were investigated through the high-resolution magic-angle spinning (HR-MAS) NMR spectroscopy technique. Cells were analyzed at their lag, exponential, and stationary phase, or after heat-inactivation. In conclusion, it was discovered that:

-the heat-treatment was an efficient method adopted for the polysaccharides extraction, since the ^{1}H and $^{1}H,^{13}C$ HSQC spectrum of the heat-inactivated cells was less resolved in respect to that of the cells alive (Fig. 41b);

-the *L. paracasei* polysaccharides NMR signals are, generally, more visible in the exponential phase, while they were fewer and with a lower intensity in the lag and, especially, in the stationary phase (Fig. 42c);

- the CPS-2 is, in general, the polysaccharide component most flexible and most exposed on the bacterium cell surface while the teichoic acid, that was not visible in the acquired spectra (Fig. 43 and 44), is an innermost and more fixed component of the cell membrane.

Regarding with the immunological activity, the milk powder enriched with *L. paracasei* CBA L74 is given to infants as food supplement to prevent the onset of eventually allergies in later life. Therefore, in the next future Prof. Canani's research group from CEINGE-

Biotecnologie Avanzate of Naples will perform the biological assays necessary to evaluate if the isolated glycans have an anti-inflammatory or some other activities, as their effect on the tight junctions of the epithelium in an in-vitro human cell assay.

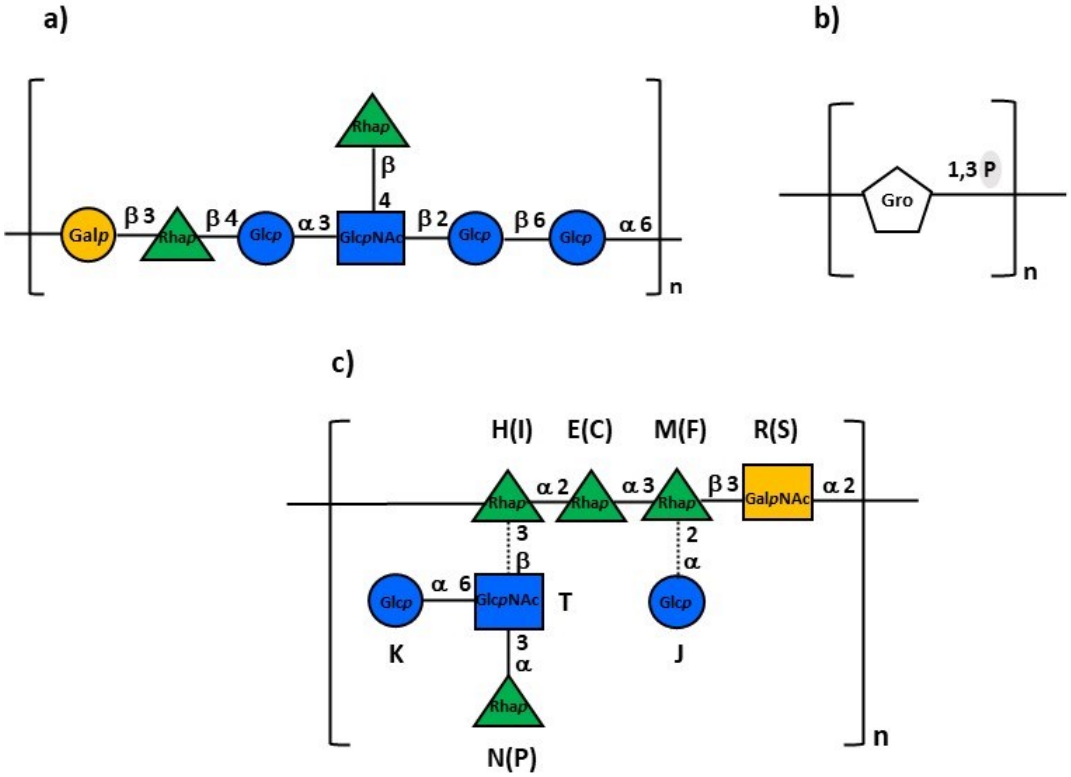

Figure 79. Chemical structures of *L. paracasei*: a) CPS-1; b) TA; c) CPS-2. When the dimer K→6T is absent, residue N becomes P and is directly linked to the C3 of the residue H; when the residue J is present, the residues H, E, M and R become, respectively, residues I, C, F, and S reported in brackets. All structures are reported according to the Symbolic Nomenclature for Glycans (SNFG).

As for ***B. subtilis* 168**, two different glycans were isolated from the bacterial cells and characterized: a phosphoglycerol-based teichoic acid polymer, not stoichiometrically substituted with an α-glucose (Fig. 80a), and a capsular polysaccharide (Fig. 80b), made of a D-GalNAc and a D-Glc unit along with phosphate linked as diester. After that, Prof. Volker's research group at Georg-August University tested their immunological activities in Arabidopsis by leaf infiltration assays. The treatment of the Arabidopsis leaf with the teichoic acid showed a dose-dependent effect (Fig. 80a), whereas the treatment with the capsular polysaccharide at every concentration did not cause any phenotype change (Fig. 80b). These data could be promising because, although the benefits of *B. subtilis* for crop production have been widely recognized, its successful application often fails due to its

inability to persist in the rhizosphere. Therefore, *B. subtilis* TA alone, at the right concentration, can replace the use of the entire bacterium as an antimicrobial compound for agricultural production.

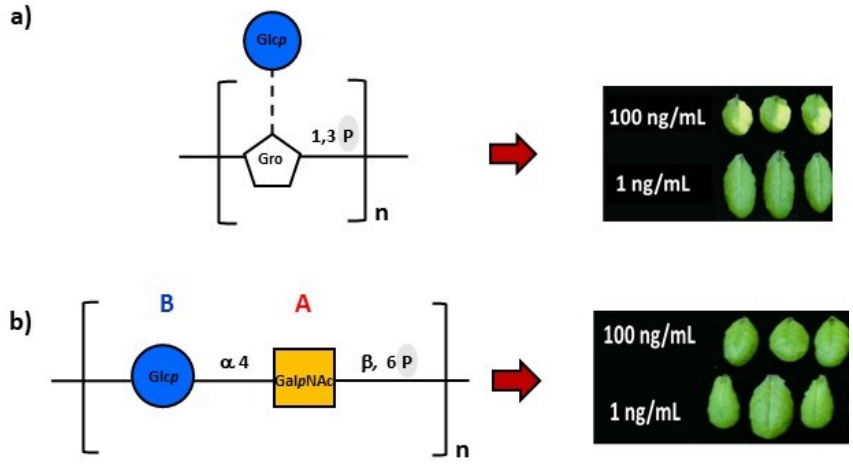

Figure 80. a) Chemical structures of the TA from *B. subtilis* 168, along with the leaf wilting concentration dependent after the injection of a solution of teichoic acid 100 ng/mL; b) chemical structures of the CPS from *B. subtilis* 168, along with the no effects observed in Arabidopsis infiltration assays, after the injection of the CPS. Both the chemical structures are reported according to the Symbolic Nomenclature for Glycans (SNFG).

As for ***R. gnavus* ATCC 35913**, an EPS was isolated and structurally characterized from its cells. It has the same structure of the EPS isolated from *R. gnavus* E1 strain, with a repeating unit made of 4 rhamnoses with a not stoichiometric ramification consisting of a terminal β-glucose (Fig. 81a). This structure is novel according to the CSBD database, and differs from the EPS structure of another strain of *R. gnavus*, the type strain ATCC 29149. This last one presents only three rhamnoses in the repeating unit, and has a ramification in a stoichiometric ratio, consisting of two α-glucose units linked together in positions 1,6 (Fig. 81b) (Henke et al., 2019). In literature, it has been previously reported that there are two different clades of *R. gnavus*, and only one of these is enriched in IBD patients and therefore could contribute to the overall symptoms connected with this disease (Hall et al., 2017). This discrepancy could be attributed to the different polysaccharide structures of the various *R. gnavus* strains. Therefore, biological assays were carried out on these three aforementioned types of *R. gnavus* strain (ATCC 35913, E1 and ATCC 29149) and their EPS, in order to see any divergence in their immunological activity. As indicator of this activity were investigated the stimulation of the production of pro and anti-inflammatory cytokines and the induction of the Nf-kB signal related to the immune response in monocytes. Hence, it emerged that ATCC 35913 was the most immunogenic strain among the overall *R. gnavus*

strains considered (Fig. 81c is provided as a single example, more in details in Fig. 64). In agreement with this observation, also its EPS showed a high ability to induce the Nf-kB mediated response in human THP1-Blue™ reporter cells (Fig. 81d is provided as a single example, more in details in Fig. 66). Hence, according to the expectations, the obtained data suggest that the immunological activity of *R. gnavus* may vary depending on the strain and the cell surface glycosylation. This evidence could be promising for a generally better understanding of the inflammatory bowel diseases, with the final aim of preventing and treating them.

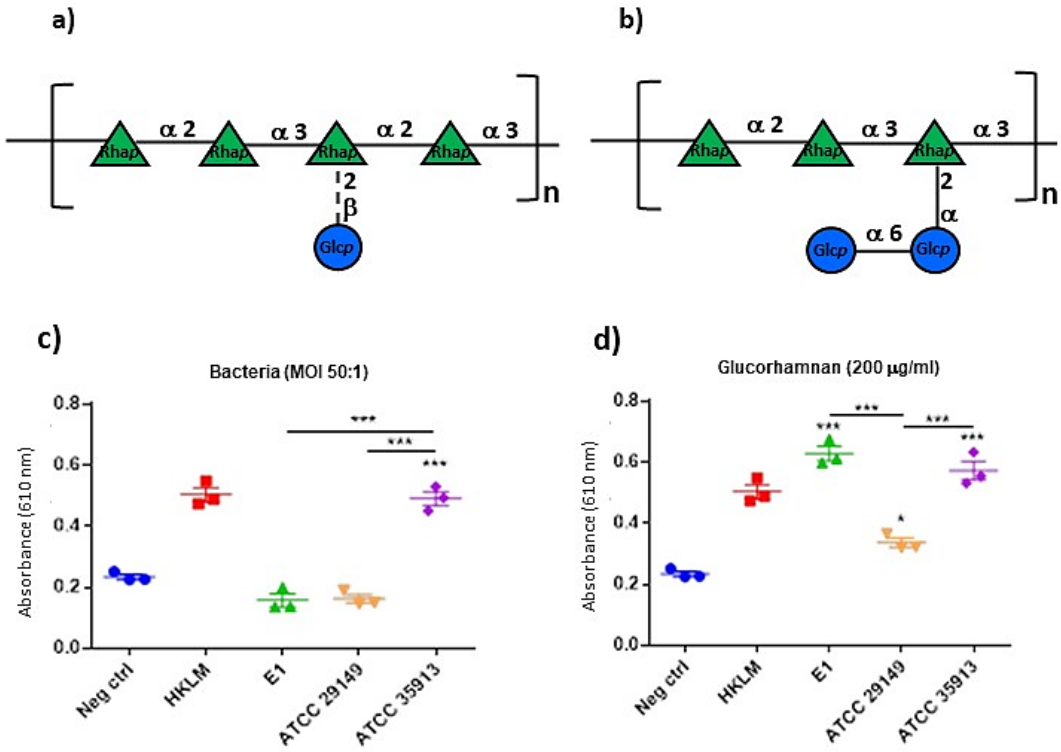

Figure 81. The panels above report the chemical structures of: a) the glucorhamnan isolated from *R. gnavus* ATCC 35913 and E1 strains; b) the glucorhamnan isolated from *R. gnavus* type (ATCC 29149) strain. All the structures are reported according to the Symbolic Nomenclature for Glycans (SNFG). The panels below report the NF-κB activation after THP1-Blue™ NF-κB cells incubation with: c) *R. gnavus* ATCC 29149, ATCC 35913 or E1 strains; d) their associated glucorhamnans. HKLM (heat-killed *Listeria monocytogenes*) was used as positive control.

As for ***E. faecium* U0317**, through opsonophagocytic assays (OPA) it was successfully identified an immunogenic CPS. This glycan was subsequently purified and characterized, leading to the discovery of a new polysaccharide structure, not yet reported elsewhere (Bychowska et al., 2011) (Hübner, Theilacker, Kaczynski, & Holst, 2016) (Kodali et al., 2015).

Precisely, the repeating unit (a tetrasaccharide motif) presents a double substituted residue with one of the substituents being Gro-*P* (Fig. 82a). Additionally, by conjugating this CPS to the carrier protein BSA, it was developed a glycoconjugate, as confirmed by SDS-PAGE (Fig. 82b). The final aim was to demonstrate its ability to elicit antibodies that mediate the opsonic killing of the parental strain *E. faecium* U0317, highlighting the potential application of this glycoconjugate as a vaccine antigen. Therefore, mice were immunized with BSA, CPS and with the glycoconjugate, and the final blood sample obtained post-immunization was assessed in an opsonophagocytic assay. Finally, it was observed an evident opsonic killing activity in the sera generated against the glycoconjugate, and a minimal opsonic activity for the unconjugated components, BSA and CPS (Fig. 82c), suggesting that the isolated polysaccharide from *E. faecium* U0317 could be utilized as a component to develop a multivalent vaccine against encapsulated enterococci.

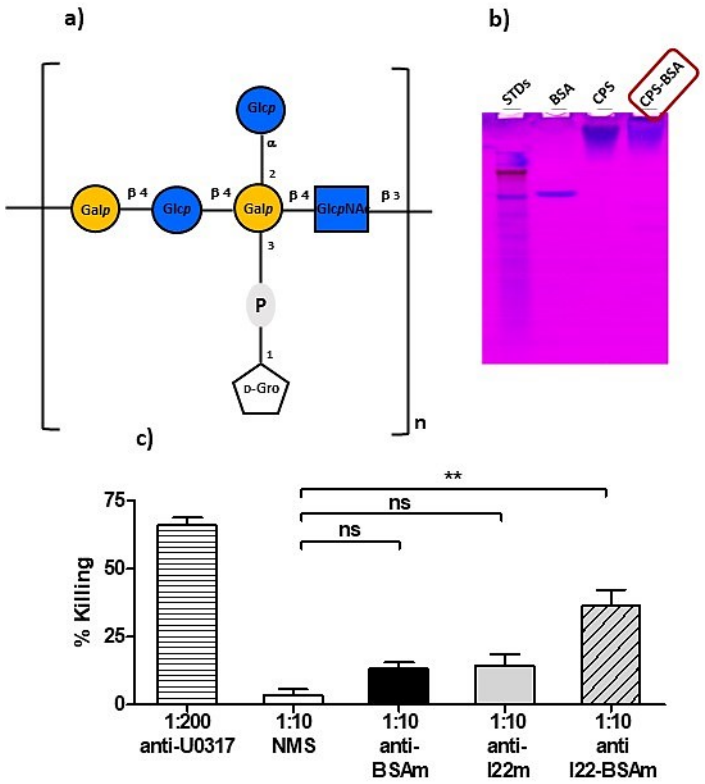

Figure 82. a) Chemical structures of the CPS isolated from *E. faecium* U0317 strain. b) SDS-PAGE gel of glycoconjugates compared to CPS and BSA alone, stained with Stains All. c) Opsonophagocytic assay of mouse sera generated against the glycoconjugate CPS-BSA and unconjugated components. The bars represent the mean of the data, and the error bars represent the standard error of the mean. ns ≥ 0.5, *P ≤ 0.05, **P < 0.01.

In summary, in this work there were used some bacterial member of the human, (as regards *L. reuteri*, *L. rhamnosus*, *L. paracasei*, *R. gnavus* and *E. faecium*), and plant (as regards *B. subtilis*) microbiota as natural sources of polysaccharides to be employed for novel applications in the field of human-healthy promotion. Thus, the bacterial glycans were isolated and widely characterized by GC-MS spectrometry and NMR spectroscopy and in most cases, thanks to several collaborators, their biological activity has been evaluated. Therefore, we characterized:

-a WTA, an LTA and two different CPS from *L. reuteri*;

-a CPS from *L. rhamnosus* GG (ATCC 53103);

-a TA and two different CPS from *L. paracasei* CBA L74;

-a TA and a CPS from *B. subtilis* 168;

-two EPS, one from *R. gnavus* ATCC 35913 and the other from *R. gnavus* E1, which differ from each other only for a branching sugar on the linear chain, which is non-stoichiometric in the first case and stoichiometric in the second one;

-a CPS from *E. faecium* U0317.

Finally, the final goal was achieved by studying the immunological properties of:

-the CPS from *L. rhamnosus* GG, which has various probiotic activities and can be used for the prevention of CMA in children;

-the teichoic acid from *B. subtilis* 168, which is able to trigger a dose-dependent inflammatory response in Arabidopsis, and can be used as an antimicrobial to improve the crop production;

-the EPS from *R. gnavus* ATCC 35913 and E1 strain, which are able to modulate the immunological response in in-vitro human cellular models and may represent an important key to understand, preventing and treating IBD;

-the CPS from *E. faecium* U0317, which has an immunogenic activity in mouse, amplified when conjugated to a carrier protein, and therefore can represent an alternative strategy for the preventions of infections caused by multidrug-resistant enterococci.

Chapter 4

Material and methods

4.1. Strains, bacterial and growth conditions

4.1.1. *Lactobacillus reuteri*

At Pohang University of Science and Technology, Prof. Sin Hyeog Im's team grew *L. reuteri* in MRS broth and extracted its polysaccharides. Therefore, the crude polysaccharides of *L. reuteri* were subsequently purified and analyzed at the University of Naples Federico II.

4.1.2. *Lacticaseibacillus rhamnosus* GG

Lactobacillus rhamnosus GG cells (5 x 10^9 CFU) from the commercial supplement in powder formula were grown in 4 L of MRS (VWR chemicals), at 37°C, with shaking at 100 rpm overnight, and recovered by centrifugation at 7000 rpm, 15 min, 4 °C (5.43 g).

4.1.3. *Lactobacillus paracasei*

Cow's skim milk powder was fermented with *L. paracasei* CBA L74 by Prof. Roberto Canani's team group, in a frame of a collaboration with an industry. The bacterium was later inactivated by heating at 85 °C for 20 s and the product was freeze-dried.
The freeze-dried cells of *L. paracasei* CBA L74 were grown at Federico II University of Naples in 4 L of MRS (VWR chemicals) medium at 37 °C, shaking at 100 rpm for 24 h. The cells were finally recovered by centrifugation 7000 rpm, 15 min, 4 °C.

4.1.4. *Bacillus subtilis*

At Georg-August University, Prof. Lipka Volker's team grew *B. subtilis* 168 in LB broth, at 37 °C, under aerobic atmosphere. The bacterium was finally inactivated in autoclave and the obtained crude polysaccharides were sent to the University of Naples for chemical characterization.

4.1.5. *Ruminococcus gnavus*

At Quadram Institute Bioscience, Prof. Juge's team grew *R. gnavus* ATCC35913 and ATCC29149 in BHI-YH medium (Oxoid LTD, UK) supplemented with 5 g/l of BactoTM yeast extract (Becton, Dickinson and Company, Sparks, MD) and 5 mg/l of haemin (Sigma-Aldrich, USA), at 37 °C in an anaerobic cabinet (85% N2, 10% H2, 5% CO2) (Don Whitley, Shipley UK). After 24 h, cells were harvested by a first cycle of centrifugation 40 min, 4000 g, 4°C, then 1 h, 5000 g, 4°C, and finally 30 min, 7000 g, 4°C.

4.1.6. *Enterococcus faecium*

At Ludwig Maximilians University, Dr. Diana Milena Laverde Gómez's team grew *E. faecium* U0317 in Columbia broth (Becton Dickinson) supplemented with 2% glucose at 37°C until an optical density of 0.8 at 600 nm was reached. After that, the bacterium polysaccharide was extracted and purified, and sent to the University of Naples Federico II for further chemical analysis.

4.2. Polysaccharides isolation procedures

The first step for the study of microbic polysaccharides is their extraction from intact bacterial cells and purification. Different extraction procedures can be performed,

depending on the bacterial species and the type of polysaccharide (capsular polysaccharides, exopolysaccharides, teichoic and lipoteichoic acids and so on) to be analysed. The chemical nature and the location of the polysaccharides on the bacterial membrane mostly influence the choice of the extraction procedure to be applied.
Usually, the extraction with *n*-butanol is performed for the recovery of lipoteichoic acid (LTA) due to its lipophilic nature (Vinogradov, Sadovskaya, Cornelissen, & van Sinderen, 2015b).
Capsular polysaccharides (CPS) and teichoic acids (TA) can be extracted with strong (hydrofluoric acid hydrolysis) or mild treatment (hot water treatment), depending on how firmly the polysaccharide is anchored to the membrane and on the bacterial species considered. We observed that the hot water treatment (120 °C for 20') works better in the extraction of bacilli polysaccharides while for the extraction of polysaccharides from *Ruminococcus gnavus* ATCC 35913, the combination of n-butanol + hydrofluoric hydrolysis protocols is the better choice to obtain the final product clean, without the need of further purifications procedures.

4.2.1. *n*-Butanol extraction procedure

In order to remove lipoteichoic acid, bacterial cells were treated as described by Morath et al. (Morath, Geyer, & Hartung, 2001), with some modifications. Briefly, the pellet was suspended in a mixture of H_2O/ButOH 1:1 (V/V), and CH_3COOH was added until a pH 4.7 was reached. The suspension was left under stirring for 30 min at room temperature (RT). After centrifugation at 7000 rpm, 4 °C, for 30 min, the aqueous phase was lyophilized.

4.2.2. HF hydrolysis procedure

After the *n*-butanol treatment, the bacterial pellet was directly treated with 48% aqueous hydrofluoric acid at 4 °C for 48, followed by neutralization with concentrated ammonia (28%). The solution was centrifuged (4 °C, 8000 rpm, 30 min) and the pellet was washed three times with water. The supernatant was dialyzed in MilliQ water (membrane cut-off 1 kDa) for 120 h and freeze-dried. Sample were not further purified and used directly for chemical and spectroscopical analysis.

4.2.3 Hot water treatment

Dry cells were suspended in MilliQ water and heat-inactivated in the autoclave at 120°C for 20 min. After the inactivation, the solution was centrifuged (4 °C, 8000 rpm, 10 min) and the supernatant was recovered and filtered over a 0.45 mm filter and freeze-dried.

4.2.4. Chromatographic purification procedures

The crude polysaccharides were purified through a combination of chromatographic techniques. It was used a size exclusion chromatography on Sephacryl® S-300 HR resin (1.5 x 45 cm, Cytiva 17-0599-01), packed and eluted with ammonium bicarbonate 50 mM, ammonium, and the eluate was monitored by a refractive index detector. A subsequent anion exchange chromatography on Q-sepharose® Fast-Flow (1 x 1.5 cm, Cytiva 17-0510-01) was useful to isolate the teichoic acids (almost in a resin/sample ratio of 1 mL : 5 mg) since its phosphate groups interact with the quaternary (Q) strong anion exchange groups

of the resin. The elution was done with a stepwise gradient of NaCl (10, 100, 200, 400, 700, 1000 mM); the teichoic acids are eluted with 200 mM < NaCl < 1 M. Each solution was concentrated by freeze-drying and desalted on BioGel® P-10, ran in water, and the eluate was monitored by a refractive index detector. Typically, chromatograms displayed a first peak in the void volume, and an intense peak related to salts.

4.2.5. Enzymatic digestion of nucleic acids and proteins

The rupture of the cells during the various extraction procedures determines the leakage of the nucleic acids and proteins in the extracellular medium thus the sample was subjected to an enzymatic digestion in order to remove them. The material was dissolved in a buffer (100 mM Tris, 50 mM NaCl, 10 mM $MgCl_2$, pH 7.5) at a concentration 1 mg/mL. Then, RNAse and DNAse (1 mg/100 μL) were added and left at 37 °C, under stirring. After 6 h, proteinase K (0,5 mg/50 μL) was added and the solution was left at 37 °C for other 10 h, under stirring. The resulting product was dialysed (membrane cut-off 12-14 kDa) over 3 days to eliminate the oligonucleotides and the peptides released by the enzymatic digestion (De Castro et al., 2010).

4.2.6. SDS-PAGE

Detection of CPS was performed through SDS-PAGE (sodium dodecyl sulfate in a PolyAcrylamide Gel Electrophoresis) with alcian blue (for the detection of anionic polysaccharides) followed by a silver staining (Kittelberger & Hilbink, 1993). This technique separates biological macromolecules according to their electrophoretic mobility, namely the molecules motion in a uniform electric field. The mobility is a consequence of the size and charge of the molecules. SDS is an anionic detergent that links the molecules, causing their denaturation and imparting an even distribution per unit mass, which allow their mobility toward anode. Electrophoretic gel consists of a polymer of acrylamide cross-linked with bisacrylamide, upon which large molecules remain on the top and small molecules migrate on the bottom. Size pores can be changed by using different percentage of these two components: since CPSs have usually a high molecular weight,a 12% polyacrylamide was chosen for the purpose of this work. Electrophoretic gels are made up of stacking or upper gel and separating or lower gel. The two layers have different composition and pH, so the samples are concentrated at the interphase among the upper and the lower gel before the effective separation across the sieves of the lower gel. In the lower gel was added the BLUeye prestained Protein Ladder (2 μl) as protein marker, in order to determine the molecular weight of each sample. Aliquots from each sample (1 mg/mL) are mixed with the sample buffer 5x (4:1 v/v) and denaturated for 5 min at 100 °C. Sample buffer solution consists of: 1 M TRIS pH 6.8 (0.6 mL); SDS 20 % (2 mL); glycerol (2.5 mL); mercaptoethanol (0.5 mL); bromophenol blue 3% (33 μL) and water. Electrophoretic run was conducted at 150 V and by using TRIS-Glycine (TRIS 25 mM, glycine 192 mM, SDS 0.1%, pH 8.3) as running buffer. After the run, gel was left in fixing solution (100 mL of AcOH 5% + EtOH 40%) for 30' and consequently in alcian blue O.N. After that, the alcian blue was removed and the gel was again put into a fresh fixing solution for 30'. The following silver nitrate stain consists in:

-oxidation with $NaIO_4$ (100 mg) in 100 mL of fixing solution for 10 min;

-washes with H_2O for 30 min X 3 times;
-silver solution (0.1% AgNO3 in 100 mL of H_2O);
-washes with H_2O for few sec;
-color development with 3% Na_2CO_3 + CH_2O (20 μL) in 100 mL of H_2O until the desired color intensity is reached;
-stop of the stain development with 1% AcOH for 5 min;
-final washes with H_2O and drying.

4.3. Polysaccharides molecular weight determination

The molecular weight was determined by size exclusion chromatography on TSK G-5000 PW_{XL} (30 cm x 7.8 mm), eluted with NH_4HCO_3 50 mM (flow =0.8 mL/min), and monitoring the eluate with a refractive index detector, by using a HPLC Agilent 1100. First, a calibration curve was built by injecting 10 μg of dextran polysaccharides of known molecular weight (5, 12, 50, 150, 410 and 670 kDa, stock solution: 1 mg/ml). It related by a linear regression the elution volume and log10 of the molecular weight. Then, 10 μg of each sample was injected, and the molecular weight was calculated based on the calibration parameters of the column. Moreover, the ratio between the molecular weight of the polysaccharides and that of their repeating unit determined the average number of repeating units assembled.

4.4. Polysaccharides composition and structure determination

Polysaccharide chemical analysis can be done through a combination of different analytical techniques. In particular, the chemical structure can be determined by NMR spectroscopy and GC-MS, after a series of chemical derivatizations.

4.4.1. GC-MS

It is first necessary that the polysaccharides are hydrolysed into their respective monosaccharide components, which must finally be made volatile to be able to study them through gas chromatography-mass spectrometry (GC-MS) technique. Based on this requirement, it was always done a final chemical derivatisation of these molecules into acetylated compounds. In this research activities, the acetylated methyl glycosides (MGA), octyl-glycosides (OMG) and partially methylated and acetylated alditols (AAPM) methods were applied (De Castro et al., 2010). Finally, all these derivatives were analysed by using a GC-MS Agilent Technologies 7820A (Santa Clara, CA, USA) equipped with a mass selective detector 5977B, an automatic injector 7693A and a HP-5ms capillary column (Agilent, 30 m x 0.25 mm i.d., 0,25 μm as film thickness, flow rate 1.2 mL/min, He as carrier gas). Electron impact mass spectra were recorded with ionization energy of 70 eV. The temperature program used was: 150 °C for 3 min, 150 up to 280 °C at 3 °C/min, 300 °C for 5 min.

4.4.1.1. Acetylated methyl glycosides (MGA)

The monosaccharide content was established by the acetylated O-methyl glycoside derivatives method. When it was present a teichoic acid or in general a phosphodiester bridge in the polysaccharide structure, it was first hydrolysed with 50 μl of HF 50% at 25 °C for 5 h. Then, the sample (0.2 mg) was treated with 1 mL HCl/MeOH (1.25 M, 80 °C, 16 h)

followed by an acetylation step with 50 μl acetic anhydride in 100 μl pyridine (80 °C, 30 min).

4.4.1.2. Acetylated octyl glycosides (OAG)

The absolute configuration of the monosaccharides was determined by analyzing their acetylated 2-(-)-octyl derivatives obtained by the reaction with an optically pure alcohol (R-(-)-octanol). Identification of the derivatives was inferred by GC–MS analysis by comparing the retention time of the peaks in the sample with those from the in-house built standards (acetylated monosaccharides functionalized with pure octanol and its racemic mixture). The procedure consists in the treatment of the pure capsular polysaccharides with 100 μL of R-(-)- octanol and 15 μL of acetyl chloride at 60 °C, O.N. Octanol excess was eliminated under air flux. Finally, the octyl glycosides were acetylated by adding 100 μL of pyridine and 50 μL of acetic anhydride at 80 °C for 30 min (Leontein, Lindberg, & Lönngren, 1978). As for the CPS of *E. faecium*, the stereochemistry of the glycerol substituent was performed by following the procedure (Rundlöf & Widmalm, 1996). Briefly, the sample was dissolved in a solution of TEMPO (2,2,6,6-Tetramethyl-1-piperidinyloxy, 2.5 mg), NaBr (28.5 mg) and NaOCl (13% aq), for 1 h, at 0 °C, at pH 10.8, to oxidize all the free primary alcoholic functions. Consequently, an hydrolysis with HF 50% (50 μL), for 5 h at 25 °C was performed to release the glyceric acid residue, then transformed in the corresponding acetylated 2-(-)-octyl ester derivative by the same aforementioned procedure.

4.4.1.3. Partially methylated alditols acetates (AAPM)

The sugar linkage pattern was defined by the partially methylated and acetylated alditols method. The sample (0.5 mg) was solved in anhydrous DMSO (1 mL) and a spun of spatula of powdered NaOH was added. The suspension was stirred at RT for 4 h, sonicating often to facilitate the dissolution of NaOH in DMSO. After that, the deprotonated alcoholic groups were methylated with 200 μl of CH_3I, left stirring t RT, O.N. The solution was extracted with $H_2O/CHCl_3$ (3:1 v/v) five times, by centrifuging at 2500 rpm for 3 min and replacing the top layer with H_2O each time. Then, the $CHCl_3$ phase was evaporated and the sample was subsequently hydrolysed with 200 μl of trifluoroacetic acid 2 M, at 120 °C for 2 h. After that, the anomeric function was marked and reduced by adding the tip of a small spun of $NaBD_4$ and 200 μl of EtOH. The sample was kept capped at RT for 1 h. The $NaBD_4$ excess was destroyed with few drops of glacial AcOH, subsequently neutralized with MeOH and evaporated under air flow. Finally, sample was acetylated with acetic anhydride (50 μl) and pyridine (100 μl) (Ciucanu & Kerek, 1984).

4.4.2. NMR spectroscopy

^{31}P and a ^{31}P-^{1}H HSQC spectra were measured on a Bruker DRX-400 MHz spectrometer, equipped with a QNP inverse probe operating at 298 K. HSQC was acquired by setting a $^{3}J_{H,P}$ coupling constant value of 20 Hz.

^{1}H and 2D NMR spectra were recorded using a Bruker 600 MHz spectrometer (University of Naples Federico II), equipped with an inverse cryoprobe with gradients along the z axis, and a Bruker 1200 MHz (CNRS of the University of Lille). The samples were solved in 550 μL of D_2O and the spectra were calibrated with internal acetone (δ_H= 2.225 ppm; δ_C = 31.45 ppm). Total Correlation Spectroscopy (TOCSY) and Nuclear Overhauser Enhancement

Spectroscopy (NOESY) experiments were performed using data sets (t1 × t2) of 2048 × 512 points. Heteronuclear Single-Quantum Coherence (HSQC) and Heteronuclear Multiple Bond Correlation (HMBC) experiments were performed in the ^{1}H-detection mode by single-quantum coherence with proton decoupling in the ^{13}C domain using data sets of 2048 × 512 points. HSQC was performed using sensitivity improvement and the phase-sensitive mode using echo/antiecho gradient selection, with multiplicity editing during the selection step (States, Haberkorn, & Ruben, 1982). HMBC was optimised on long-range coupling constants, with a low-pass J filter to suppress one-bond correlations, using gradient pulses for selection. Moreover, a 60 ms delay was used for the evolution of long-range correlations. HMBC was optimized on long-range coupling constants, with a low-pass J filter to suppress one-bond correlations, using gradient pulses for selection, and a 60 ms delay was used for the evolution of long-range correlations. HMBC spectra were optimized for 6 – 15 Hz coupling constants. For transformation, the data matrix in both homo- and heteronuclear experiments was extended to 4096 × 2048 points and transformed by applying a qsine or a sine window function (Speciale et al., 2022). Spectra were transformed and analyzed with Bruker Topspin NMR DATA analysis software.

Concerning with the other parameters of spectra acquisition the conditions were as follows:

-for *L. reuteri,* spectra were acquired at 298 K. With regard to the teichoic acid analysis, TOCSY and NOESY mixing time was set to 100 and 300 ms, respectively, and 32 scans for each spectrum were recorded; HSQC experiment were recorded with 40 scans;

-for *R. gnavus*, spectra were acquired at 298 K. TOCSY and NOESY mixing time was set to 100 and 200 ms, respectively, and 24 scans for each spectrum were recorded;

-for *B. subtilis,* spectra were recorded at 298 K. TOCSY and T-ROESY experiments were performed with a mixing times of 100 and 400 ms, respectively. Concerning with the teichoic acid, 40 scans for COSY, 32 for TOCSY, 64 for HSQC and 80 for HMBC were recorded. In the CPS NMR analysis, COSY were acquired with 32 scans, T-ROESY and TOCSY with 40, HSQC with 60, HMBC with 80 and HSQC-TOCSY with 100 scans;

-for *E. faecium*, spectra were recorded at 315 K. TOCSY and NOESY experiments were both performed with a mixing times of 100 ms. 24 scans for COSY, TOCSY and NOESY, 40 for HSQC, 70 for HMBC and 100 for HSQC-TOCSY were recorded;

-for *L. rhamnosus,* spectra were acquired at 298 K. HSQC experiment was recorded with 24 scans;

-for *L. paracasei,* spectra of the mixture of TA+CPS-1 were acquired at 298 K. TOCSY and NOESY mixing time was set to 100 and 200 ms, respectively, and were recorded, along with COSY experiment, with 24 scans. 100 scans were recorded for HMBC and HSQC-TOCSY and 60 for HSQC experiments. Spectra of the CPS-1 pure isolate were recorded at 315 K, with a number of scans of 32 for TOCSY and 70 for HSQC experiment. TOCSY mixing time was set to 100 ms. Finally, the CPS-2 spectra were recorded at 315 K. TOCSY and NOESY mixing time was set to 100 and 200 ms, respectively, and 16 scans for each one and for COSY spectrum were recorded. 128, 512 and 192 scans were acquired for HSQC, HMBC and HSQC-TOCSY spectrum, respectively.

4.4.3. HR-MAS NMR spectroscopy technique

The high-resolution magic-angle spinning (HR-MAS) NMR spectroscopy can be used to investigate the molecular surface components on the intact cells (Ainsworth et al., 2014) (Maes et al., 2009). The expression of *L. paracasei* surface polysaccharides in its different grow phases and after inactivation was analysed by this technique. The bacterium was grown in MRS broth (0.5 L) and collected at various time intervals corresponding to its growth phases. Cells in their lag growth phase were harvested after 4 h, corresponding to an O.D. of 0.3; cells in their exponential phase were harvested after 5 h, corresponding to an O.D. of 0.5, and cells in their stationary phase were harvested after almost 15 h, corresponding to an O.D. of 3. Finally, after almost 48 h, the growth was stopped, the bacterium was centrifuged and the pellet was collected. Dry cells were suspended in MilliQ water and heat-inactivated in the autoclave at 120°C for 20 min. The suspension was centrifuged and the supernatant containing polysaccharides was recovered apart from the pellet, on which the subsequent HR-MAS analyses were performed. Thus, cell pellets were washed several times with deuterium oxide to remove culture medium residues and protonated water. The 4-mm ZrO_2 rotors were filled with 50 µl of cells alive or with 90 µl of inactivated pellet. All of them were centrifuged at 4000 rpm, for 4 min, at RT.

Monodimensional ^{1}H and bidimensional ^{1}H-^{13}C HSQC NMR experiments were performed by Dr. Xavier Trivelli, belonging to the research group of Prof. Jann Guèrardel of the CNRS of the University of Lille. The instrument used was an 18.8 T, Avance NEO 800 MHz Bruker spectrometer, equipped with a ^{1}H-^{13}C-^{31}P probe with uniaxial gradients spinning at 5 kHz, at 293 K. Proton and ^{13}C resonate at 800 and 201 MHz, respectively. All of the experiments were sourced from the Bruker library pulse programs, and delays and powers were optimized for each (Sadovskaya et al., 2017). All the spectral widths were 8,197 Hz (^{1}H) with 1,024 points for free induction decay resolution and 28,168 Hz (^{13}C), giving 8.0 and 220 Hz/point. The spectra of *L. paracasei* inactivated cells and of the bacterium cells in their lag, exponential and stationary phase, were acquired during 424, 376, 688, and 352 scans, respectively.

4.5. Immunological assays on *L. rhamnosus* and its polysaccharide

All these assays were performed by Prof. Roberto Canani's research group from CEINGE-Biotecnologie Avanzate of Naples.

4.5.1. Human enterocyte cell lines and peripheral blood mononuclear cells

Caco-2 cells were used as validated model of gut barrier (American Type Culture Collection, Middlesex, UK; accession number: HTB-37) (Sambuy et al., 2005). Cells were grown in Dulbecco's modified Eagle's medium (DMEM; Gibco, Berlin, Germany) with L-glutamine and a high concentration of glucose (4.5 g/L), supplemented with 10% fetal bovine serum (FBS, Gibco), 1% non-essential amino acids (Gibco), 1% sodium pyruvate (Gibco), and 1% penicillin/streptomycin (Gibco). The cells were incubated at 37°C in a atmosphere containing 5% CO_2. The culture medium was changed every 2 days.

Peripheral blood samples were obtained from four pediatric patients with a cow's milk allergy IgE-mediated. Blood samples were analysed in an anonymized manner with the permission of the Ethics Committee of the University Federico II of Naples. PBMCs were

isolated from heparinized peripheral blood (8 ml) by Ficoll density gradient centrifugation (Ficoll Histopaque-1077, Sigma, St. Louis, Missouri, USA). Briefly, cells were stratified on 3 ml of Ficoll and centrifuged, 2500 rpm for 10 min, at RT. The opaque interface containing mononuclear cells was carefully aspirated and cells were washed with 10 ml of PBS and centrifuged again, at 1400 rpm for 10 min, at RT. The upper layer was discarded and PBMCs (2×10^5 cells/well) were cultured in duplicates in 96-well plates in 200 µl culture medium (RPMI 1640, Gibco) containing 10% FBS (Gibco), 1% non-essential amino acids (Gibco), 1% sodium pyruvate (Gibco), and 1% penicillin/streptomycin (Gibco).

4.5.2. Caco-2 and PBMC stimulation

Caco-2 cells were stimulated after 15 days post-confluence with heat inactivated bacterium (1 µg/ml), or CPS (100 µg/ml) or ID35 (10 µg/ml) or CPS+ID35, for 48 h. For PBMCs stimulation, beta-lactoglobulin (BLG; 200 µg/ml) was added in the presence or in absence of heat inactivated bacterium (1 µg/ml), or CPS (100 µg/ml), or ID35 (10 µg/ml), or CPS+ID35, for 5 days. In both cases, cells exposed to only medium were used as negative control.

4.5.3. Quantitative Real-Time PCR

Total RNA was extracted from stimulated Caco-2 and PBMCs cells with TRIzol reagent (Gibco BRL, Paisley, UK). RNA samples were quantified using the NanoDrop 2000c spectrophotometer (Thermo Scientific) and purity was verified by A260/280 and A260/230 absorbance ratios. To evaluate the gene expression of the interferon alpha 2 (*Ifna2*, Hs00265051_s1), the transforming growth factor beta 1 (*th2*, Hs00998133_m1), and the prostaglandin-endoperoxide synthase 2 (*Ptgs2*, Hs00153133_m1), quantitative real-time PCR analysis was performed using Taqman Gene Expression Master Mix (Applied Biosystems, Vilnius, Lithuania). The TaqMan probes for these genes were inventoried and tested by Applied Biosystems manufacturing facility (QC). Gene expression of the mucin 2 (*Muc2*), main protein involved in the regulation of mucus thickness, and *lactase* enzyme, marker of enterocytes differentiation, was evaluated using a SYBR green Master Mix (Applied Biosystems, Grand Island, NY, USA).

4.5.4. Determination of cytokines production by PBMCs

The quantities of IL-4, IL-5, IL-13 and IL-10 in cell supernatant were measured using specific human ELISA assay kits (Elabscience Biotechnology Inc. Wuhan, Hubei).

4.5.5. Treg population analysis by flow cytometry

Tregs were identified as CD4+/CD25+/FoxP3 positive cells by flow cytometry analysis. The staining was developed by using Treg detection human kit (Miltenyi Biotech, Bergisch Gladbach, Germany) and the results were analyzed by BD CANTO II flow cytometer and DIVA software (Becton-Dickinson, Franklin Lakes, New Jersey, USA). 100000 events were acquired after gating of lymphocytes based on the FSC/SSC dot plot.

4.6. Immunological assays on *B. subtilis* polysaccharides

These assays were performed by Prof. Lipka Volker's research group from Georg-August Universitat, Department of Plant Cell Biology (GE). With the aim to observe an immunological response, Arabidopsis leaves have been treated through leaf puncture with both the teichoic acid and the CPS of the bacterium. The range of concentrations used were 100-1 μg/ml and 100-1 ng/ml. The bacterium alone ($O.D_{600}$ = 0.02) represented the positive control, while MilliQ water was the negative control. Leaf wilting has been considered as a symptom of a hyperinflammatory or autoimmune response.

4.7. Immunological assays on *R. granvus* strains and its polysaccharide

All of these experiments were carried out by Prof. Juge's team from Quadram Institute Bioscience (UK).

4.7.1. Bone marrow-derived dendritic cells (BMDCs)

C57BL/6 mice from the Disease Modelling Unit at the University of East Anglia (Norwich, UK) were killed and disinfected with EtOH 75%. A syringe was inserted into the bone cavity to rinse the bone marrow into a sterile culture dish with RPMI-1640 medium supplemented with 10 % FBS. The cell suspension in the dish was centrifuged and the cell pellet was resuspended with Tris-NH_4Cl red blood cell (RBC) lysis buffer to lyse the RBCs. After a second centrifugation step the supernatant was discarded, and the pellet was washed with PBS. Isolated monocytes were cultured in cell culture dishes at a density of 5.0×10^5 cells/ml in Gibco's serum-free AIM-V medium (Invitrogen, Carlsbad, CA, USA) supplemented with 80 ng/ml granulocyte monocyte stimulating factor (Gentaur Molecular Products, Brussels, Belgium), at 37°C in an atmosphere supplemented with 5 % CO_2.

4.7.2. Epithelial cell models

T84 and LS174T cell lines were obtained from the European Collection of Authenticated Cell Cultures. T84 and mucin-producing LS174T human colon carcinoma cells were cultured in T75 flasks at a density of $1.0x10^5$ cells/ml in Dulbecco's Modified Eagle's medium/Nutrient F-12 Ham (DMEM/F12 1:1) and DMEM medium, respectively, supplemented with 10% foetal bovine serum, 2 mM glutamine, 100 U/mL of penicillin and 100 μg/mL of streptomycin, at 37°C atmosphere containing 5% CO2.

4.7.3. Cells stimulation

Bacteria at MOI 20:1 or 200 μg/ml of glucorhamnan in DMEM/F12 medium were added to the apical part of the transwells in order to see the interaction with the epithelial cell models. The medium was used as negative control. The cells were incubated 37°C with 5% CO_2, 18 h.

BMDCs ($5x10^5$ cells per well) were incubated with the bacteria (MOI: 50:1) or purified glucorhamnan (200 μg/ml) at 37°C, for 18 hours in 96-well microplates. LPS from *E. coli* O111:B4 (100 μg/ml) (InvivoGen, San Diego, USA) was used as a positive, while mBMDCs cultured without bacteria or glucorhamnan were used as negative control. Then, the microwell plates were centrifuged at 510 × g for 3 min and the supernatant was collected.

4.7.4. Cytokine quantification

Quantification of TNF-α and IL-10 secretion was done by ELISA, using the protocols from Biolegend (San Diego, USA). Quantification of IL-29 was carried using Human IL-29 (IFN lambda 1). Briefly, the supernatant (50 µl) from the cells co-cultures was added into microwells (96-well microplates) and then incubated with the mouse capture antibody and the mouse detection antibody, avidin-HRP (Biolegend, San Diego, USA). After each step, the cells were washed with PBS enriched with 0.05% Tween-20. After incubation with 3,3',5,5'-Tetramethylbenzidine (TMB) for 15 min, the colour development was monitored by using a Bio-Rad Benchmark Plus microtiter plate reader at A570/450 nm.

4.8. Immunological assays and glycoconjugation of *E. faecium* polysaccharide

4.8.1. Rabbit immunization

Rabbit immunizations with heat inactivated *E. feacium* U0317 were performed by Charles River Laboratories (Kropec et al., 2011). New Zealand white rabbits were immunized with heat-killed *E. faecium* strain at a concentration of $1.4x10^{12}$ CFU per dose, by intravenous injection three times a week, for 3 weeks.

4.8.2. Opsonophagocytic inhibition assays

These experiments were done by Dr. Diana Milena Laverde Gómez's team, from Ludwig Maximilians University. The bacterial strain *E. faecium* U0317 was grown overnight in TSB from a single colony that was derived from a TSA fresh plate. The cells were harvested by centrifugation, washed three times with PBS, and separated into three batches for subsequent treatments (Hammerschmidt, Talay, Brandtzaeg, & Chhatwal, 1997). The first batch was heat-inactivated at 65°C for one hour; the second batch was treated with proteinase K (0.1 mg/mL) and calcium chloride (5 mM), incubated at 54°C for four hours and then heat-inactivated at 65°C for an hour; the third batch was treated with sodium metaperiodate (1 M) for 24 hours at room temperature. The sodium metaperiodate was finally neutralized with an excess (2 M) of ethylene glycol (Karl Roth). All the treated cells were then washed three times with PBS and adjusted to a concentration of around $2.5x10^{11}$ CFU/mL in PBS for the OPIA.

4.8.3. Conjugation of purified polysaccharides L22 from *E. faecium* U0317 with BSA

This experiment was done by Dr. Luis Felipe Romero Saavedra, from Ludwig Maximilians University. BSA was conjugated with L22 by activation of its hydroxyl groups with CDAP (1-cyano-4-dimethylaminopyridinium tetrafluoroborate) (Lees, Barr, & Gebretnsae, 2020). L22 was dissolved in H_2O (10 mg/mL) and a freshly solution of CDAP in acetonitrile (10:1) was added. The mixture was stirred for 30 seconds, and triethylamine (0.2 M) was added to neutralize the pH. For the coupling with the carrier protein 100 µL of the corresponding protein (10 mg/mL) was added to the mixture. The reaction was left at RT, O.N. After that, the glycoconjugate was purified through an Amicon ultrafiltration filter unit with Ultracel-100 membrane. Finally, the content of the sugar and protein was determined by hexose and Bradford assays (Romero-Saavedra et al., 2019).

4.8.4. Immunodotblot

The immunodotblot technique was utilized by Dr. Diana Milena Laverde Gómez's team to assess the immunoreactivity of polysaccharide fractions with anti-U0317 serum. Hybond ECL Membrane (GE healthcare, UK) was used for dot blotting proteins. The membrane was loaded with 2 µL of each polysaccharide-containing fraction and incubated at 4°C, for 2 h, in blocking buffer (BB) consisting on PBS + 3% skim milk. After that, it was washed three times with washing buffer (WB), composed of PBS + 0.05% Tween 20, and incubated at RT for 1 h with the anti-U0317 primary antibody diluted 1:500 in BB (the primary antibody excess was removed by washings with WB). After that, the membrane was incubated with goat anti-rabbit IgG secondary antibody marked with alkaline phosphatase (1:1000 in BB) at RT for 1 h. Thus, the membrane was washed four times with WB and put into a color development solution, consisting on 100 µL of 5-Bromo-4-chloro-3-indolyl-phosphate (BCIP) and 100 µL of nitro blue tetrazolium (NBT) diluted in 10 mL alkaline phosphatase color development buffer. When the color appeared, the reaction was stopped by washing the membrane with distilled water. Immunoreactivity is confirmed if the membrane becomes purple within 5 minutes of exposure to the substrate solution.

4.8.5. Opsonophagocytic assay and opsonophagocytic inhibition assay

These assays were performed by Dr. Diana Milena Laverde Gómez's team as described elsewhere (Laverde et al., 2020). For the OPA, there were used: baby rabbit serum as the complement source, rabbit or mouse sera raised against various antigenic determinants, the target bacterial strain, and freshly isolated polymorphonuclear leukocytes (PMN's). The lyophilized baby rabbit serum was resuspended in sterile RPMIF medium (RPMI + 15% fetal bovine serum), and diluted to a final concentration of 6.7% in RPMIF. The mixture was absorbed at 4 °C, for 60 min with the target bacterial strain obtained from a freshly grown TSA plate. After that, the entire solution was centrifuged and filtered. For the PMN's collection, fresh human blood was collected from healthy adult volunteers and mixed with an equal volume of heparin-dextran buffer. After incubation (37°C for 45 min), the upper phase containing leukocytes was centrifuged and washed with RPMIF. The cells were then resuspended in ammonium chloride (10 mL, 1%), and incubated at RT, for 20 min. Finally, the PMN's were washed again with RPMF and resuspended to obtain a final concentration of 2×10^7 cells/mL. The bacteria were grown O.N. on a TSA plate, then single colonies were grown at 37°C until an OD_{650} of 0.400. Finally, bacterial cells were washed, and diluted with RPMF to obtain a final concentration of 2×10^7 CFU/mL. For the assay, 100 µl both PMN's, antibody dilutions, absorbed baby rabbit complement, and bacterial suspension were mixed, and incubated at 37 °C for 90 min. After that, samples were diluted, plated in TSA, and incubated O.N. at 37 °C. By comparison of the colony forming units (CFUs) surviving in tubes containing bacteria, PMN's, complement, and antibody, to those where PMN's were lacking the % of bacterial killing has been estabilished. The experiment was repeated at least twice, using different blood donors, under the same conditions. For the opsonophagocytic inhibition assay (OPIA), from 0.08 to 100 µg/mL of purified polysaccharide fractions, or 1.25x10^11 CFU/mL of treated bacterial cells were used. These inhibitors were incubated at 4 °C for 60 min, with an equal volume of serum dilution. Thus, the same aforementioned opsonophagocytic assay was performed, using the mixture of

inhibitor/serum dilution in place of the serum dilution used in a standard opsonophagocytic assay. The assays were conducted with an antibody dilutions resulting in 70 to 80% opsonic killing of the bacteria. The inhibition of killing was determined as the % of surviving CFUs after opsonophagocytic killing when the inhibitor was used, compared to the % of surviving CFUs when no inhibitor was added.

4.8.6. Mice immunizations

Female BALB/c mice, aged between six to eight weeks (Charles River Laboratories) were immunized by Dr. Diana Milena Laverde Gómez's team, with polysaccharide L22, BSA, and L22-BSA glycoconjugate. 10 µg of each antigen emulsified in 100 µL of complete Freund's adjuvant was employed for the vaccination. Two days after, the mice received a boost subcutaneously with the same antigen dose emulsified in 100 µL of incomplete Freund's adjuvant and an intraperitoneal boost on days 5, 14, and 21 days after, with 5 µg of antigen suspended in saline. Finally, 23 days after mice were euthanized, and their blood was collected. After centrifuging, 4000 rpm for 5 min at 4 °C, the resulting upper phase, containing the blood serum, was employed for the opsonophagocytic assay. Anyway, two mice were sacrificed on day 0, before any vaccinations were administered, and their blood serum was used as pre-immune control serum.

Acknowledgements

I would like to express my heartfelt thanks to my principal investigators Prof. De Castro and Prof Molinaro from University of Naples Federico II for all the scientific heritage handed down to me. To date, my passion for sugar has, if possible, increased even more.

As well, I really want to express my sincere thanks to all the Synthesis and Structure of Carbohydrates in Naples group (SSCN), especially Dr. Forgione M., Dr. Marseglia, Dr. Di Carluccio, Dr. Iovine, Dr. Lembo and Dr. Fabregat not only for their constant support, but also for making every single day of this journey more special and carefree. Thank you for making the difference.

Also, I would like to extend my gratitude to Prof. Speciale, Dr. Notaro, Prof. Lombardi, Prof. Silipo, Prof. Lanzetta, Prof. Bedini, Prof. Iadonisi, Prof. Corsaro, Prof. Di Lorenzo, Prof. Marchetti, Prof. Casillo, Prof. Traboni, Dr. Lenza, Dr. Fanina, Dr. D' Amico, Dr. Esposito, Dr. Frogione R., Dr. Tiemblo, Dr. Amor and Dr. Pither, it was a real pleasure to meet you.

In addition, I would like to thank the UGSF of the CNRs of Lille, and in particular Prof. Guerardel, Dr. Trivelli, Dr. Vidal, Dr. Alessandra, Dr. Reginald, Dr. Bouckaert, Dr. Yannick and Dr. Biot for their welcome and their precious support in the realization of a beautiful part of my Ph.D project.

I also have to really thank to Prof. Verna, Prof. Canani, Prof. Volker, Prof. Juge and Dr. Romero and all their research team for giving us the carbohydrate sources and performing the immunological assays necessary to exploit our goals.

Special thanks go to my family, for always representing, without a shadow of a doubt, my strong point and my safe home.

Another special thanks goes to my second grandmother, my grandparents and my uncle who watch me from up there. You are the little stars that I always carry with me in my dark moments.

Last, but not least, I wish to thank all my friends, my boyfriend and my acquired family in Naples, for their constant presence and for helping to make every day special.

References

Agudelo Higuita, N. I., & Huycke, M. M. (2014). *Enterococcal Disease, Epidemiology, and Implications for Treatment*. In M. S. Gilmore, D. B. Clewell, Y. Ike & N. Shankar (Eds.), *Enterococci: From Commensals to Leading Causes of Drug Resistant Infection*. Boston: Massachusetts Eye and Ear Infirmary

Aguilar-Toalá, J. E., Arioli, S., Behare, P., Belzer, C., Berni Canani, R., Chatel, J.-M., Zhou, Z. (2021). Postbiotics — when simplification fails to clarify. *Nature Reviews Gastroenterology & Hepatology,* 18(11), 825-826.

Aguilar-Toalá, J. E., Garcia-Varela, R., Garcia, H. S., Mata-Haro, V., González-Córdova, A. F., Vallejo-Cordoba, B., & Hernández-Mendoza, A. (2018). Postbiotics: An evolving term within the functional foods field. *Trends in Food Science & Technology,* 75, 105-114.

Aguirre, M., & Collins, M. D. (1993). Lactic acid bacteria and human clinical infection. *J Appl Bacteriol,* 75(2), 95-107.

Ainsworth, S., Sadovskaya, I., Vinogradov, E., Courtin, P., Guerardel, Y., Mahony, J., van Sinderen, D. (2014). Differences in lactococcal cell wall polysaccharide structure are major determining factors in bacteriophage sensitivity. *mBio,* 5(3), e00880-00814.

Altveş, S., Yildiz, H. K., & Vural, H. C. (2020). Interaction of the microbiota with the human body in health and diseases. *Biosci Microbiota Food Health,* 39(2), 23-32.

Arboleya, S., Sánchez, B., Solís, G., Fernández, N., Suárez, M., Hernández-Barranco, A. M., Gueimonde, M. (2016). Impact of Prematurity and Perinatal Antibiotics on the Developing Intestinal Microbiota: A Functional Inference Study. *Int J Mol Sci,* 17(5).

Ardita, C. S., Mercante, J. W., Kwon, Y. M., Luo, L., Crawford, M. E., Powell, D. N., Neish, A. S. (2014). Epithelial adhesion mediated by pilin SpaC is required for *Lactobacillus rhamnosus* GG-induced cellular responses. *Appl Environ Microbiol,* 80(16), 5068-5077.

Attridge, S. R., & Holmgren, J. (2009). *Vibrio cholerae* O139 capsular polysaccharide confers complement resistance in the absence or presence of antibody yet presents a productive target for cell lysis: implications for detection of bactericidal antibodies. *Microb Pathog,* 47(6), 314-320.

Balloux, F., & van Dorp, L. (2017). Q&A: What are pathogens, and what have they done to and for us? *BMC Biol,* 15(1), 91.

Basturk, A., Isik, İ., Atalay, A., & Yılmaz, A. (2020). Investigation of the Efficacy of *Lactobacillus rhamnosus* GG in Infants With Cow's Milk Protein Allergy: a Randomised Double-Blind Placebo-Controlled Trial. *Probiotics Antimicrob Proteins,* 12(1), 138-143.

Bednorz, C., Guenther, S., Oelgeschläger, K., Kinnemann, B., Pieper, R., Hartmann, S., Wieler, L. H. (2013). Feeding the probiotic *Enterococcus faecium* strain NCIMB 10415 to piglets specifically reduces the number of *Escherichia coli* pathotypes that adhere to the gut mucosa. *Appl Environ Microbiol,* 79(24), 7896-7904.

Berg, G., Köberl, M., Rybakova, D., Müller, H., Grosch, R., & Smalla, K. (2017). Plant microbial diversity is suggested as the key to future biocontrol and health trends. *FEMS Microbiology Ecology,* 93(5).

Berg, G., & Martinez, J. L. (2015). Friends or foes: can we make a distinction between beneficial and harmful strains of the *Stenotrophomonas maltophilia* complex? *Front Microbiol,* 6, 241.

Berg, G., Rybakova, D., Fischer, D., Cernava, T., Vergès, M.-C. C., Charles, T., Schloter, M. (2020). Microbiome definition re-visited: old concepts and new challenges. *Microbiome,* 8(1), 103.

Berni Canani, R., De Filippis, F., Nocerino, R., Laiola, M., Paparo, L., Calignano, A., Ercolini, D. (2017). Specific Signatures of the Gut Microbiota and Increased Levels of Butyrate in Children Treated with Fermented Cow's Milk Containing Heat-Killed *Lactobacillus paracasei* CBA L74. *Appl Environ Microbiol,* 83(19).

Bhakdi, S., Klonisch, T., Nuber, P., & Fischer, W. (1991). Stimulation of monokine production by lipoteichoic acids. *Infect Immun,* 59(12), 4614-4620.

Blake, C., Christensen, M. N., & Kovács Á, T. (2021). Molecular Aspects of Plant Growth Promotion and Protection by *Bacillus subtilis*. *Mol Plant Microbe Interact,* 34(1), 15-25.

Bos, M. P., Robert, V., & Tommassen, J. (2007). Biogenesis of the gram-negative bacterial outer membrane. *Annu Rev Microbiol,* 61, 191-214.

Brown, S., Santa Maria, J. P., Jr., & Walker, S. (2013). Wall teichoic acids of gram-positive bacteria. *Annu Rev Microbiol,* 67, 313-336.

Brown, S., Xia, G., Luhachack, L. G., Campbell, J., Meredith, T. C., Chen, C., Walker, S. (2012). Methicillin resistance in *Staphylococcus aureus* requires glycosylated wall teichoic acids. 109(46), 18909-18914.

Bulgarelli, D., Schlaeppi, K., Spaepen, S., Ver Loren van Themaat, E., & Schulze-Lefert, P. (2013). Structure and functions of the bacterial microbiota of plants. *Annu Rev Plant Biol,* 64, 807-838.

Bychowska, A., Theilacker, C., Czerwicka, M., Marszewska, K., Huebner, J., Holst, O., Kaczyński, Z. (2011). Chemical structure of wall teichoic acid isolated from *Enterococcus faecium* strain U0317. *Carbohydr Res,* 346(17), 2816-2819.

Chaparro, J. M., Badri, D. V., & Vivanco, J. M. (2014). Rhizosphere microbiome assemblage is affected by plant development. *The ISME Journal,* 8(4), 790-803.

Chapter 1 - Basic Biology of Oral Microbes. (2015). In X. Zhou & Y. Li (Eds.), *Atlas of Oral Microbiology* (pp. 1-14). Oxford: Academic Press

Cicenia, A., Scirocco, A., Carabotti, M., Pallotta, L., Marignani, M., & Severi, C. (2014). Postbiotic Activities of Lactobacilli-derived Factors. 48, S18-S22.

Ciucanu, I., & Kerek, F. (1984). A simple and rapid method for the permethylation of carbohydrates. *Carbohydrate Research,* 131(2), 209-217.

Coats, S. R., Pham, T. T., Bainbridge, B. W., Reife, R. A., & Darveau, R. P. (2005). MD-2 mediates the ability of tetra-acylated and penta-acylated lipopolysaccharides to antagonize *Escherichia coli* lipopolysaccharide at the TLR4 signaling complex. *J Immunol,* 175(7), 4490-4498.

Costerton, J. W., Cheng, K. J., Geesey, G. G., Ladd, T. I., Nickel, J. C., Dasgupta, M., & Marrie, T. J. (1987). Bacterial biofilms in nature and disease. *Annu Rev Microbiol,* 41, 435-464.

Cress, B. F., Englaender, J. A., He, W., Kasper, D., Linhardt, R. J., & Koffas, M. A. (2014). Masquerading microbial pathogens: capsular polysaccharides mimic host-tissue molecules. *FEMS Microbiol Rev,* 38(4), 660-697.

Crost, E. H., Coletto, E., Bell, A., & Juge, N. (2023). *Ruminococcus gnavus*: friend or foe for human health. *FEMS Microbiology Reviews,* 47(2).

Dasgupta, S., & Kasper, D. L. (2010). *Chapter 3 - Novel Tools for Modulating Immune Responses in the Host—Polysaccharides from the Capsule of Commensal Bacteria*. In F. W. Alt (Ed.), *Advances in Immunology* (pp. 61-91): Academic Press

De Angelis, M., & Gobbetti, M. (2011). *Lactic Acid Bacteria | Lactobacillus spp.: General Characteristics*. In (pp. 78-90)

De Boer, W. R., Kruyssen, F. J., & Wouters, J. T. (1976). The structure of teichoic acid from *Bacillus subtilis* var, niger WM as determined by C nuclear-magnetic-resonance spectroscopy. *Eur J Biochem,* 62(1), 1-6.

De Castro, C., Parrilli, M., Holst, O., & Molinaro, A. J. M. i. e. (2010). Microbe-associated molecular patterns in innate immunity: Extraction and chemical analysis of gram-negative bacterial lipopolysaccharides. 480, 89-115.

de Vrese, M., Laue, C., Papazova, E., Petricevic, L., & Schrezenmeir, J. (2019). Impact of oral administration of four *Lactobacillus* strains on Nugent score - systematic review and meta-analysis. *Benef Microbes,* 10(5), 483-496.

Dertli, E., Colquhoun, I. J., Gunning, A. P., Bongaerts, R. J., Le Gall, G., Bonev, B. B., Narbad, A. (2013). Structure and biosynthesis of two exopolysaccharides produced by *Lactobacillus johnsonii* FI9785. *J Biol Chem,* 288(44), 31938-31951.

Devriese, L., Baele, M., & Butaye, P. (2006). *The Genus Enterococcus*. In M. Dworkin, S. Falkow, E. Rosenberg, K.-H. Schleifer & E. Stackebrandt (Eds.), *The Prokaryotes: Volume 4: Bacteria: Firmicutes, Cyanobacteria* (pp. 163-174). New York, NY: Springer US

Dramsi, S., Magnet, S., Davison, S., & Arthur, M. (2008). Covalent attachment of proteins to peptidoglycan. *FEMS Microbiol Rev,* 32(2), 307-320.

Edwards, J., Johnson, C., Santos-Medellín, C., Lurie, E., Podishetty, N. K., Bhatnagar, S., Sundaresan, V. (2015). Structure, variation, and assembly of the root-associated microbiomes of rice. 112(8), E911-E920.

Edwards, M. S., Kasper, D. L., Jennings, H. J., Baker, C. J., & Nicholson-Weller, A. (1982). Capsular sialic acid prevents activation of the alternative complement pathway by type III, group B streptococci. *J Immunol,* 128(3), 1278-1283.

Eilam, O., Zarecki, R., Oberhardt, M., Ursell, L. K., Kupiec, M., Knight, R., Ruppin, E. (2014). Glycan Degradation (GlyDeR) Analysis Predicts Mammalian Gut Microbiota Abundance and Host Diet-Specific Adaptations. 5(4), 10.1128/mbio.01526-01514.

Enomoto, T., Shimizu, K., & Shimazu, S. (2006). [Suppression of allergy development by habitual intake of fermented milk foods, evidence from an epidemiological study]. *Arerugi,* 55(11), 1394-1399.

Fischer, W., Koch, H. U., Rösel, P., Fiedler, F., & Schmuck, L. (1980). Structural requirements of lipoteichoic acid carrier for recognition by the poly(ribitol phosphate) polymerase from *Staphylococcus aureus* H. A study of various lipoteichoic acids, derivatives, and related compounds. *J Biol Chem,* 255(10), 4550-4556.

Fischer, W., Laine, R. A., & Nakano, M. (1978). On the relationship between glycerophosphoglycolipids and lipoteichoic acids in gram-positive bacteria: II. Structures of glycerophosphoglycolipids. *Biochimica et Biophysica Acta (BBA) - Lipids and Lipid Metabolism,* 528(3), 298-308.

Flandroy, L., Poutahidis, T., Berg, G., Clarke, G., Dao, M. C., Decaestecker, E., Rook, G. (2018). The impact of human activities and lifestyles on the interlinked microbiota and health of humans and of ecosystems. *Sci Total Environ,* 627, 1018-1038.

Flom, J. D., & Sicherer, S. H. (2019). Epidemiology of Cow's Milk Allergy. *Nutrients,* 11(5).

Francino, M. P. (2015). Antibiotics and the Human Gut Microbiome: Dysbioses and Accumulation of Resistances. *Front Microbiol,* 6, 1543.

Garcia-Gutierrez, E., Mayer, M. J., Cotter, P. D., & Narbad, A. (2019). Gut microbiota as a source of novel antimicrobials. *Gut Microbes,* 10(1), 1-21.

Garcia-Vello, P., Sharma, G., Speciale, I., Molinaro, A., Im, S.-H., & De Castro, C. (2020). Structural features and immunological perception of the cell surface glycans of *Lactobacillus plantarum*: a novel rhamnose-rich polysaccharide and teichoic acids. *Carbohydrate Polymers,* 233, 115857.

Gauthier, A. E., Rotjan, R. D., & Kagan, J. C. (2022). Lipopolysaccharide detection by the innate immune system may be an uncommon defence strategy used in nature. *Open Biol,* 12(10), 220146.

Glauert, A. M., & Thornley, M. J. (1969). The topography of the bacterial cell wall. *Annu Rev Microbiol,* 23, 159-198.

Grabinger, T., Glaus Garzon, J. F., Hausmann, M., Geirnaert, A., Lacroix, C., & Hennet, T. (2019). Alleviation of Intestinal Inflammation by Oral Supplementation With 2-Fucosyllactose in Mice. *Front Microbiol,* 10, 1385.

Granier, A., Goulet, O., & Hoarau, C. (2013). Fermentation products: immunological effects on human and animal models. *Pediatric Research,* 74(2), 238-244.

Hacquard, S., Garrido-Oter, R., González, A., Spaepen, S., Ackermann, G., Lebeis, S., Schulze-Lefert, P. (2015). Microbiota and Host Nutrition across Plant and Animal Kingdoms. *Cell Host & Microbe,* 17(5), 603-616.

Hacquard, S., & Schadt, C. W. (2015). Towards a holistic understanding of the beneficial interactions across the Populus microbiome. 205(4), 1424-1430.

Hall, A. B., Yassour, M., Sauk, J., Garner, A., Jiang, X., Arthur, T., Huttenhower, C. (2017). A novel *Ruminococcus gnavus* clade enriched in inflammatory bowel disease patients. *Genome Medicine,* 9(1), 103.

Hammerschmidt, S., Talay, S. R., Brandtzaeg, P., & Chhatwal, G. S. (1997). SpsA, a novel pneumococcal surface protein with specific binding to secretory immunoglobulin A and secretory component. *molecular microbiology,* 25(6), 1113-1124.

Hanchi, H., Mottawea, W., Sebei, K., & Hammami, R. (2018). The Genus *Enterococcus*: Between Probiotic Potential and Safety Concerns-An Update. *Front Microbiol,* 9, 1791.

Haynie, T., Gubler, S., Drees, C., Heaton, T., Mitton, T., Gleave, Q., Savage, P. B. (2021). Synthesis of the pentasaccharide repeating unit from *Ruminococcus gnavus* and measurement of its inflammatory properties. *RSC Advances,* 11(24), 14357-14361.

Heinrichs, D. E., Yethon, J. A., & Whitfield, C. (1998). Molecular basis for structural diversity in the core regions of the lipopolysaccharides of *Escherichia coli* and *Salmonella enterica*. *Mol Microbiol,* 30(2), 221-232.

Henke, M. T., Brown, E. M., Cassilly, C. D., Vlamakis, H., Xavier, R. J., & Clardy, J. (2021). Capsular polysaccharide correlates with immune response to the human gut microbe *Ruminococcus gnavus*. 118(20), e2007595118.

Henke, M. T., Kenny, D. J., Cassilly, C. D., Vlamakis, H., Xavier, R. J., & Clardy, J. (2019). *Ruminococcus gnavus*, a member of the human gut microbiome associated with Crohn's disease, produces an inflammatory polysaccharide. 116(26), 12672-12677.

Hérias, M. V., Midtvedt, T., Hanson, L. A., & Wold, A. E. (1997). *Escherichia coli* K5 capsule expression enhances colonization of the large intestine in the gnotobiotic rat. *Infect Immun,* 65(2), 531-536.

Hongpattarakere, T., Cherntong, N., Wichienchot, S., Kolida, S., & Rastall, R. A. (2012). In vitro prebiotic evaluation of exopolysaccharides produced by marine isolated lactic acid bacteria. *Carbohydrate Polymers,* 87(1), 846-852.

Hsieh, S., Porter, N. T., Donermeyer, D. L., Horvath, S., Strout, G., Saunders, B. T., Allen, P. M. (2020). Polysaccharide Capsules Equip the Human Symbiont *Bacteroides thetaiotaomicron* to Modulate Immune Responses to a Dominant Antigen in the Intestine. *J Immunol,* 204(4), 1035-1046.

Hübner, J., Theilacker, C., Kaczynski, Z., & Holst, O. (2016). Rhamno-polysaccharide from *Enterococcus faecium* clonal complex 17 and uses thereof. Google Patents.

Huebner, J., Quaas, A., Krueger, W. A., Goldmann, D. A., & Pier, G. B. (2000). Prophylactic and therapeutic efficacy of antibodies to a capsular polysaccharide shared among vancomycin-sensitive and -resistant enterococci. *Infect Immun,* 68(8), 4631-4636.

Huebner, J., Wang, Y., Krueger, W. A., Madoff, L. C., Martirosian, G., Boisot, S., Pier, G. B. (1999). Isolation and chemical characterization of a capsular polysaccharide antigen shared by clinical isolates of *Enterococcus faecalis* and vancomycin-resistant *Enterococcus faecium*. *Infect Immun,* 67(3), 1213-1219.

Ikeda-Ohtsubo, W., Brugman, S., Warden, C. H., Rebel, J. M. J., Folkerts, G., & Pieterse, C. M. J. (2018). How Can We Define "Optimal Microbiota?": A Comparative Review of Structure and Functions of Microbiota of Animals, Fish, and Plants in Agriculture. *Front Nutr,* 5, 90.

Iliev, I. D., Kitazawa, H., Shimosato, T., Katoh, S., Morita, H., He, F., Saito, T. (2005). Strong immunostimulation in murine immune cells by *Lactobacillus rhamnosus* GG DNA containing novel oligodeoxynucleotide pattern. *Cell Microbiol,* 7(3), 403-414.

Iliev, I. D., Tohno, M., Kurosaki, D., Shimosato, T., He, F., Hosoda, M., Kitazawa, H. (2008). Immunostimulatory oligodeoxynucleotide containing TTTCGTTT motif from *Lactobacillus rhamnosus* GG DNA potentially suppresses OVA-specific IgE production in mice. *Scand J Immunol,* 67(4), 370-376.

Kalynych, S., Morona, R., & Cygler, M. (2014). Progress in understanding the assembly process of bacterial O-antigen. *FEMS Microbiology Reviews,* 38(5), 1048-1065.

Kalynych, S., Morona, R., & Cygler, M. (2014). Progress in understanding the assembly process of bacterial O-antigen. *FEMS Microbiol Rev,* 38(5), 1048-1065.

Kiriukhin, M. Y., Debabov, D. V., Shinabarger, D. L., & Neuhaus, F. C. (2001). Biosynthesis of the glycolipid anchor in lipoteichoic acid of *Staphylococcus aureus* RN4220: role of YpfP, the diglucosyldiacylglycerol synthase. *J Bacteriol,* 183(11), 3506-3514.

Kittelberger, R., & Hilbink, F. (1993). Sensitive silver-staining detection of bacterial lipopolysaccharides in polyacrylamide gels. *J Biochem Biophys Methods,* 26(1), 81-86.

Kloepper, J. W., & Schroth, M. N. (1981). Plant growth-promoting rhizobacteria and plant growth under gnotobiotic conditions. *Phytopathology,* 71(6), 642-644.

Kodali, S., Vinogradov, E., Lin, F., Khoury, N., Hao, L., Pavliak, V., Donald, R. G. (2015). A Vaccine Approach for the Prevention of Infections by Multidrug-resistant *Enterococcus faecium*. *J Biol Chem,* 290(32), 19512-19526.

Koenig, J. E., Spor, A., Scalfone, N., Fricker, A. D., Stombaugh, J., Knight, R., Ley, R. E. (2011). Succession of microbial consortia in the developing infant gut microbiome. 108(supplement_1), 4578-4585.

Korpela, K., Salonen, A., Virta, L. J., Kekkonen, R. A., Forslund, K., Bork, P., & de Vos, W. M. (2016). Intestinal microbiome is related to lifetime antibiotic use in Finnish pre-school children. *Nature Communications,* 7(1), 10410.

Kozlova, Y. I., Streshinskaya, G. M., Shashkov, A. S., Evtushenko, L. I., & Naumova, I. B. (1999). Anionic carbohydrate-containing polymers of cell walls in two streptoverticille genospecies. *Biochemistry (Mosc),* 64(6), 671-677.

Kraal, L., Abubucker, S., Kota, K., Fischbach, M. A., & Mitreva, M. (2014). The prevalence of species and strains in the human microbiome: a resource for experimental efforts. *PLoS One,* 9(5), e97279.

Krinos, C. M., Coyne, M. J., Weinacht, K. G., Tzianabos, A. O., Kasper, D. L., & Comstock, L. E. (2001). Extensive surface diversity of a commensal microorganism by multiple DNA inversions. *Nature,* 414(6863), 555-558.

Kropec, A., Sava, I. G., Vonend, C., Sakinc, T., Grohmann, E., & Huebner, J. (2011). Identification of SagA as a novel vaccine target for the prevention of *Enterococcus faecium* infections. *Microbiology (Reading),* 157(Pt 12), 3429-3434.

Kšonžeková, P., Bystrický, P., Vlčková, S., Pätoprstý, V., Pulzová, L., Mudroňová, D., Tkáčiková, Ľ. (2016). Exopolysaccharides of *Lactobacillus reuteri*: Their influence on adherence of *E. coli* to epithelial cells and inflammatory response. *Carbohydr Polym,* 141, 10-19.

Lacaze, A., Zboralski, A., & Joly, D. (2021). Who Feeds The Plants? Microbes! *Frontiers for Young Minds,* 9.

Lancefield, R. C. (1933). A serological differentiation of human and other groups of hemolytic streptococci. *J Exp Med,* 57(4), 571-595.

Landersjö, C., Yang, Z., Huttunen, E., & Widmalm, G. (2002). Structural studies of the exopolysaccharide produced by *Lactobacillus rhamnosus* strain GG (ATCC 53103). *Biomacromolecules,* 3(4), 880-884.

Larsen, O. F. A., & Claassen, E. (2018). The mechanistic link between health and gut microbiota diversity. *Sci Rep,* 8(1), 2183.

Laverde, D., Romero-Saavedra, F., Argunov, D. A., Enotarpi, J., Krylov, V. B., Kalfopoulou, E., Huebner, J. (2020). Synthetic Oligomers Mimicking Capsular Polysaccharide

Diheteroglycan are Potential Vaccine Candidates against Encapsulated Enterococcal Infections. *ACS Infect Dis,* 6(7), 1816-1826.

Lebeer, S., Claes, I. J., Verhoeven, T. L., Vanderleyden, J., & De Keersmaecker, S. C. (2011). Exopolysaccharides of *Lactobacillus rhamnosus* GG form a protective shield against innate immune factors in the intestine. *Microb Biotechnol,* 4(3), 368-374.

Lederberg, J., & McCray, A. T. J. T. S. (2001). `Ome Sweet `Omics--A Genealogical Treasury of Words. 15, 8-8.

Lees, A., Barr, J. F., & Gebretnsae, S. (2020). Activation of Soluble Polysaccharides with 1-Cyano-4-Dimethylaminopyridine Tetrafluoroborate (CDAP) for Use in Protein-Polysaccharide Conjugate Vaccines and Immunological Reagents. III Optimization of CDAP Activation. *Vaccines (Basel),* 8(4).

Leontein, K., Lindberg, B., & Lönngren, J. (1978). Assignment of absolute configuration of sugars by g.l.c. of their acetylated glycosides formed from chiral alcohols. *Carbohydrate Research,* 62(2), 359-362.

Liu, C., Finegold, S. M., Song, Y., & Lawson, P. A. (2008). Reclassification of *Clostridium coccoides*, *Ruminococcus hansenii*, *Ruminococcus hydrogenotrophicus*, *Ruminococcus luti*, *Ruminococcus productus* and *Ruminococcus schinkii* as *Blautia coccoides* gen. nov., comb. nov., *Blautia hansenii* comb. nov., *Blautia hydrogenotrophica* comb. nov., *Blautia luti* comb. nov., *Blautia producta* comb. nov., *Blautia schinkii* comb. nov. and description of *Blautia wexlerae* sp. nov., isolated from human faeces. *Int J Syst Evol Microbiol,* 58(Pt 8), 1896-1902.

Liu, S., Zhao, W., Lan, P., & Mou, X. (2021). The microbiome in inflammatory bowel diseases: from pathogenesis to therapy. *Protein Cell,* 12(5), 331-345.

Maes, E., Mille, C., Trivelli, X., Janbon, G., Poulain, D., & Guérardel, Y. (2009). Molecular Phenotyping of Mannosyltransferases-Deficient *Candida albicans* Cells by High-Resolution Magic Angle Spinning NMR. *The Journal of Biochemistry,* 145(4), 413-419.

Magne, F., Gotteland, M., Gauthier, L., Zazueta, A., Pesoa, S., Navarrete, P., & Balamurugan, R. (2020). The Firmicutes/Bacteroidetes Ratio: A Relevant Marker of Gut Dysbiosis in Obese Patients? *Nutrients,* 12(5).

Maldonado, R. F., Sá-Correia, I., & Valvano, M. A. (2016). Lipopolysaccharide modification in Gram-negative bacteria during chronic infection. *FEMS Microbiol Rev,* 40(4), 480-493.

Marquis, R. E., Mayzel, K., & Carstensen, E. L. (1976). Cation exchange in cell walls of gram-positive bacteria. *Can J Microbiol,* 22(7), 975-982.

Martens, E. C., Roth, R., Heuser, J. E., & Gordon, J. I. (2009). Coordinate regulation of glycan degradation and polysaccharide capsule biosynthesis by a prominent human gut symbiont. *J Biol Chem,* 284(27), 18445-18457.

Martinez, J. (2012). Bottlenecks in the Transferability of Antibiotic Resistance from Natural Ecosystems to Human Bacterial Pathogens. 2.

Martins dos Santos, V., Müller, M., & de Vos, W. M. (2010). Systems biology of the gut: the interplay of food, microbiota and host at the mucosal interface. *Curr Opin Biotechnol,* 21(4), 539-550.

Mazmanian, S. K., & Kasper, D. L. (2006). The love-hate relationship between bacterial polysaccharides and the host immune system. *Nat Rev Immunol,* 6(11), 849-858.

Mendoza, D. d. (2014). Temperature Sensing by Membranes. 68(1), 101-116.

Micoli, F., Adamo, R., & Costantino, P. (2018). Protein Carriers for Glycoconjugate Vaccines: History, Selection Criteria, Characterization and New Trends. *Molecules,* 23(6).

Miller, S. I., & Salama, N. R. (2018). The gram-negative bacterial periplasm: Size matters. *PLoS Biol,* 16(1), e2004935.

Montminy, S. W., Khan, N., McGrath, S., Walkowicz, M. J., Sharp, F., Conlon, J. E., Lien, E. (2006). Virulence factors of Yersinia pestis are overcome by a strong lipopolysaccharide response. *Nature Immunology,* 7(10), 1066-1073.

Morath, S., Geyer, A., & Hartung, T. J. J. o. E. M. (2001). Structure-function relationship of cytokine induction by lipoteichoic acid from *Staphylococcus aureus*. 193, 393-397.

Mourenza, Á., Gil, J. A., Mateos, L. M., & Letek, M. (2020). Alternative Anti-Infective Treatments to Traditional Antibiotherapy against *Staphylococcal veterinary* Pathogens. 9(10), 702.

Mu, Q., Tavella, V. J., & Luo, X. M. (2018). Role of *Lactobacillus reuteri* in Human Health and Diseases. *Front Microbiol,* 9, 757.

Nascimento, L. C. S., Casarotti, S. N., Todorov, S. D., & Penna, A. L. B. (2019). Probiotic potential and safety of enterococci strains. *Annals of Microbiology,* 69(3), 241-252.

Nemeth, J., Oesch, G., & Kuster, S. P. (2015). Bacteriostatic versus bactericidal antibiotics for patients with serious bacterial infections: systematic review and meta-analysis. *J Antimicrob Chemother,* 70(2), 382-395.

Nikaido, H. (2003). Molecular basis of bacterial outer membrane permeability revisited. *Microbiol Mol Biol Rev,* 67(4), 593-656.

Nocerino, R., Paparo, L., Terrin, G., Pezzella, V., Amoroso, A., Cosenza, L., Berni Canani, R. (2017). Cow's milk and rice fermented with *Lactobacillus paracasei* CBA L74 prevent infectious diseases in children: A randomized controlled trial. *Clin Nutr,* 36(1), 118-125.

O'Brien, P. A., Webster, N. S., Miller, D. J., & Bourne, D. G. (2019). Host-Microbe Coevolution: Applying Evidence from Model Systems to Complex Marine Invertebrate Holobionts. 10(1), 10.1128/mbio.02241-02218.

Opoku-Temeng, C., Kobayashi, S. D., & DeLeo, F. R. (2019). *Klebsiella pneumoniae* capsule polysaccharide as a target for therapeutics and vaccines. *Computational and Structural Biotechnology Journal,* 17, 1360-1366.

Panke-Buisse, K., Poole, A. C., Goodrich, J. K., Ley, R. E., & Kao-Kniffin, J. (2015). Selection on soil microbiomes reveals reproducible impacts on plant function. *Isme j,* 9(4), 980-989.

Pankey, G. A., & Sabath, L. D. (2004). Clinical relevance of bacteriostatic versus bactericidal mechanisms of action in the treatment of Gram-positive bacterial infections. *Clin Infect Dis,* 38(6), 864-870.

Paparo, L., Aitoro, R., Nocerino, R., Fierro, C., Bruno, C., & Canani, R. B. (2018). Direct effects of fermented cow's milk product with *Lactobacillus paracasei* CBA L74 on human enterocytes. *Benef Microbes,* 9(1), 165-172.

Patel, P., Wermuth, H. R., Calhoun, C., & Hall, G. A. (2023). *Antibiotics*.

Paynich, M. L., Jones-Burrage, S. E., & Knight, K. L. (2017). Exopolysaccharide from *Bacillus subtilis* Induces Anti-Inflammatory M2 Macrophages That Prevent T Cell-Mediated Disease. *J Immunol,* 198(7), 2689-2698.

Poirel, L., Madec, J.-Y., Lupo, A., Schink, A.-K., Kieffer, N., Nordmann, P., & Schwarz, S. (2018). Antimicrobial Resistance in Escherichia coli. 6(4), 10.1128/microbiolspec.arba-0026-2017.

Porter, N. T., & Martens, E. C. (2017). The Critical Roles of Polysaccharides in Gut Microbial Ecology and Physiology. 71(1), 349-369.

Qin, J., Li, R., Raes, J., Arumugam, M., Burgdorf, K. S., Manichanh, C., Meta, H. I. T. C. (2010). A human gut microbial gene catalogue established by metagenomic sequencing. *Nature,* 464(7285), 59-65.

Raetz, C. R., & Whitfield, C. (2002). Lipopolysaccharide endotoxins. *Annu Rev Biochem,* 71, 635-700.

Ramos, Y., Sansone, S., & Morales, D. K. (2021). Sugarcoating it: Enterococcal polysaccharides as key modulators of host-pathogen interactions. *PLoS Pathog,* 17(9), e1009822.

Rampelotto, P. H. (2013). Extremophiles and extreme environments. *Life (Basel),* 3(3), 482-485.

Rappuoli, R. (2018). Glycoconjugate vaccines: Principles and mechanisms. 10(456), eaat4615.

Rappuoli, R., & De Gregorio, E. (2011). A sweet T cell response. *Nature Medicine,* 17(12), 1551-1552.

Rekha, K., Kumar, R. M., Ilango, K., Rex, A., & Usha, B. (2018). Transcriptome profiling of rice roots in early response to *Bacillus subtilis* (RR4) colonization. 96(11), 749-765.

Reygaert, W. C. (2018). An overview of the antimicrobial resistance mechanisms of bacteria. *AIMS Microbiol,* 4(3), 482-501.

Rohokale, R., & Guo, Z. (2023). Development in the Concept of Bacterial Polysaccharide Repeating Unit-Based Antibacterial Conjugate Vaccines. *ACS Infect Dis,* 9(2), 178-212.

Romero-Saavedra, F., Laverde, D., Kalfopoulou, E., Martini, C., Torelli, R., Martinez-Matamoros, D., Huebner, J. (2019). Conjugation of Different Immunogenic Enterococcal Vaccine Target Antigens Leads to Extended Strain Coverage. *J Infect Dis,* 220(10), 1589-1598.

Rundlöf, T., & Widmalm, G. (1996). A Method for Determination of the Absolute Configuration of Chiral Glycerol Residues in Natural Products Using TEMPO Oxidation and Characterization of the Glyceric Acids Formed. *Analytical Biochemistry,* 243(2), 228-233.

Ruvalcaba-Gómez, J. M., Villagrán, Z., Valdez-Alarcón, J. J., Martínez-Núñez, M., Gomez-Godínez, L. J., Ruesga-Gutiérrez, E., Villarruel-López, A. (2022). Non-Antibiotics Strategies to Control Salmonella Infection in Poultry. *Animals (Basel),* 12(1).

Sadovskaya, I., Vinogradov, E., Courtin, P., Armalyte, J., Meyrand, M., Giaouris, E., Chapot-Chartier, M. P. (2017). Another Brick in the Wall: a Rhamnan Polysaccharide Trapped inside Peptidoglycan of *Lactococcus lactis*. *mBio,* 8(5).

Sagheddu, V., Patrone, V., Miragoli, F., Puglisi, E., & Morelli, L. (2016). Infant Early Gut Colonization by Lachnospiraceae: High Frequency of *Ruminococcus gnavus*. *Front Pediatr,* 4, 57.

Salas-Jara, M. J., Ilabaca, A., Vega, M., & García, A. (2016). Biofilm Forming Lactobacillus: New Challenges for the Development of Probiotics. *Microorganisms,* 4(3).

Sambuy, Y., De Angelis, I., Ranaldi, G., Scarino, M. L., Stammati, A., & Zucco, F. (2005). The Caco-2 cell line as a model of the intestinal barrier: influence of cell and culture-related factors on Caco-2 cell functional characteristics. *Cell Biol Toxicol,* 21(1), 1-26.

Schiavi, E., Gleinser, M., Molloy, E., Groeger, D., Frei, R., Ferstl, R., O'Mahony, L. (2016). The Surface-Associated Exopolysaccharide of *Bifidobacterium longum* 35624 Plays an Essential Role in Dampening Host Proinflammatory Responses and Repressing Local TH17 Responses. *Appl Environ Microbiol,* 82(24), 7185-7196.

Scott, A. J., Oyler, B. L., Goodlett, D. R., & Ernst, R. K. (2017). Lipid A structural modifications in extreme conditions and identification of unique modifying enzymes to define the Toll-like receptor 4 structure-activity relationship. *Biochim Biophys Acta Mol Cell Biol Lipids,* 1862(11), 1439-1450.

Scott, J. R., & Barnett, T. C. (2006). Surface proteins of gram-positive bacteria and how they get there. *Annu Rev Microbiol,* 60, 397-423.

Sekirov, I., Russell, S. L., Antunes, L. C., & Finlay, B. B. (2010). Gut microbiota in health and disease. *Physiol Rev,* 90(3), 859-904.

Sender, R., Fuchs, S., & Milo, R. (2016). Revised Estimates for the Number of Human and Bacteria Cells in the Body. *PLoS Biol,* 14(8), e1002533.

Shaw, N., Heatherington, K., & Baddiley, J. (1968). The glycolipids of *Lactobacillus casei* A.T.C.C. 7469. *Biochem J,* 107(4), 491-496.

Siepert, B., Reinhardt, N., Kreuzer, S., Bondzio, A., Twardziok, S., Brockmann, G., Tedin, K. (2014). *Enterococcus faecium* NCIMB 10415 supplementation affects intestinal immune-associated gene expression in post-weaning piglets. *Vet Immunol Immunopathol,* 157(1-2), 65-77.

Silhavy, T. J., Kahne, D., & Walker, S. (2010). The bacterial cell envelope. *Cold Spring Harb Perspect Biol,* 2(5), a000414.

Silva, M., Jacobus, N. V., Deneke, C., & Gorbach, S. L. (1987). Antimicrobial substance from a human Lactobacillus strain. *Antimicrob Agents Chemother,* 31(8), 1231-1233.

Sims, I. M., Frese, S. A., Walter, J., Loach, D., Wilson, M., Appleyard, K., Tannock, G. W. (2011). Structure and functions of exopolysaccharide produced by gut commensal *Lactobacillus reuteri* 100-23. *The ISME Journal,* 5(7), 1115-1124.

Smillie, C. S., Smith, M. B., Friedman, J., Cordero, O. X., David, L. A., & Alm, E. J. (2011). Ecology drives a global network of gene exchange connecting the human microbiome. *Nature,* 480(7376), 241-244.

Smokvina, T., Wels, M., Polka, J., Chervaux, C., Brisse, S., Boekhorst, J., Siezen, R. J. (2013). *Lactobacillus paracasei* comparative genomics: towards species pan-genome definition and exploitation of diversity. *PLoS One,* 8(7), e68731.

Soemarie, Y. B., Milanda, T., & Barliana, M. I. (2021). Fermented Foods as Probiotics: A Review. *J Adv Pharm Technol Res,* 12(4), 335-339.

Sonnenborn, U. (2016). *Escherichia coli* strain Nissle 1917—from bench to bedside and back: history of a special *Escherichia coli* strain with probiotic properties. *FEMS Microbiology Letters,* 363(19).

Speciale, I., Notaro, A., Garcia-Vello, P., Di Lorenzo, F., Armiento, S., Molinaro, A., De Castro, C. (2022). Liquid-state NMR spectroscopy for complex carbohydrate structural analysis: A hitchhiker's guide. *Carbohydr Polym,* 277, 118885.

States, D. J., Haberkorn, R., & Ruben, D. J. J. o. M. R. (1982). A two-dimensional nuclear overhauser experiment with pure absorption phase in four quadrants☆. 48, 286-292.

Stearns, J. C., Lynch, M. D., Senadheera, D. B., Tenenbaum, H. C., Goldberg, M. B., Cvitkovitch, D. G., Neufeld, J. D. (2011). Bacterial biogeography of the human digestive tract. *Sci Rep,* 1, 170.

Sun, Z., Harris, H. M. B., McCann, A., Guo, C., Argimón, S., Zhang, W., O'Toole, P. W. (2015). Expanding the biotechnology potential of lactobacilli through comparative genomics of 213 strains and associated genera. *Nature Communications,* 6(1), 8322.

Surana, N. K., & Kasper, D. L. (2017). Moving beyond microbiome-wide associations to causal microbe identification. *Nature,* 552(7684), 244-247.

Talarico, T. L., Casas, I. A., Chung, T. C., & Dobrogosz, W. J. (1988). Production and isolation of reuterin, a growth inhibitor produced by *Lactobacillus reuteri*. *Antimicrob Agents Chemother,* 32(12), 1854-1858.

Tan, W., Zhou, Z., Li, W., Lu, H., & Qiu, Z. (2021). *Lactobacillus rhamnosus* GG for Cow's Milk Allergy in Children: A Systematic Review and Meta-Analysis. *Front Pediatr,* 9, 727127.

Tannock, G. W. (2004). A special fondness for lactobacilli. *Appl Environ Microbiol,* 70(6), 3189-3194.

Thang, C. L., Baurhoo, B., Boye, J. I., Simpson, B. K., & Zhao, X. (2011). Effects of *Lactobacillus rhamnosus* GG supplementation on cow's milk allergy in a mouse model. *Allergy Asthma Clin Immunol,* 7(1), 20.

Togo, A. H., Diop, A., Bittar, F., Maraninchi, M., Valero, R., Armstrong, N., Million, M. (2018). Description of *Mediterraneibacter massiliensis*, gen. nov., sp. nov., a new genus isolated from the gut microbiota of an obese patient and reclassification of *Ruminococcus faecis*, *Ruminococcus lactaris*, *Ruminococcus torques*, *Ruminococcus gnavus* and *Clostridium glycyrrhizinilyticum* as *Mediterraneibacter faecis* comb. nov., *Mediterraneibacter lactaris* comb. nov., *Mediterraneibacter torques* comb. nov., *Mediterraneibacter gnavus* comb. nov. and *Mediterraneibacter glycyrrhizinilyticus* comb. nov. *Antonie Van Leeuwenhoek,* 111(11), 2107-2128.

Treisman, G. J. (2017). *Chapter 42 - The Role of the Brain–Gut–Microbiome in Mental Health and Mental Disorders*. In M. H. Floch, Y. Ringel & W. Allan Walker (Eds.), *The Microbiota in Gastrointestinal Pathophysiology* (pp. 389-397). Boston: Academic Press

Tsang, J. (2017). Bacterial plasmid addiction systems and their implications for antibiotic drug development. *Postdoc J,* 5(5), 3-9.

Urban-Chmiel, R., Marek, A., Stępień-Pyśniak, D., Wieczorek, K., Dec, M., Nowaczek, A., & Osek, J. (2022). Antibiotic Resistance in Bacteria-A Review. *Antibiotics (Basel),* 11(8).

Vaishnava, S., Yamamoto, M., Severson, K. M., Ruhn, K. A., Yu, X., Koren, O., Hooper, L. V. (2011). The antibacterial lectin RegIIIgamma promotes the spatial segregation of microbiota and host in the intestine. *Science,* 334(6053), 255-258.

Valle, J., Da Re, S., Henry, N., Fontaine, T., Balestrino, D., Latour-Lambert, P., & Ghigo, J.-M. (2006). Broad-spectrum biofilm inhibition by a secreted bacterial polysaccharide. 103(33), 12558-12563.

van Dalen, R., Peschel, A., & van Sorge, N. M. (2020). Wall Teichoic Acid in *Staphylococcus aureus* Host Interaction. *Trends Microbiol,* 28(12), 985-998.

van Dalen, R., Peschel, A., & van Sorge, N. M. (2020). Wall Teichoic Acid in *Staphylococcus aureus* Host Interaction: (Trends in Microbiology. In press. *Trends Microbiol,* 28(10), 869.

Van Gerven, N., Waksman, G., & Remaut, H. (2011). Pili and flagella biology, structure, and biotechnological applications. *Prog Mol Biol Transl Sci,* 103, 21-72.

Varki, A., Cummings, R. D., Aebi, M., Packer, N. H., Seeberger, P. H., Esko, J. D., Kornfeld, S. (2015). Symbol Nomenclature for Graphical Representations of Glycans. *Glycobiology,* 25(12), 1323-1324.

Verma, R., Lee, C., Jeun, E. J., Yi, J., Kim, K. S., Ghosh, A., Im, S. H. (2018). Cell surface polysaccharides of *Bifidobacterium bifidum* induce the generation of Foxp3(+) regulatory T cells. *Sci Immunol,* 3(28).

Vieira, A. T., Fukumori, C., & Ferreira, C. M. (2016). New insights into therapeutic strategies for gut microbiota modulation in inflammatory diseases. *Clin Transl Immunology,* 5(6), e87.

Vinogradov, E., Sadovskaya, I., Cornelissen, A., & van Sinderen, D. (2015a). Structural investigation of cell wall polysaccharides of *Lactobacillus delbrueckii* subsp. *bulgaricus* 17. *Carbohydr Res,* 413, 93-99.

Vinogradov, E., Sadovskaya, I., Cornelissen, A., & van Sinderen, D. (2015b). Structural investigation of cell wall polysaccharides of *Lactobacillus delbrueckii* subsp. *bulgaricus* 17. *Carbohydrate Research,* 413, 93-99.

Vollmer, W. (2008). Structural variation in the glycan strands of bacterial peptidoglycan. *FEMS Microbiol Rev,* 32(2), 287-306.

von Mutius, E., & Vercelli, D. (2010). Farm living: effects on childhood asthma and allergy. *Nature Reviews Immunology,* 10(12), 861-868.

Walter, A., Unsleber, S., Rismondo, J., Jorge, A. M., Peschel, A., Gründling, A., & Mayer, C. (2020). Phosphoglycerol-type wall and lipoteichoic acids are enantiomeric polymers differentiated by the stereospecific glycerophosphodiesterase GlpQ. *J Biol Chem,* 295(12), 4024-4034.

Walter, J. (2008). Ecological role of lactobacilli in the gastrointestinal tract: implications for fundamental and biomedical research. *Appl Environ Microbiol,* 74(16), 4985-4996.

Wang, B., Yao, M., Lv, L., Ling, Z., & Li, L. (2017). The Human Microbiota in Health and Disease. *Engineering,* 3(1), 71-82.

Wang, L., Wang, Q., & Reeves, P. R. (2010). The variation of O antigens in gram-negative bacteria. *Subcell Biochem,* 53, 123-152.

Wang, Z., Sun, Q., Zhang, H., Wang, J., Fu, Q., Qiao, H., & Wang, Q. (2021). Insight into antibacterial mechanism of polysaccharides: A review. *LWT,* 150, 111929.

Whitfield, C., Kaniuk, N., & Frirdich, E. (2003). Molecular insights into the assembly and diversity of the outer core oligosaccharide in lipopolysaccharides from *Escherichia coli* and Salmonella. *J Endotoxin Res,* 9(4), 244-249.

Whitfield, C., Wear, S. S., & Sande, C. (2020). Assembly of Bacterial Capsular Polysaccharides and Exopolysaccharides. *Annu Rev Microbiol,* 74, 521-543.

Zhou, X., Willems, R. J. L., Friedrich, A. W., Rossen, J. W. A., & Bathoorn, E. (2020). *Enterococcus faecium*: from microbiological insights to practical recommendations for infection control and diagnostics. *Antimicrobial Resistance & Infection Control,* 9(1), 130.

Zhou, X., Zhang, D., Qi, W., Hong, T., Xiong, T., Wu, T., Nie, S. (2021). Exopolysaccharides from *Lactobacillus plantarum* NCU116 Facilitate Intestinal Homeostasis by Modulating Intestinal Epithelial Regeneration and Microbiota. *Journal of Agricultural and Food Chemistry,* 69(28), 7863-7873.

Zhou, Z., Ding, W., Li, C., & Wu, Z. (2017). Synthesis and immunological study of a wall teichoic acid-based vaccine against *E. faecium* U0317. *Journal of Carbohydrate Chemistry,* 36(4), 205-219.

Żółkiewicz, J., Marzec, A., Ruszczyński, M., & Feleszko, W. (2020). Postbiotics-A Step Beyond Pre- and Probiotics. *Nutrients,* 12(8).